

# Mesozoic-Cenozoic evolution of the Eastern Kunlun Range, central Tibet, and implications for basin evolution during the Indo-Asian collision

Chen Wu<sup>1,2,\*</sup>, Andrew V. Zuza<sup>3</sup>, Zhiguang Zhou<sup>1</sup>, An Yin<sup>1,2</sup>, Michael W. McRivette<sup>4</sup>, Xuanhua Chen<sup>5</sup>, Lin Ding<sup>6</sup>, and Jianzhen Geng<sup>7</sup>

<sup>1</sup>STRUCTURAL GEOLOGY GROUP, CHINA UNIVERSITY OF GEOSCIENCES (BEIJING), BEIJING 100083, CHINA

<sup>2</sup>DEPARTMENT OF EARTH, PLANETARY, AND SPACE SCIENCES, UNIVERSITY OF CALIFORNIA, LOS ANGELES, CALIFORNIA 90095-1567, USA

<sup>3</sup>NEVADA BUREAU OF MINES AND GEOLOGY, UNIVERSITY OF NEVADA, RENO, NEVADA, 89557, USA

<sup>4</sup>DEPARTMENT OF GEOLOGICAL SCIENCES, ALBION COLLEGE, ALBION, MICHIGAN 49224, USA

<sup>5</sup>INSTITUTE OF GEOMECHANICS, CHINESE ACADEMY OF GEOLOGICAL SCIENCES, BEIJING 100081, CHINA

<sup>6</sup>INSTITUTE OF TIBETAN PLATEAU RESEARCH, CHINESE ACADEMY OF SCIENCES, P.O. BOX 9825, BEIJING 100085, CHINA

<sup>7</sup>ISOTOPIC LABORATORY, TIANJIN INSTITUTE OF GEOLOGY AND MINERAL RESOURCES, TIANJIN 300170, PR CHINA

## ABSTRACT

The present-day Tibetan plateau, which is the largest highland on Earth, formed primarily due to the India-Asia collision since 50–60 Ma. The development of the plateau has been associated with the Cenozoic development of two large intra-plateau sedimentary basins in north-central Tibet: the Qaidam and Hoh Xil basins to the north and south of the Eastern Kunlun Range, respectively. We conducted an integrated study of these two basins and the Eastern Kunlun Range that separates them to understand the timing and mechanisms of their development in order to decipher the growth and uplift history of the plateau. Crustal shortening in the Fenghuoshan-Nangqian and Qilian Shan-Nan Shan thrust belts initiated no later than the early Eocene, which formed the northern and southern boundaries of the combined Hoh Xil and Qaidam basins in central Tibet. The distinct two-stage development of the Hoh Xil basin suggests emergence of a topographic barrier between the Hoh Xil basin in the south and Qaidam basin in the north in the early Neogene, which is supported by the existing and new apatite fission-track data from the Eastern Kunlun Range that suggest rapid cooling after ca. 20 Ma. Previous and newly collected geochronological, petrological, and thermochronological data are best interpreted in the context of the Paleogene Paleo-Qaidam hypothesis, which requires Hoh Xil and Qaidam basins to have been parts of a single integrated basin during the early stage of the Cenozoic Tibetan plateau development.


LITHOSPHERE, v. 11, no. 4, p. 524–550; GSA Data Repository Item 2019162 | Published online 18 April 2019

<https://doi.org/10.1130/L1065.1>

## INTRODUCTION

Understanding how the Cenozoic Tibetan plateau has been developed in response to the Indo-Asian collision has important implications for deciphering the dynamics of large-scale intracontinental deformation and their impacts on a wide range of geologic processes (Harrison et al., 1992; Molnar et al. 1993, 2010; Liu-Zeng et al., 2008; Yin, 2010; Favre et al., 2015; Ding et al., 2017; Haproff et al., 2018). Current models for the formation of the plateau vary from vertically uniform lithospheric shortening, lower-crustal flow, continental subduction, convective removal of mantle lithosphere, large-scale underthrusting, to accumulation of Cenozoic sediment (e.g., England and Houseman, 1986, 1989; Dewey et al., 1988; Royden, 1996; Tapponnier et al., 2001; DeCelles et al., 2002; Wang et al., 2011; Yu et al., 2015). A detailed knowledge of uplift and deformation across the plateau is necessary to establish a unified understanding of plateau evolution.

The Hoh Xil and Qaidam basins of central-northern Tibet (Fig. 1) are two intra-plateau basins that figure importantly in the above debate. Specifically, the timing and geometry of their formation can inform us on the spatial and temporal uplift of bounding thrust-related ranges. The two basins are currently separated by the active 1000-km-long left-slip Kunlun Fault in Tibet (e.g., Cowgill et al., 2003; Robinson et al., 2003; Fu and Awata, 2007; Duvall et al., 2013; Yuan et al., 2013; Zuza et al., 2017), which is located within the Eastern Kunlun Range (Fig. 1). It has been proposed that these two basins were once connected as a single Paleogene basin (Figs. 2A and 2B), which is known as the Paleo-Qaidam basin (Yin et al., 2008a, 2008b). Existing thermochronologic data for the Eastern Kunlun Range include <sup>40</sup>Ar/<sup>39</sup>Ar, fission-track, and (U-Th)/He results from across the range. Sparse <sup>40</sup>Ar/<sup>39</sup>Ar and apatite fission-track data reveal slow Jurassic cooling and rapid Neogene cooling across the Eastern Kunlun Range (Jolivet et al., 2001; Wang et al., 2004; Y. Liu et al., 2005a; Yuan et al., 2006; Chen et al., 2011; Duvall et al., 2013; Wang et al., 2016; Yuan et al., 2013; Wang et al., 2017), and this inferred Neogene uplift of the Eastern Kunlun Range raises the question of whether Qaidam and Hoh Xil basins were originally connected. However, some fission-track and (U-Th)/He studies have resulted in a wide range of ages for rapid

Chen Wu  <http://orcid.org/0000-0003-0647-3530>  
\*wuchen2016@cugb.edu.cn; wuchenlovegeology@gmail.com

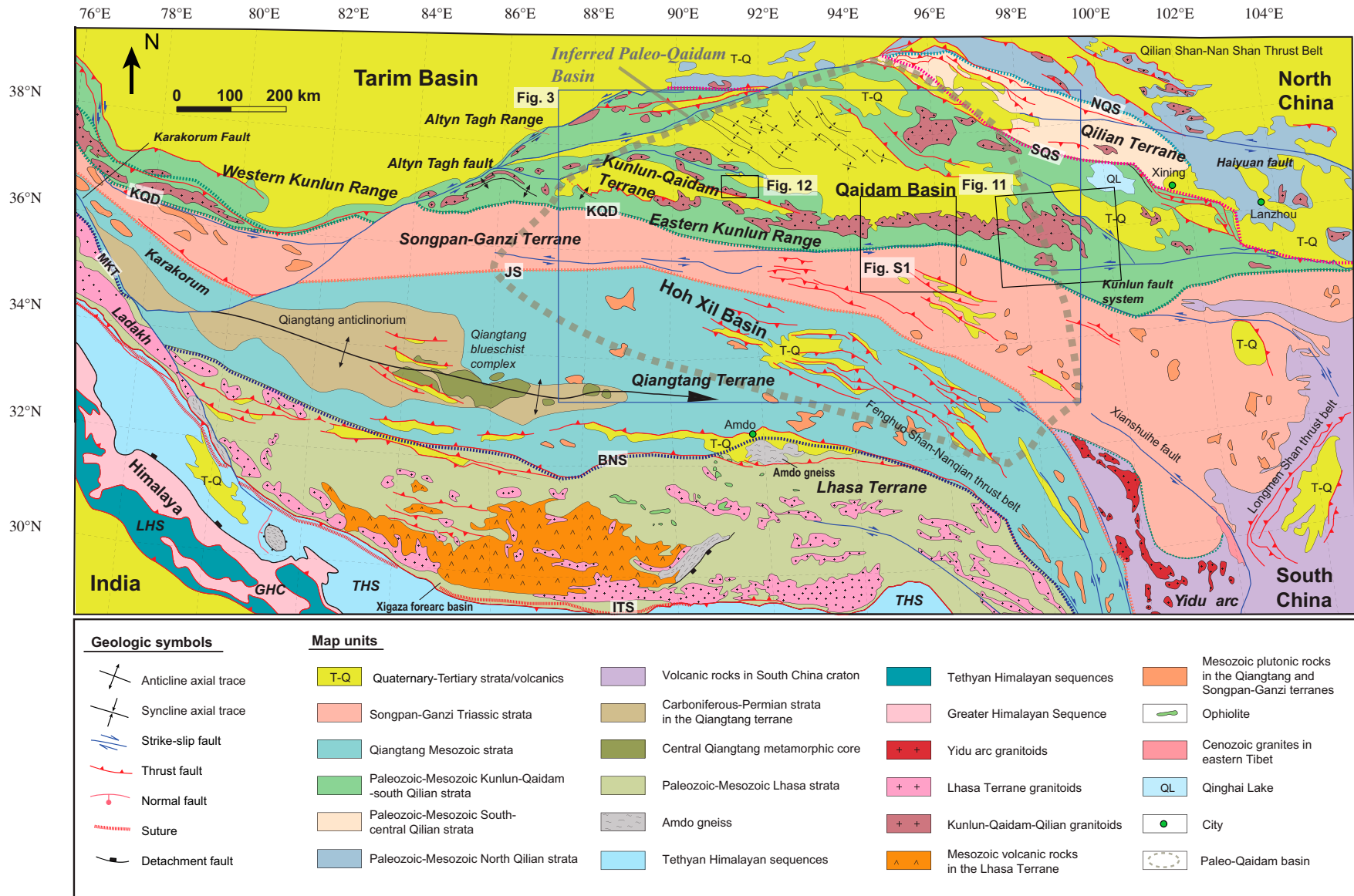


**Figure 1.** An index geologic map of Tibet after Yin and Harrison (2000) that shows the locations of the study areas. The two major Cenozoic sedimentary basins of the central Tibetan plateau, the Qaidam and Hoh Xil basins, are superposed on the Kunlun terrane and Songpan-Ganzi and northern Qiangtang terranes, respectively. The bold dashed line indicates the areal extent of the inferred Paleogene Paleo-Qaidam basin. Note the abbreviations of major lithologic and tectonic units are defined as: THS—Tethyan Himalayan sequences (Proterozoic to Late Cretaceous passive continental margin strata); LHS—Lesser Himalayan metasedimentary series; GHC—Greater Himalayan Sequence; ITS—Indus-Tsangpo suture; BNS—Bangong-Nujiang suture; JS—Jinsha suture; KQD—Kunlun-Qinling-Dabie suture; SQS—south Qilian suture; NQS—north Qilian suture; MKT—Main Karakorum Thrust.

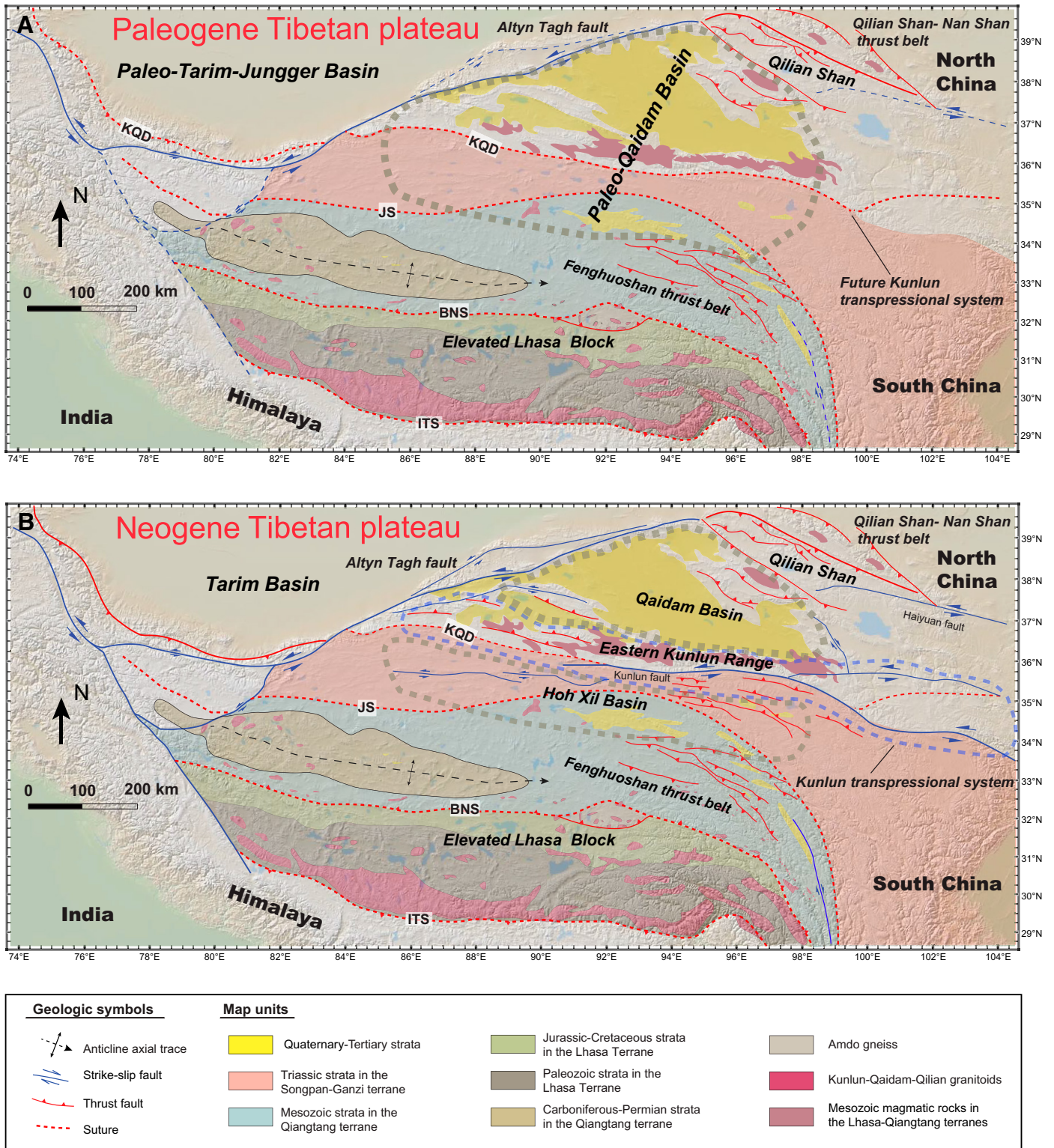


Figure 2. (A) Paleogene tectonic configuration of the Tibetan plateau in present-day geographic coordinates. The Paleo-Qaidam basin lies between the elevated Lhasa block and the Fenghuo Shan thrust belt in the south and the elevated Qilian Shan in the north. The region northwest of the Tibetan plateau was a large topographic depression, with the linked Tarim and Junggar basins across the Tian Shan because the Tian Shan was not uplifted until the early Miocene (Yin et al., 2008a, 2008b). (B) Neogene tectonic configuration of the Tibetan plateau in present-day geographic coordinates. The initiation of the Eastern Kunlun left-slip transpressional system caused the uplift of the Eastern Kunlun Range, which has partitioned the Paleo-Qaidam basin into the Hoh Xil basin to the south and the Qaidam basin to the north. These two maps (A) and (B) based on Yin et al. (2008b). Note: ITS—Indus-Tsangpo suture; BNS—Bangong-Nujiang suture; JS—Jinsha suture; KQD—Kunlun-Qinling-Dabie suture. Digital topographic map was derived from the Global Multi-Resolution Topography (GMRT) Synthesis by Ryan et al. (2009) (<http://www.geomapp.org>).

cooling ranging from ca. 40 to 0 Ma (e.g., Clark et al., 2010; Dai et al., 2013; Duvall et al., 2013). The Paleo-Qaidam hypothesis implies that the original Qaidam basin was much larger in the early Cenozoic and bounded by different structures (i.e., Paleo-Qaidam basin) (Figs. 2A and 2B). In addition, this model emphasizes the role of large basin development and discrete northward jumping of thrust systems (e.g., Meyer et al., 1998).

In this contribution, we conducted an integrated field and analytical study involving detailed geologic mapping, sedimentology, sandstone petrologic analyses, U-Pb detrital zircon geochronology, tectonic setting analysis, and thermochronologic analysis across the Hoh Xil basin–Eastern Kunlun Range–Qaidam basin of western China (Fig. 1). We first outline the regional tectonic framework of Tibet and introduce the studied sedimentary basins to place our provenance analysis in perspective. Our new field and analytical observations allow us to (1) establish the structural framework and uplift history of the Eastern Kunlun Range, and (2) interpret whether a large Paleogene basin existed in central-north Tibet. We ultimately present new constraints on the tectonic reconstruction of the central-north Tibet and evolution of its Cenozoic basins.

## REGIONAL TECTONIC FRAMEWORK

The primary tectonic domains of the Tibetan plateau include, from north to south, the Qilian terrane, Kunlun–Qaidam terrane, Songpan–Ganzi terrane, Qiangtang terrane, Lhasa terrane, and the Himalayas (e.g., Allégre et al., 1984; Dewey et al., 1988; Yin and Harrison, 2000; Gehrels et al., 2011) (Fig. 1). Below is a brief review of the geology of these domains, which is necessary to adequately interpret sedimentary provenance and any detrital zircon data set. Three major phases of magmatism occurred at the Qilian terrane (Cowgill et al., 2003; Gehrels et al., 2003a, 2011; Yin et al., 2007b; Wu et al., 2017; Zuza et al., 2018): (1) at 960–820 Ma as small isolated plutons intruding the North China craton, (2) at 520–400 Ma as arc related plutons and volcanic complexes, and (3) at ca. 270 Ma as isolated plutons of the Permian Kunlun arc. Mesozoic extensional structures and related basin deposits have been documented around the Qilian terrane (e.g., Chen et al., 2003; Chen et al., 2014). In addition, Proterozoic magmatism or metamorphic events at 1700–2000 Ma (Chen et al., 2013; Liao et al., 2014) and 2350–2550 Ma (Lu, 2002; Lu et al., 2006; Gong et al., 2012; X.J. Yu et al., 2017c; S. Yu et al., 2017b) occurred in the South Qilian Shan and northern Qaidam basin.

The Kunlun–Qaidam terrane includes the Eastern Kunlun Range and Qaidam basin, and consists of Precambrian basement intruded by Ordovician–Devonian plutons, and Permian to Triassic arc sequences, including the prominent Permian–Triassic Kunlun batholith exposed in the Eastern Kunlun Range (Fig. 1; Mock et al., 1999; Cowgill et al., 2003; Robinson et al., 2003; Gehrels et al., 2003a, 2003b; Mo et al., 2007; X.H. Chen et al., 2012b; Cheng et al., 2016; C. Wu et al., 2016a; Dong et al., 2018; Wu et al., 2019). At the western end of the Eastern Kunlun Range, Cretaceous plutons have also been documented (Robinson et al., 2003). Some minor Neoproterozoic ages have also been reported in recent studies (e.g., He et al., 2016a, 2016b, 2018). The Triassic Yidun arc bounding the southeastern side of the Songpan–Ganzi terrane is the eastern extent of the Permian–Triassic Kunlun batholith and is locally intruded by Cretaceous (ca. 95–105 Ma) granites (Reid et al., 2007; C. Wu et al., 2016a; Jackson et al., 2018). The Qaidam basin is bounded by the Altyn Tagh Range to the northwest, and the Paleozoic granitoids are widely exposed in the Altyn Tagh region. Six episodes of granitic magmatism can be distinguished at ca. 517 Ma, 501–496 Ma, 462–451 Ma, 426–385 Ma, 352–343 Ma, and ca. 265 Ma in the south Altyn Tagh (e.g., Kang et al., 2011; Liu et al., 2009; C.L. Wu et al., 2016b); whereas numerous early Paleozoic granitoid plutons (i.e., 500–405 Ma) are exposed throughout

the north Altyn Tagh (e.g., Sobel and Arnaud, 1999; C.L. Wu et al., 2005, 2016b; Kang et al., 2011).

The Songpan–Ganzi terrane is composed mainly of a Triassic submarine-fan turbidite complex deposited during the closure of the Paleo-Tethys Ocean (Fig. 1; Yin and Nie, 1996; Nie et al., 1994; Weislogel et al., 2006, 2010; Enkelmann et al., 2007; Zhang et al., 2014; C. Wu et al., 2016a). Post-orogenic plutons, with ages ranging from 175 Ma to 200 Ma, occur across the Songpan–Ganzi Terrane (Roger et al., 2004; Zhang et al., 2014). Along the northern and eastern margins of the Qiangtang terrane, the subduction of the Jinsha Ocean was mostly accommodated by both northward and southward subduction during the Triassic to possibly earliest Jurassic (Fig. 1) (Murphy et al., 1997; Yin and Harrison, 2000; Pullen et al., 2008; Ding et al., 2013; Zhang et al., 2014; C. Wu et al., 2016a). The terrane is composed of 220–170 Ma plutonic rocks (e.g., Roger et al., 2003, 2004; Gynn et al., 2006; Zhang et al., 2014), and 170–100 Ma intrusive rocks in the southern Qiangtang terrane (Li et al., 2014; D. Liu et al., 2017a, 2018; Hao et al., 2016). However, the U-Pb zircon dating reveals the presence of Eocene granitoids (Roger et al., 2000; Spurlin et al., 2005) and post-collision volcanic rocks (<44 Ma) are widely scattered across the Qiangtang terrane (e.g., Hacker et al., 2000; Chung et al., 2005; Jolivet et al., 2003; Ding et al., 2003, 2007). The voluminous Late Jurassic to late Paleogene Gangdese batholith exposed in the southern Lhasa terrane is overlain by the locally deformed late Paleocene–early Eocene Linzizong volcanic rocks (e.g., Yin et al., 1994; Harrison et al., 2000; Mo et al., 2005; Kapp, et al., 2007a, 2007b; Volkmer et al., 2007). Post-collision volcanism and dike intrusion occurred widely across the Lhasa terrane between 26 and 10 Ma (Miller et al., 1999; Williams et al., 2001; Mo et al., 2006, 2007).

## MESOZOIC-CENOZOIC SEDIMENTS IN CENTRAL TIBET

### Jurassic–Cretaceous strata

Jurassic sediments are present across much of central and northern Tibet (Figs. 1 and 3). In Qaidam basin, Jurassic strata are exposed along the northeastern and western basin margins; they are divided into the lower, middle, and upper units (Qian et al., 2018) and represent important hydrocarbon source units as described elsewhere (Chen et al., 2010). The overlying Cretaceous dark-red beds disconformably overlie upper Jurassic strata, although the units are generally parallel (C. Wu et al., 2016a). In the Songpan–Ganzi terrane, Jurassic rocks are restricted to local occurrences of coal-bearing deltaic deposits (Weislogel, 2008; Ding et al., 2013). Farther south, Jurassic sediments of the Yanshiping Group are widely exposed in the Qiangtang terrane (Figs. 3 and 4A–4C; e.g., Leeder et al., 1988; C.S. Wang et al., 2001a; Fang et al., 2016). This thick Jurassic sequence overlies Middle to Late Triassic shallow marine strata that were likely deposited in sub-basins marginal to the closing Songpan–Ganzi remnant ocean basin (Yin et al., 1988; Yin and Harrison, 2000; Zhang et al., 2006). Paleocurrent directions obtained from channel sandstones and cross stratification in Yanshiping Group sediments are generally directed south (Leeder et al., 1988). Northern derivation of detritus suggests that the marine depositional environment in the Jurassic was located near the southern margin of the Qiangtang terrane (Leeder et al., 1988).

### Cenozoic Hoh Xil Basin

The Cenozoic Hoh Xil basin developed on the older Songpan–Ganzi and northern Qiangtang terranes (Fig. 1), and is composed of the basal Cretaceous–Eocene Fenghuoshan Group and Tuotuohe Group, the overlying Yaxicuo Group, and the capping Wudaoliang Group (Liu and Wang,

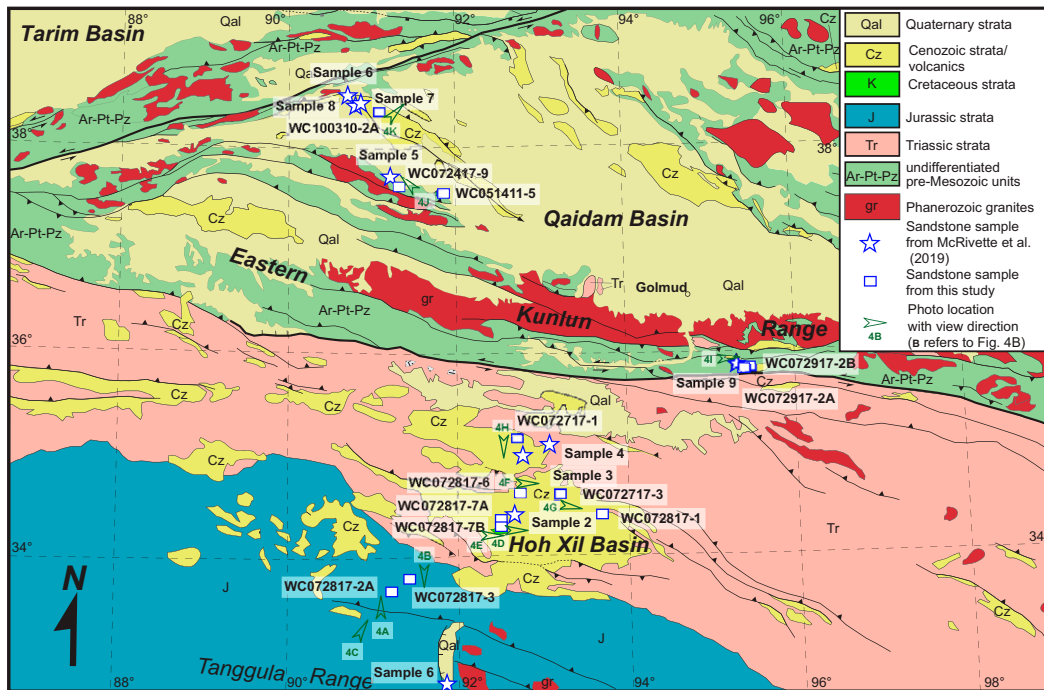


**Figure 3.** Geologic map of the central Tibetan plateau, including the Qaidam and Hoh Xil basin and the Eastern Kunlun Range. Locations of sandstone samples collected for petrographic analysis and U-Pb detrital zircon geochronology are indicated by the white stars from McRivette et al. (2019) and white rectangles from this study.

2001; Li et al., 2018). Together, the Cenozoic strata exceed ~5800 m in thickness (Liu and Wang, 2001) and extend from the Tanggula Shan northward to the Kunlun Range, which overlies the Mesozoic sedimentary units (Fig. 3). The contact between the Fenghuoshan Group and the underlying strata in the central portion of the basin has previously been described as a Cenozoic thrust placing the Fenghuoshan Group strata over Neogene sediments (Leeder et al., 1988; Staisch et al., 2016; McRivette et al., 2019). We observed this contact to be clearly depositional as indicated by the presence of wide channels of the Fenghuoshan Group incised into the underlying Cretaceous strata (Figs. 4D and 4E). To the southwest, the underlying Cretaceous strata are in normal-fault contact with Triassic flysch deposits (Fig. 4E).

Magnetostratigraphic analyses of the Fenghuoshan and Yaxicuo Groups indicate their deposition ages at 51–31 Ma (early Eocene–early Oligocene) and ca. 31–30 Ma (early Oligocene), respectively (Liu et al., 2003). However, the age of the Fenghuoshan Group is suggested to range from ca. 72 to 51 Ma with the most recent magnetostratigraphic analyses (Jin et al., 2018). Fossil assemblages further establish an Eocene age for the Fenghuoshan Group (Smith and Xu, 1988). However, new results from Staisch et al. (2014) suggest that the Fenghuoshan Group was deposited from 85 to 51 Ma. The lower-age bound is derived from Late Cretaceous fossils in the lower part of the group (Li et al., 2015) and the upper age was determined via a zircon age in interbedded tuff (Staisch et al., 2014). Recently, a tuff layer within the Fenghuoshan Group yielded a weighted mean U-Pb age of ca. 63 Ma (Jin et al., 2018). The Fenghuoshan Group was sourced from the Qiangtang terrane, and may share a sediment source with Cretaceous sedimentary rocks in the Nima Basin (Staisch et al., 2014). Dai et al. (2012) and Li et al. (2018) also provide detrital zircon data to argue that the Qiangtang terrane is the main source terrane for the Fenghuoshan Group. Furthermore, Staisch et al. (2014) interpreted the Tuotuohe and Yaxicuo Groups as coeval early Oligocene sedimentary units that unconformably overlie the Fenghuoshan Group. The significant deformation of the Fenghuoshan and Yaxicuo Group strata relative to the overlying Wudaoliang Group

and the extensive erosional surface upon which the latter was deposited require that a depositional hiatus must have occurred across the vast majority of Hoh Xil basin in the late Oligocene (e.g., Wang et al., 2002; Wu et al., 2008; Staisch et al., 2016).

The Eocene to early Oligocene Tuotuohe Group unconformably overlies the Fenghuoshan Group and is exposed along the South Fenghuoshan thrust fault and in the Tuotuohe subbasin, located to the south of the Fenghuoshan Range (Fig. 4F; Qinghai BGMR, 1991). The inclusion of Fenghuoshan Group clasts within the Tuotuohe Group strata indicates that it was, at least in part, sourced from the Fenghuoshan Range (Staisch et al., 2014). The Yaxicuo Group is 670–2000 m thick and is interpreted to have been deposited in fluvial and lacustrine environments (Fig. 4G; Z.F. Liu et al., 2005b; Liu and Wang, 2001). There are paleocurrent studies that indicate the Yaxicuo Group also received detritus from the north (Wang et al., 2008).

In the Wudaoliang Group, with a total thickness from <100 m to ~800 m (Fig. 4H) (Liu and Wang, 2001), paleocurrent data are sparse, though southward flow has been documented near the base of the unit (Z.F. Liu et al., 2005b). It is assigned an early Miocene age based on fossil and pollen assemblages (Yin et al., 1988; Wu et al., 2008), consistent with magnetostratigraphy indicating the basal rocks were deposited between 23.8 Ma and 21.8 Ma (Z.F. Liu et al., 2005b; Wang et al., 2008). The most robust constraint for the upper age limit of the Wudaoliang Group is ca. 11 Ma based on late Miocene to Pliocene sporopollen assemblages in localized overlying sediments (Wu et al., 2008).

### Cenozoic Sediments within the Eastern Kunlun Range

Cenozoic sediments exposed within the Eastern Kunlun Range are typically associated with active south-directed thrusts (Yin et al., 2007a; Chen et al., 2010) (Figs. 3 and 4J). Sediment deposition in the western segment of the Eastern Kunlun Range started in the latest Oligocene in a lacustrine setting (Chen et al., 2010); they are interpreted to be parts of a larger Oligocene Qaidam basin which were subsequently incorporated

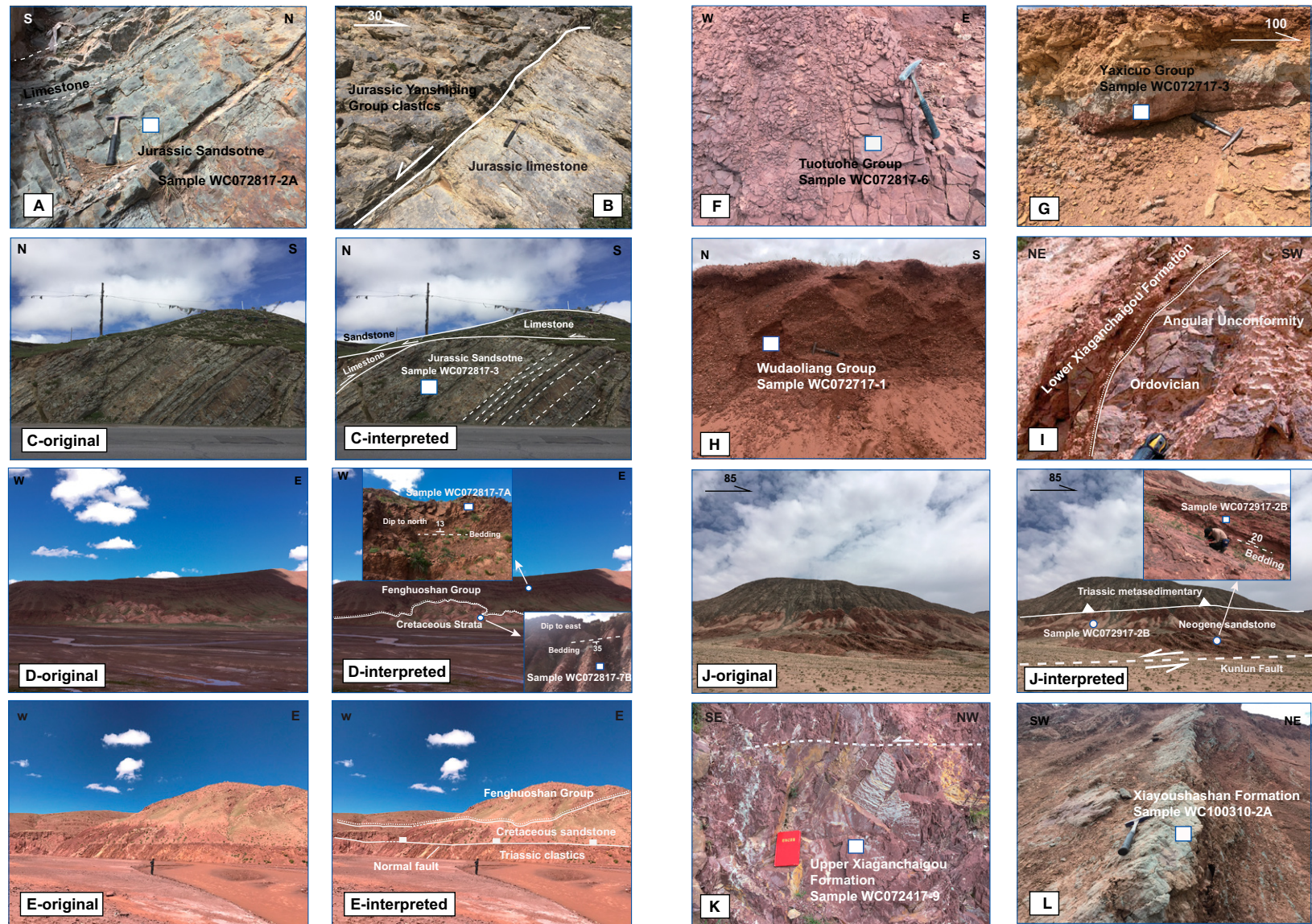


**Figure 4.** Field photographs from the central-north Tibet displaying important geologic relationships discussed in text. (A) Outcrop of the Middle Jurassic sandstone sample WC072817-2A, showing the contact between the limestone and sandstone. (B, C) Complex thrusting in the Late Jurassic strata, showing the outcrop of the Middle Jurassic sandstone sample WC072817-3. (D) Unconformity between the Fenghuoshan Group of Hoh Xil basin and underlying Cretaceous strata. The erosional/depositional character of this contact is clearly shown by the incised paleo-channels on the left and right sides of the outcrop. The outcrops of sandstone samples WC072817-2A and WC072817-2B from the Fenghuoshan Group and Cretaceous strata are indicated, respectively. (E-original and E-interpreted) Normal fault juxtaposing Cretaceous strata in the hanging-wall and Triassic flysch in the footwall. (F) Location of the Tuotuohe Group sandstone sample WC072817-6. (G-H) Outcrops of the Yaxicuo Group and Wudaoliang Group sandstone samples WC072717-3 and WC072717-1, respectively. (I) Depositional contact between the Lower Xiaganchaigou Formation and Paleozoic rocks exposed in the Eastern Kunlun Range along the southern margin of Qaidam basin, with a handheld GPS unit for scale. (J-original and J-interpreted) Exposure of Neogene strata adjacent to the Kunlun fault in the interior of the Eastern Kunlun Range. The strata are in the footwall of an active north dipping thrust fault. Outcrops of the Neogene sediment samples WC072917-2A and WC072917-2B. (K-L) Outcrops of the Upper Xiaganchaigou Formation sandstone sample WC072417-9 and Xiayoushahan Formation sandstone sample WC100310-2A, respectively.

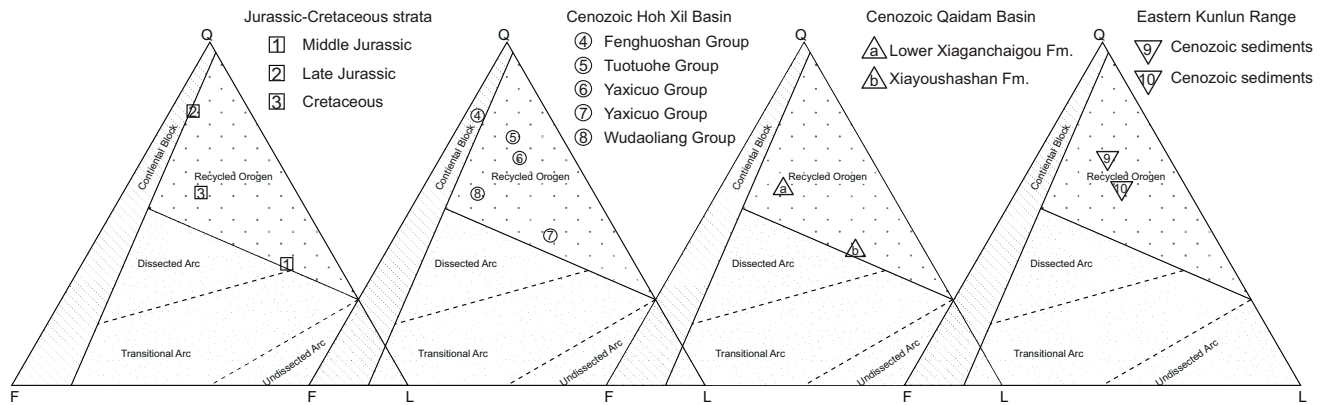


Figure 5. Modal composition of sandstone samples analyzed in this study displayed in a QFL plot after Dickinson (1985).

into the Eastern Kunlun Range due to encroachment of thrusting from the range to the basin (Yin et al., 2007a; Chen et al., 2010). In the central and eastern segments of the Eastern Kunlun Range, Cenozoic sediments may have started to develop in the Neogene in alluvial fan settings (Fig. 3; Wu et al., 2008). These deposits have been interpreted to be the northern proximal facies of a large Miocene lake in the Hoh Xil region during the deposition of the Wudaoliang Group (Fig. 3; Wu et al., 2008). As a result, the depositional ages and tectonic settings of the sediments within the range and their relationships to the nearby Qaidam and Hoh Xil basins remain poorly understood.

### Cenozoic Qaidam Basin

Qaidam basin is currently the largest topographic depression inside Tibet (e.g., Yin et al., 2002; Rieser et al., 2005; Chen et al., 2011; Wang et al., 2017). In the north, the south-directed North Qaidam thrust system juxtaposes Jurassic and older rocks over the Cenozoic strata (Fig. 3) (Yin et al., 2008a). In the south, the Cenozoic basin strata overlie Paleozoic and older rocks of the Kunlun Range in a depositional contact (Yin et al., 2007a). This contact is well exposed along the southwestern margin of Qaidam basin (Chen et al., 2011) and the contact surface can be traced via seismic reflection profiles as a north-dipping basement reflector below the basin fill (Yin et al., 2007a). The overall structure of the Cenozoic basin is a broad synclinorium bounded by active thrust faults in the northern and south that initiated at ca. 50 Ma and 30–20 Ma, respectively (Fig. 3) (Yin et al., 2008b).

Age assignments for Cenozoic strata in the Qaidam basin come from biostratigraphy, magnetostratigraphy, fission track, and  $^{40}\text{Ar}/^{39}\text{Ar}$  dating of detritus in exposed strata. These data are subsequently correlated across the basin using a dense network of seismic reflection profiles and drill hole data (e.g., Yang et al., 1992; Xia et al., 2001; Sun et al., 2005; Rieser et al., 2006a, 2006b; Fang et al., 2007; Yin et al., 2008b; Lu and Xiong, 2009; Chen et al., 2011; McRivette et al., 2019; Ke et al., 2013; Yu et al., 2014; Cheng et al., 2016; Bush et al., 2016; Ji et al., 2017; A. Chen et al., 2017a; Wang et al., 2017). Cenozoic stratigraphic division and age assignments from oldest to youngest units are as follows (Chen et al., 2010): Paleocene to lower Eocene Lulehe Formation (Yang et al., 1992; Rieser et al., 2006a; Ke et al., 2013; Yu et al., 2014; Ji et al., 2017), middle Eocene to lower Oligocene Xiaganchaigou Formation (Yang et al., 1992; Sun et al., 2005; Yu et al., 2014; Li et al., 2016; Ji et al., 2017), upper Oligocene Shangganchaigou Formation (Sun et al., 1999; Yu et al., 2014; Li et al., 2016; Chang et al., 2015; Ji et al., 2017), lower to middle Miocene Xiayoushashan Formation (Sun et al., 1999; Chang et al., 2015; Ji et al., 2017; Li et al., 2016), middle

to upper Miocene Shangyoushashan Formation (Sun et al., 1999; Wang et al., 2007; Fang et al., 2007; Chang et al., 2015; Li et al., 2016; Ji et al., 2017), and upper Miocene and Pliocene Shizigou Formation (Sun et al., 1999; Fang et al., 2007; Wang et al., 2007; Yu et al., 2014; Li et al., 2016). The total thickness of Cenozoic Qaidam deposits exceeds 16 km in the west and progressively thins eastward to less than 2 km in the east (Yin et al., 2008b; Chen et al., 2010).

## METHODS

### Sandstone Petrology

Analysis of the modal compositions of 12 sandstone samples involved counting at least 350 grains using the Gazzi-Dickinson method on each thin section (Dickinson, 1970; Ingersoll et al., 1984; Dickinson, 1985). The grain types were identified and tabulated following Ingersoll et al. (1984) and Dickinson (1985). As the purpose of this study is to determine the first-order trends, we only tabulated quartz (Q), feldspar (F), and lithic fragments (L) in our analysis. K-feldspar and plagioclase were differentiated optically. Detailed sample locations and results are presented in the GSA Data Repository in Table S1 and Table S2<sup>1</sup>, respectively. In summary, Jurassic and Cretaceous samples plot between “continental block” and “recycled orogen” fields on the ternary diagram (Fig. 5). The Paleocene–Eocene Fenghuoshan Group sandstone plots in the “continental block,” whereas the Eocene–early Miocene samples from Hoh Xil basin, Cenozoic Kunlun Range sediments and middle Eocene–Pliocene samples from Qaidam basin plot in the “recycled orogen” field (Fig. 5).

### U-Pb Zircon Geochronology

Twelve sandstone samples were analyzed for detrital zircon geochronology. Zircon grains were separated from 3 to 10 kg whole-rock samples by standard crushing, sieving, heavy liquid, and magnetic separation techniques. They were mounted in epoxy blocks and polished to obtain an even surface, and then cleaned in an ultra-sonic washer containing a 5%  $\text{HNO}_3$  bath prior to laser ablation–inductively coupled plasma–mass spectrometry (LA-ICP-MS) analysis. To identify the internal structure and texture of the zircon grains and to select potential positions for U-Pb analysis, cathodoluminescence (CL) images of zircons were taken on a

<sup>1</sup>GSA Data Repository Item 2019162, Tables S1–S4 and Figure S1, is available at <http://www.geosociety.org/datarepository/2019>, or on request from [editing@geosociety.org](mailto:editing@geosociety.org).

JXA-880 electron microscope and an image analysis software was used under operating conditions of 20 kV and 20 nA at the Institute of Mineral Resources, Chinese Academy of Geological Sciences, Beijing, China.

The zircons separated from the samples were analyzed for U, Th, and Pb using the LA-ICP-MS facility at the Isotopic Laboratory, Tianjin Institute of Geology and Mineral Resources of China Geological Survey. Laser sampling was performed using a Neptune multi-collector-inductively coupled-plasma mass spectrometer (Thermo Fisher Ltd.) to a NEW WAVE 193 nm-FX ArF Excimer laser-ablation system (ESI Ltd.). The MC-ICP-MS is a double focusing multi-collector ICP-MS. The maximum mass dispersion was 17%. This machine has nine Faraday cups, one fixed central channel and eight motorized Faraday cups. The Excimer LA system pulse width is less than 4 ns and all analyses were conducted with a beam diameter of 30  $\mu\text{m}$ , an 8 Hz repetition rate, and energy density of 11 J/cm<sup>2</sup>. Approximately 100 zircon grains were analyzed per sample in this study. Detailed operating conditions of the laser ablation system and the MC-ICP-MS instrument and data reduction are listed in Table S3. GJ-1 was used as an external standard for U-Pb dating analyses (Jackson et al., 2004). Common-Pb corrections were made using the method of Andersen (2002). NIST SRM 610 glass was used as an external standard to calculate U, Th, and Pb concentrations of zircons. Every eight analyses were followed by two analyses of the standard zircon GJ-1. <sup>207</sup>Pb/<sup>206</sup>Pb, <sup>206</sup>Pb/<sup>238</sup>U, <sup>207</sup>Pb/<sup>235</sup>U, and <sup>208</sup>Pb/<sup>232</sup>Th ratios were calculated using ICP-MS Data Cal 8.4. Following the convention of the “best age” approach to reporting U-Pb detrital zircon ages, the range in the cutoffs between reporting <sup>206</sup>Pb/<sup>238</sup>U and <sup>206</sup>Pb/<sup>207</sup>Pb ages was made so as to not split distinct age clusters between U-Pb and Pb-Pb ages (e.g., Gehrels et al., 2011). Therefore, the cutoff between <sup>206</sup>Pb/<sup>238</sup>U and <sup>206</sup>Pb/<sup>207</sup>Pb was determined by the sample and was in the range of 900–1050 Ma. Reported uncertainties for age determination of individual grains are at the 1 $\sigma$  level and reflect measurement errors only. Analyses with >10% uncertainty, >20% normal discordance, or >5% reverse discordance are not considered further. The resulting interpreted ages are shown on normalized relative age-probability diagrams. Relative age probability plots show each age and its uncertainty (for measurement error only) as a normal distribution, and sum all ages from a sample into a single curve.

### Kolmogorov-Smirnov Tests and Multidimensional Scaling

The Kolmogorov-Smirnov (K-S) statistical method is a nonparametric test for the equality of continuous one-dimensional probability distributions of two samples. The tested samples are displayed in cumulative probability diagrams, and their largest vertical difference in the plot is defined as the  $D$  value. Typically, a threshold value of  $\alpha = 0.01$  or  $0.05$  is set. That is, if the  $D$  value is  $>D_{\text{critical}}$  ( $\alpha = 0.05$ ), the null hypothesis ( $H_0$ ) that the two samples are drawn from the same population can be rejected.

The critical value  $D$  can be calculated by  $D_{\text{critical}} = 1.36 \sqrt{\frac{N_1 + N_2}{N_1 N_2}}$  for  $\alpha$

$= 0.05$ , where  $N_1$  and  $N_2$  are the number of dated zircon grains from the two samples. In this study, we dated ~100 zircon grains for each sample, and the corresponding critical value of  $D_{\text{critical}}$  is 0.192. The  $P$  value in K-S tests denotes the threshold of the significance level at which fail to reject the null hypothesis ( $H_0$ ). The  $P$  value must be greater than 0.05 for it to be statistically permissible to interpret two samples as being derived from the same parent distribution at the 95% confidence level.

Multidimensional scaling (MDS) of detrital zircon data attempts to transform the dissimilarity between samples to distance in  $N$ -dimensional space. Samples are represented as a point, typically in two-dimensional

or three-dimensional Cartesian space, with greater distances between two points indicating greater dissimilarity between the two U-Pb age distributions. The transformation is accomplished by iterative rearrangement of the data in  $N$ -dimensional space to minimize the misfit (“stress”) between the calculated distances and the disparities, which is calculated as:

$$\left( \frac{\sum_{ij} (f(x_{ij}) - d_{ij})^2}{\sum_{ij} d_{ij}^2} \right)^{0.5} \quad (1)$$

where  $d_{ij}$  is the distance and  $f(x_{ij})$  is the disparity between the  $i$ th and  $j$ th element. Disparity is calculated as a linear (1:1) transformation of the input dissimilarities. In a low-stress MDS plot, the distances between points linearly correlate with the dissimilarities between samples. Metric nonclassical MDS was implemented using an in-house MATLAB algorithm. Dissimilarity was calculated as the complement of the Cross-correlation coefficient:  $1 - R^2$  (Saylor and Sundell, 2016).

### Apatite Fission-Track Thermochronology

Apatite fission-track (AFT) thermochronology is based on crystal-lattice damage manifested as linear tracks resulting from the constant-rate spontaneous fission of trace levels of <sup>238</sup>U in apatite grains. Fission tracks in apatite are incompletely annealed over the temperature range of ~60–110 °C, which is termed the partial annealing zone (Gleadow, 1981; Ketchum et al., 2007). The decrease in temperature of a sample through the partial annealing zone as a function of time is reflected by the distribution of lengths for the partially annealed tracks. We conducted AFT analyses from 12 samples determine the low-temperature thermal history of the central and eastern segments of the Eastern Kunlun Range. This information in turn permits us to infer the onset of exhumation across this range.

Fission-track ages were measured using the external detector method (Gleadow, 1981) and calculated using the zeta calibration method (Hurford and Green, 1983). Ages were calculated using the Zeta calibration method (Hurford and Green, 1983; Hurford, 1990) with a Zeta value of  $322.1 \pm 3.6$  (1 s). Apatite grains were separated from ~5-kg materials for each sample using standard mineral separation techniques. Polished grain mounts were prepared and etched to reveal spontaneous fission tracks. Apatite grain mounts were etched in 6.6% HNO<sub>3</sub> at 25 °C for 30 s. All samples were irradiated at the China Institute of Atomic Energy reactor facility, Beijing. Low-U muscovite external detectors covering apatite grain mounts were etched in 40% hydrofluoric acid at 25 °C for 20 min to reveal induced fission tracks. In order to increase the number of observable horizontal confined tracks, the samples were exposed to <sup>252</sup>Cf (Donelick and Miller, 1991). Horizontal confined fission-track lengths (e.g., Laslett et al., 1987; Gleadow et al., 1986) were measured only in prismatic apatite crystals because of the anisotropy of annealing of fission tracks in apatite (Green et al., 1986).

## RESULTS

### U-Pb Detrital Zircon Geochronology

#### Jurassic-Cretaceous Strata Samples

The youngest zircon ages from the middle and upper sections of Jurassic Yanshiping Group sandstones (samples WC072817-2A and WC072817-3 in Figs. 3, 4A, and 4C) constrain the maximum depositional ages of these samples to ca. 165 Ma ( $n = 3$ ) and ca. 159 Ma ( $n = 3$ ), respectively (Figs. 6C and 6E). These ages are consistent with the Middle and Late Jurassic ages previously assigned to these strata (e.g., Leeder et al., 1988; C.S. Wang et al., 2001a; Fang et al., 2016). Sample



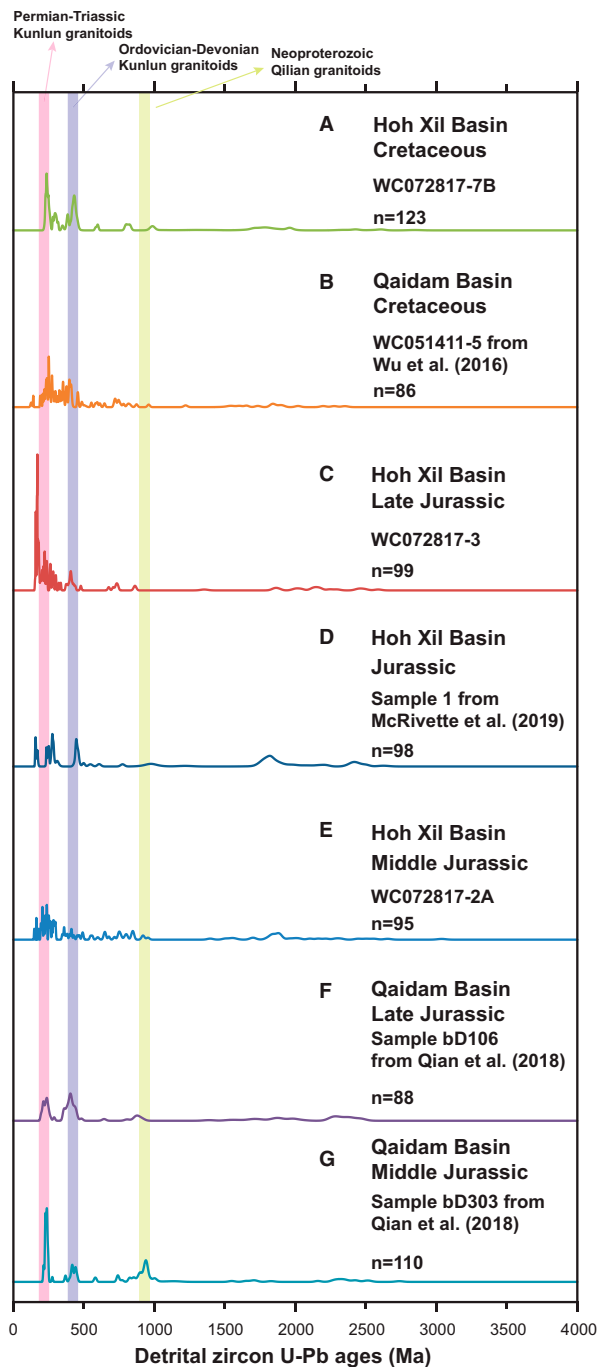


**Figure 6.** Normalized relative probability plots of detrital zircon U-Pb ages from the Jurassic-Cretaceous sediments from this study, McRivette et al. (2019), C. Wu et al. (2016a), and Qian et al. (2018). See Table S4 for detailed data.

WC072817-2A has 200–288 Ma (ca. 210 Ma peak) and 360–490 Ma (ca. 410 Ma peak) zircon populations (Fig. 6E). The largest age cluster is in the early Proterozoic between 1750 Ma and 1950 Ma with a peak at ca. 1888 Ma. Minor age clusters occur at ca. 165 Ma, ca. 361 Ma, 755–855 Ma, and 2350–2550 Ma (Fig. 6E). Zircons from sample WC072817-3 have age populations at 157–230 Ma (ca. 172 Ma peak) and 380–480 Ma (ca. 410 Ma peak) (Fig. 6C). Minor age populations also occur at ca. 224 Ma and 2050–2550 Ma (Fig. 6C). The age spectrums of a Jurassic

sandstone sample from McRivette et al. (2019) and two Qaidam basin Jurassic samples from Qian et al. (2018) are shown as Figures 6D, 6F, and 6G, respectively.

The dominant age population of the Cretaceous sandstone sample WC072817-7B within the Hoh Xil basin (Figs. 3, 4D) is at 220–460 Ma with peaks of ca. 236 Ma and ca. 429 Ma (Fig. 6A). Two other significant populations are at 797–1000 Ma (ca. 822 Ma peak) and 1600–2100 Ma (broad peak centered at ca. 1834 Ma) (Fig. 6A). Minor age populations exist at 1000–1500 Ma and 2300–2800 Ma (Fig. 6A). One sample was collected from fine-grained arkosic arenite on the southwestern margin Qaidam basin (C. Wu et al., 2016a; sample WC051411-5). C. Wu et al. (2016a) interpreted the Cretaceous unit, from which the sample was collected, to have been deposited in a fluvial setting based on their sedimentary textures and structures observed in the field. The U-Pb dating of detrital zircon analysis is shown as Figure 6B.

#### **Cenozoic Samples from Hoh Xil Basin**

The dominant zircon-age population of Fenghuoshan Group sandstone sample WC072817-7A (Figs. 3, 4D, and 4E) is at 390–480 Ma (Fig. 7G). Two other significant populations are at 210–300 Ma and 1600–2100 Ma (broad ca. 1840 Ma peak) (Fig. 7G). Minor age populations exist at 300–390 Ma, 750–850 Ma, 900–1000 Ma, ca. 1430 Ma, and ca. 2.5 Ga (Fig. 7G). The dominant age population of the Fenghuoshan Group sandstone from McRivette et al. (2019) is shown as Figure 7H. The dominant age populations of the Eocene Tuotuohe Group sandstone sample WC072817-6 (Figs. 3 and 5F) are at 160–280 Ma and 380–490 Ma (Fig. 7F). Two other significant populations are at 560–670 Ma (ca. 625 Ma peak) and 710–965 Ma (ca. 850 Ma peak) (Fig. 7F). Minor age populations exist at ca. 1.5–2.5 Ga with two broad peaks centered at ca. 1.8 Ga and ca. 2.5 Ga (Fig. 7F).

The dominant zircon-age populations of Oligocene Yaxicuo Group sandstone sample WC072717-3 are 168–300 Ma and 375–485 Ma (Fig. 7D). Two other significant populations are at 700–850 Ma (720 Ma peak) and 1.5–2.1 Ga (two broad ca. 1.58 Ga and ca. 1.8 Ga peaks) (Fig. 7D). Minor age populations exist at 950–1200 Ma, 1300–1400 Ma, and ca. 2542 Ma (Fig. 7D). The dominant zircon-age population of another Yaxicuo Group sandstone (sample WC072817-1) is 64–300 Ma, with peaks of ca. 66 Ma, ca. 164 Ma and ca. 253 Ma (Fig. 7E). Two other minor populations are at 350–480 Ma and 2.0–2.55 Ga (Fig. 7E).

Four zircon-age populations were observed in the Miocene Wudaoliang Group sample WC072717-1 (Figs. 3 and 4H): 220–320 Ma, with two peaks at ca. 248 Ma and ca. 310 Ma, 400–500 Ma (ca. 434 Ma peak), Neoproterozoic ages peaking at ca. 907 Ma, and Paleoproterozoic ages peaking at ca. 1836 Ma (Fig. 7A). Several grains also yielded ca. 2.5 Ga ages. Sample WC072717-1 yielded a single ca. 28 Ma zircon grain, and although this value is not a robust estimate of the maximum depositional age because it is based only one zircon analysis (Fig. 7A). McRivette et al. (2019) collected two sandstone samples from lower and upper sections of the early Miocene Wudaoliang Group and three age populations are evident for both samples (Figs. 7B and 7C) that is consistent with our age results.

#### **Cenozoic Eastern Kunlun Range Samples**

The inferred Neogene-age sandstone sample WC072917-2A is a medium-grained red sandstone whereas sample WC072917-2B is a medium-grained gray-brown sandstone (Fig. 4J). The majority of zircons of sample WC072917-2A comprise two main populations: 210–290 Ma (ca. 240 Ma peak) and 390–470 Ma (ca. 428 Ma peak) (Fig. 8A). A smaller broad peak is defined by zircons with middle Proterozoic ages at 900–1090 Ma (Fig. 8A). There are several zircon grains with ages

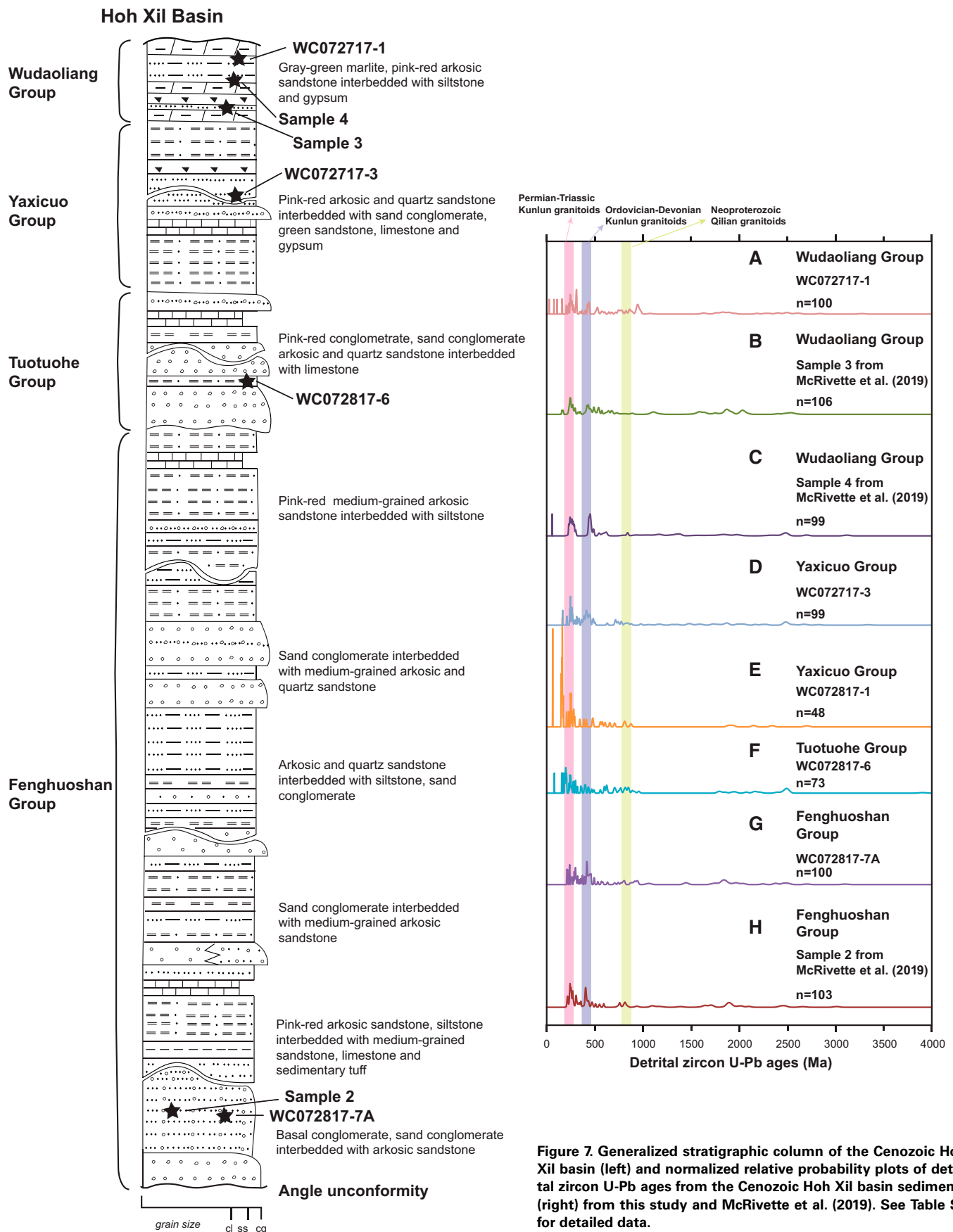


**Figure 7.** Generalized stratigraphic column of the Cenozoic Hoh Xil basin (left) and normalized relative probability plots of detrital zircon U-Pb ages from the Cenozoic Hoh Xil basin sediments (right) from this study and McRivette et al. (2019). See Table S4 for detailed data.

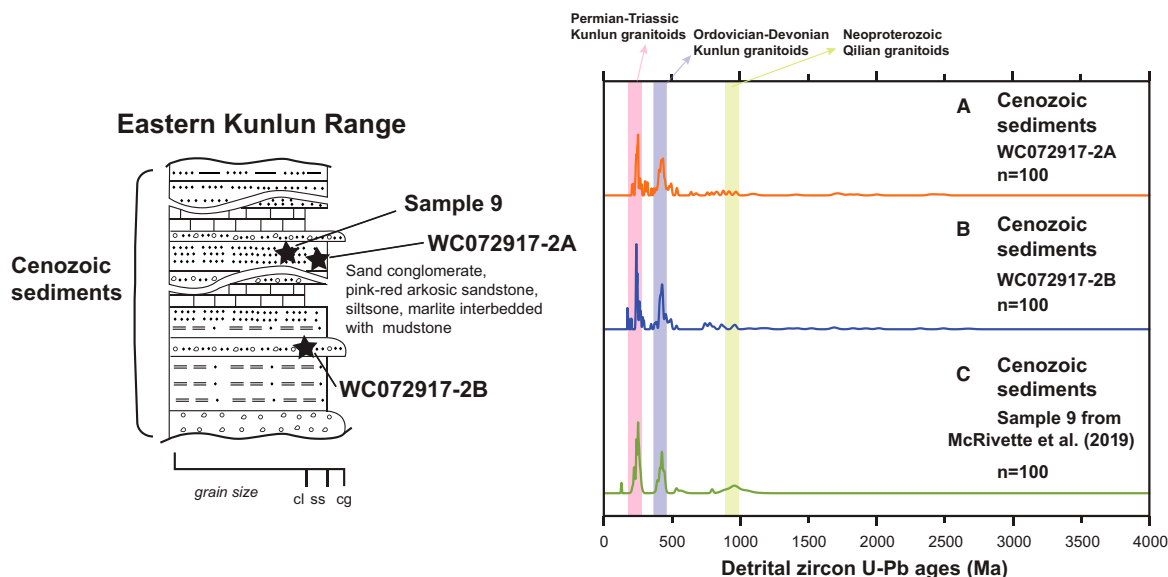


**Figure 8. Generalized stratigraphic column of the Cenozoic Eastern Kunlun sediments (left) and normalized relative probability plots of detrital zircon U-Pb ages from the Eastern Kunlun Range Cenozoic sediments (right) from this study and McRivette et al. (2019). See Table S4 for detailed data.**

between ca. 1.5 Ga and ca. 2.5 Ga (Fig. 8A). The majority of zircons of sample WC072917-2B comprise two main populations: 210–290 Ma (ca. 240 Ma peak) and 390–470 Ma (ca. 430 Ma peak) (Fig. 8B). There are numerous Neoproterozoic zircons and several grains with ages between ca. 1.5 Ga and ca. 2.5 Ga (Fig. 8B). McRivette et al. (2019) present zircon ages from an inferred Neogene-age sandstone sample from an intermontane basin within the Eastern Kunlun Range, it shows similar age populations (Fig. 8C).

### Cenozoic Samples from Qaidam Basin

Zircon ages from the Lower Xiaganchaigou Formation sandstone sample 5 (Figs. 3, 4I, and 9F) from McRivette et al. (2019) are clustered at 210–290 Ma and 370–480 Ma (Fig. 9F). Numerous ages extend from the middle to late Proterozoic, and smaller age populations are also present at 1.8–2.0 Ga and ca. 2.5 Ga (Fig. 9F). Cheng et al. (2016) reported the zircon ages of Lower Xiaganchaigou Formation sandstone from the Huatugou section within the northwest Qaidam basin that range from ca. 2660 Ma to ca. 180 Ma, with two prominent peaks at ca. 430 Ma and ca. 260 Ma. Over 65% of the detrital zircon ages for the Upper Xiaganchaigou Formation sandstone sample WC072417-9 (Figs. 3 and 4K) are <500 Ma and comprise two age populations at 350–500 Ma and 220–280 Ma (Fig. 9E). The remaining detrital zircon ages are widely scattered throughout the Proterozoic, with a minor ca. 872 Ma peak, and extend into the Middle to Late Archean (Fig. 9E).

Over 85% of the detrital zircon ages for the late Oligocene Shangganchaigou Formation (sample 6 in Figs. 3 and 9D) from McRivette et al. (2019) are <500 Ma and comprise two age populations at 350–500 Ma and 220–280 Ma (Fig. 9D). A few ages fall between the two age populations. The remaining detrital zircon ages are widely scattered throughout the Proterozoic and extend into the Middle to Late Archean (Fig. 9D). Over 85% of the detrital zircon ages for the Xiayoushashan Formation sandstone sample WC100310-2A (Figs. 3 and 4L) are <500 Ma and comprise two age populations at 220–280 Ma and 350–500 Ma (Fig. 9C). Zircon grains analyzed from the Xiayoushashan Formation sandstone within the Huatugou section by Cheng et al. (2016) provided ages ranging from ca.

2380 Ma to ca. 235 Ma, with a small peak at ca. 260 Ma, a major peak at ca. 400 Ma, and a subpeak at ca. 960 Ma.

Most zircons in the late Miocene Shangyoushashan Formation sandstone sample (Fig. 3) from McRivette et al. (2019) are of Paleozoic and Mesozoic ages, defining two age groups at 250–290 Ma and 395–510 Ma (Fig. 9B). The majority of the older zircon ages are evenly distributed between 825 Ma and 1240 Ma (Fig. 9B). Cheng et al. (2016) reported two Shangyoushashan Formation sandstones (samples SZG2 and CSL4) within the Huatugou section. U-Pb zircon ages of sample SZG2 are between ca. 2020 Ma and ca. 235 Ma with two peaks at ca. 440 Ma and ca. 250 Ma. Some additional ages (less than 20%) are spread between ca. 1990 Ma and ca. 520 Ma, with a smaller population at ca. 870 Ma. Analyses from sample CSL4 yield ages between ca. 2378 Ma and ca. 235 Ma, with three peaks at ca. 880 Ma, ca. 430 Ma, and ca. 220 Ma.

Detrital zircon ages of the Pliocene Shizigou Formation sandstone sample (Fig. 3) from McRivette et al. (2019) are also primarily <500 Ma, with a dominant cluster at 375–480 Ma (ca. 436 Ma peak) and a smaller population at 225–290 Ma (ca. 270 Ma peak) (Fig. 9A). Older zircon ages are scattered throughout the Proterozoic. Cheng et al. (2016) reported zircon analyses of a Shizigou Formation sandstone from the Huatugou section within the Qaidam basin with three zircon-age peaks at ca. 890 Ma, ca. 430 Ma, and ca. 240 Ma.

Kolmogorov-Smirnov Tests and Multidimensional Scaling Tables 1A and 1B display comparison of age spectra of samples from Jurassic-Cretaceous and Cenozoic strata, respectively. The large  $P$  values (i.e., >0.05) imply that the age spectra of samples WC051411-5 and bD106 may have been drawn from the same parent population as sample WC072817-7B (Table 1A). However, the  $D$  value between the age spectra of the sample WC072817-7B and that of samples WC051411-5 and bD106 are only 0.145 and 0.164 (Table 1A), respectively, which are < $D_{\text{critical}}$  ( $\alpha = 0.05$ ). The large  $P$  values (i.e., >0.05) imply that the age spectra of samples bD106, sample 1, and bD303 may have been drawn from the same parent population as sample WC072817-2A (Table 1A). In contrast, the  $D$  value between the age spectra of the WC072817-2A and that of bD106 and bD303 are only 0.140 and 0.129 (Table 1A), respectively, which are < $D_{\text{critical}}$  ( $\alpha = 0.05$ ).

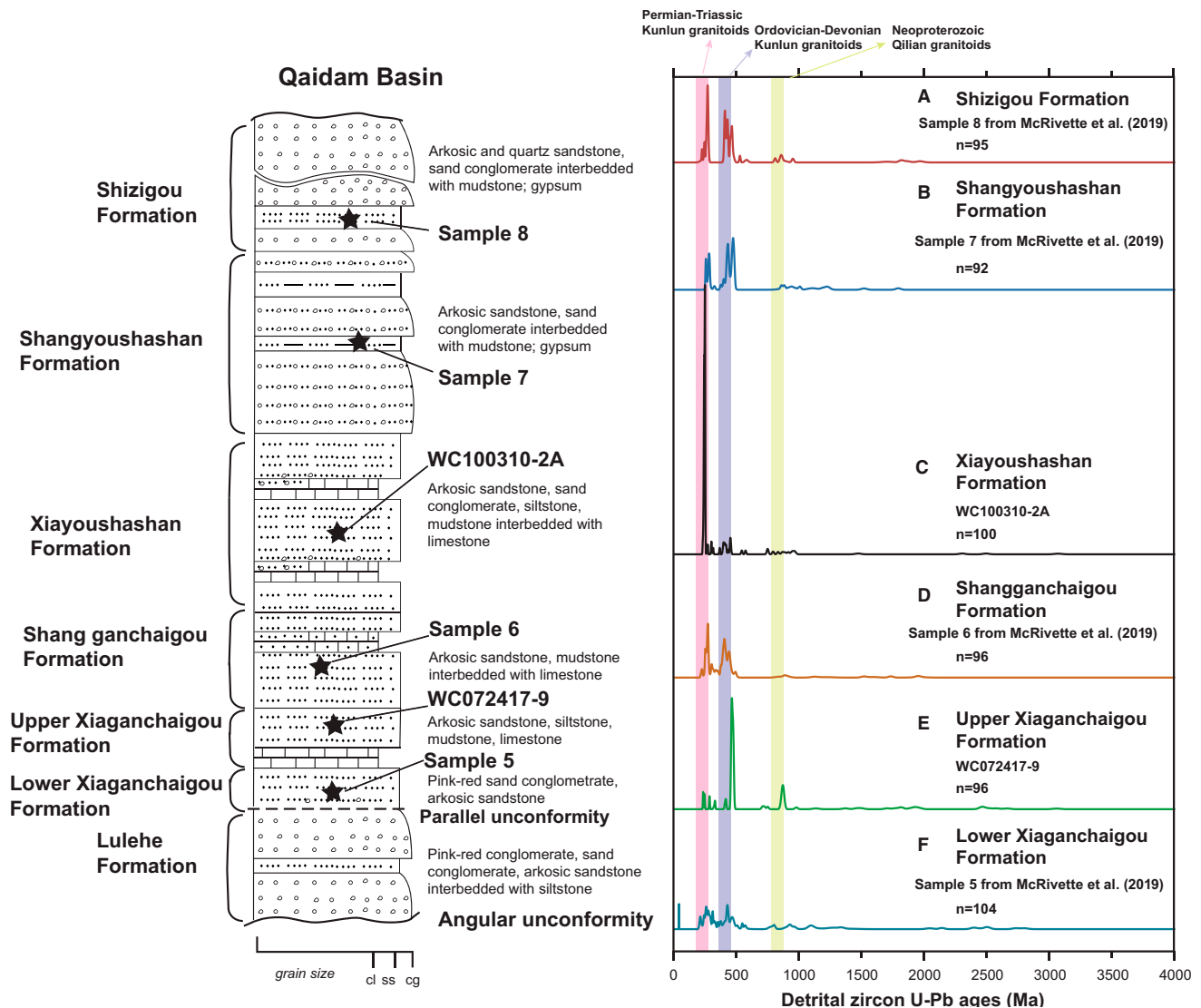


**Figure 9.** Generalized stratigraphic column of the Cenozoic Qaidam basin (left) and normalized relative probability plots of detrital zircon U-Pb ages from the Qaidam basin Cenozoic sediments (right) from this study and McRivette et al. (2019). See Table S4 for detailed data.

The large  $P$  values (i.e.,  $>0.05$ ) imply that the age spectra of Tuotuohe Group (WC072817-6), Yaxicuo Group (WC072817-1 and WC072717-3), Wudaoliang Group (i.e., WC072717-1, sample 3 and sample 4), Cenozoic Eastern Kunlun sediments (i.e., WC072917-2A, WC072917-2B, and sample 9), and Lower Xiaganchaigou Formation (sample 5) samples may have been drawn from the same parent population as the Fenghuoshan Group sandstone samples (i.e., WC072817-7A and sample 2) (Table 1B). The  $D$  values between the age spectra of the Fenghuoshan Group sample and that of these above samples are  $>D_{\text{critical}}$  ( $\alpha = 0.05$ ) (Table 1B). The samples from Cenozoic Hoh Xil basin sediments, Cenozoic Eastern Kunlun sediments, and Lower Xiaganchaigou Formation sandstone may have been drawn from the same parent function as Wudaoliang Group sandstone samples as supported by K-S test results with large  $P$  values (i.e.,  $>0.05$ ). This result is also consistent with those  $D$  values (Table 1B). A K-S comparison of the zircon-age spectra of Fenghuoshan Group, Wudaoliang Group, and Cenozoic Qaidam basin sandstone samples (i.e., sample 5, sample 6, sample 7, and sample 8) may imply that they were drawn from the

sample parent population as Cenozoic Eastern Kunlun sediments as evidenced by the large  $P$  values (i.e.,  $>0.05$ ), which is consistent with the results of  $D$  values (Table 1B).

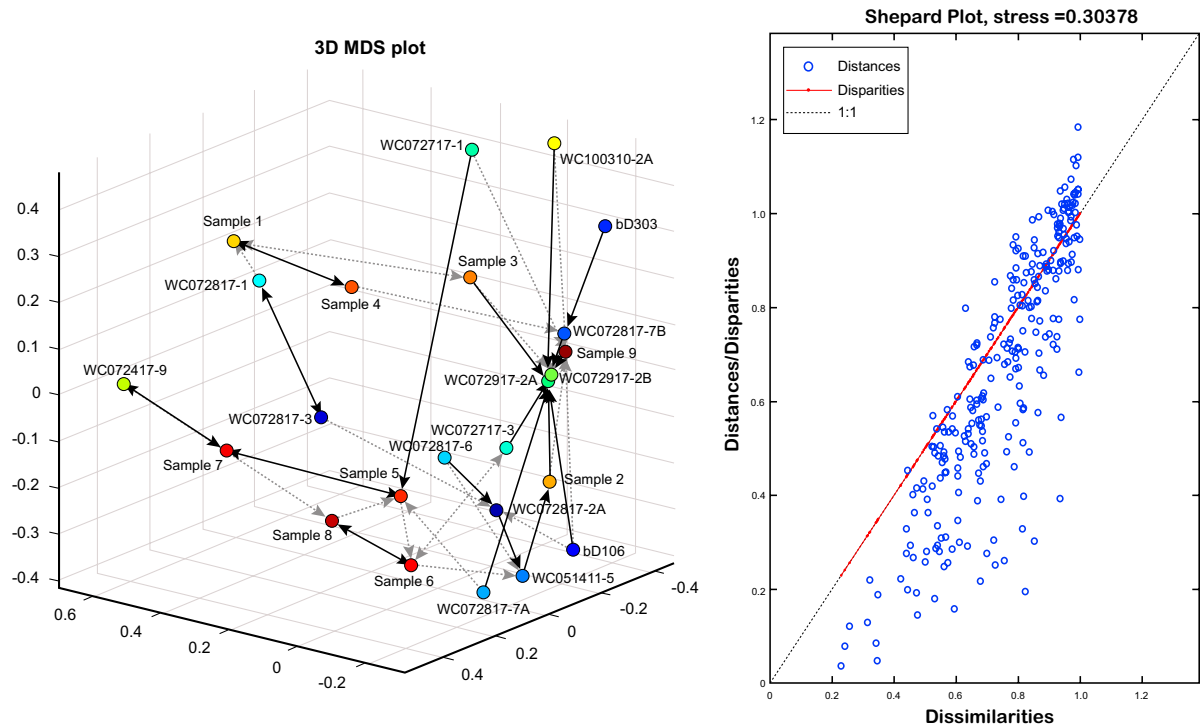
In the three-dimensional MDS plot (left panel in Fig. 10), the black solid lines and the gray dashed lines point from each sample to its closest neighbor and second closest neighbor respectively. The Shepard plot (right panel in Fig. 10) shows the distances in the MDS that represent dissimilarities between the data sets well (stress is low, 0.30378). The MDS shows that, for all our analyzed samples, there is a systematic similarity in sediment provenance between Jurassic Qaidam basin samples (bd106 and bd303), Cretaceous Hoh Xil sandstone sample WC072817-7B, Cenozoic Hoh Xil basin samples, and Cenozoic Eastern Kunlun sediments (i.e., WC072917-2A, WC072917-2B, and sample 9) (Fig. 10). The closest neighbor of the Cenozoic Hoh Xil basin samples and Jurassic-Cretaceous Qaidam sandstone samples is the Jurassic Hoh Xil sandstone samples (Fig. 10). The closest neighbor of the Qaidam Miocene-Pliocene strata and Hoh Xil Wudaoliang Group sandstone samples are the Qaidam Eocene-Oligocene samples (Fig. 10).

TABLE 1. *P* AND *D* VALUES USED IN TWO-SAMPLE KOLMOGOROV-SMIRNOV TEST RESULTS FOR JURASSIC-CRETACEOUS (A) AND CENOZOIC (B) SEDIMENTS

<b>A</b>		(7E)	(7C)	(7A)	(7B)	(7D)	(7F)	(7G)										
<i>P</i> -value	<i>D</i> -value																	
(7E) WC072817-2A	–	0.000	0.005	0.018	<b>0.096</b>	<b>0.510</b>	<b>0.195</b>											
(7C) WC072817-3	0.296	–	0.000	0.000	0.000	0.000	0.000											
(7A) WC072817-7B	0.232	0.391	–	<b>0.209</b>	0.001	<b>0.125</b>	0.017											
(7B) WC051411-5	0.220	0.326	0.145	–	0.000	0.008	0.001											
(7D) Sample 1	0.192	0.419	0.297	0.357	–	<b>0.089</b>	0.000											
(7F) bD106	0.120	0.391	0.164	0.245	0.199	–	0.046											
(7G) bD303	0.149	0.359	0.202	0.277	0.315	0.196	–											

<b>B</b>		(8G)	(8H)	(8F)	(8E)	(8D)	(8A)	(8B)	(8C)	(9A)	(9B)	(9C)	(10F)	(10E)	(10D)	(10C)	(10B)	(10A)
<i>P</i> -value	<i>D</i> -value																	
(8G) WC072817-7A	–	<b>0.739</b>	<b>0.223</b>	0.000	<b>0.998</b>	<b>0.771</b>	<b>0.318</b>	<b>0.720</b>	0.004	0.021	0.001	<b>0.071</b>	0.000	0.000	0.000	0.003	0.001	
(8H) Sample 2	0.106	–	<b>0.299</b>	0.000	<b>0.890</b>	<b>0.719</b>	<b>0.116</b>	<b>0.358</b>	0.033	<b>0.070</b>	0.002	<b>0.187</b>	0.000	0.000	0.000	0.015	0.009	
(8F) WC072817-6	0.161	0.163	–	0.002	<b>0.296</b>	<b>0.624</b>	<b>0.100</b>	<b>0.385</b>	0.001	0.007	0.005	<b>0.135</b>	0.000	0.000	0.000	0.002	0.001	
(8E) WC072817-1	0.464	0.404	0.344	–	0.000	0.000	0.000	0.000	0.000	0.000	0.001	0.000	0.000	0.000	0.000	0.000	0.000	0.000
(8D) WC072717-3	0.056	0.091	0.151	0.436	–	<b>0.494</b>	<b>0.301</b>	<b>0.878</b>	0.003	0.022	0.000	<b>0.083</b>	0.000	0.000	0.000	0.003	0.001	
(8A) WC072717-1	0.094	0.109	0.116	0.396	0.118	–	<b>0.038</b>	<b>0.552</b>	0.000	0.000	0.000	0.038	0.001	0.000	0.000	0.000	0.000	0.000
(8B) Sample 3	0.139	0.190	0.192	0.437	0.141	0.204	–	<b>0.373</b>	0.000	0.000	0.000	0.004	0.003	0.000	0.000	0.000	0.000	0.000
(8C) Sample 4	0.110	0.158	0.153	0.396	0.093	0.126	0.147	–	0.003	0.006	0.001	<b>0.148</b>	0.004	0.000	0.000	0.014	0.005	
(9A) WC072917-2A	0.250	0.224	0.294	0.396	0.254	0.330	0.359	0.287	–	<b>0.998</b>	<b>0.311</b>	<b>0.554</b>	0.000	<b>0.217</b>	0.000	<b>0.097</b>	<b>0.604</b>	
(9B) WC072917-2B	0.215	0.203	0.259	0.392	0.214	0.305	0.336	0.271	0.055	–	<b>0.529</b>	<b>0.732</b>	0.000	<b>0.114</b>	0.000	<b>0.125</b>	<b>0.531</b>	
(9C) Sample 9	0.310	0.324	0.291	0.384	0.338	0.325	0.418	0.349	0.152	0.128	–	<b>0.082</b>	0.000	0.026	0.002	0.003	0.043	
(10F) Sample 5	0.197	0.180	0.190	0.386	0.193	0.215	0.276	0.191	0.121	0.105	0.212	–	0.000	0.009	0.000	<b>0.321</b>	<b>0.174</b>	
(10E) WC072417-9	0.315	0.363	0.317	0.583	0.328	0.276	0.261	0.279	0.533	0.503	0.593	0.412	–	0.000	0.000	0.000	0.000	0.000
(10D) Sample 6	0.371	0.351	0.408	0.422	0.361	0.459	0.498	0.410	0.159	0.182	0.246	0.266	0.677	–	0.000	0.000	<b>0.236</b>	
(10C) WC100310-2A	0.557	0.486	0.398	0.422	0.537	0.495	0.534	0.502	0.421	0.413	0.298	0.507	0.691	0.544	–	0.000	0.000	
(10B) Sample 7	0.286	0.269	0.321	0.480	0.291	0.376	0.405	0.275	0.196	0.188	0.314	0.161	0.382	0.355	0.602	–	<b>0.167</b>	
(10A) Sample 8	0.323	0.293	0.359	0.427	0.327	0.399	0.451	0.314	0.127	0.135	0.250	0.194	0.539	0.180	0.548	0.202	–	



**Figure 10.** Three-dimensional multidimensional scaling (3D MDS) plot of the Mesozoic-Cenozoic Hoh Xil basin–Eastern Kunlun Range–Qaidam basin sandstone samples. Dissimilarity is based on the complement of the cross-correlation coefficient. The black solid lines and the gray dash lines in the MDS plot (left panel) point from each sample to its closest neighbor and second closest neighbor respectively.

### Apatite Fission-Track Thermochronology

We collected 11 Paleozoic granite samples for AFT analyses from the eastern (Fig. 11) and central (Fig. 12) segments of the Eastern Kunlun Range. Results of nine samples (Fig. S1) from our previous work (Chen et al., 2011) are also summarized for comparison. AFT results are listed in Table S4. Sample locations and AFT pooled ages are shown on Figure 13. AFT ages for almost all analyzed samples range between  $17 \pm 1$  Ma and  $58 \pm 3$  Ma ( $1\sigma$ ), with the exception of sample WC100110-1B, which has a significantly older AFT age of  $82 \pm 4$  Ma ( $1\sigma$ ). Because fission-track systematics in apatite are characterized by a partial annealing zone between  $\sim 60$  and  $110$  °C, AFT ages and measured fission-track length distributions can be inverted to produce compatible thermal history paths. All models were further constrained by a surface temperature of  $10$  °C. We performed inverse modeling of the AFT data using the AFTSolve software of Ketcham et al. (2000) and the kinetic annealing model for apatite of Ketcham et al. (1999). Figure 13 shows the measured track-length distributions and modeled time-temperature paths for AFT analyses in the left column and the best-fit AFT modeled history in the right column.

The AFT age results provide information about the timing of uplift of the Eastern Kunlun Range. West of the Golmud-Lhasa Highway, samples display a southward-younging trend for the onset of rapid cooling. All samples, except sample MM4-30-04-1C (Fig. S1; Chen et al., 2011), show rapid cooling through the apatite partial annealing zone after 20 Ma (Fig. 13), which is consistent with the pooled AFT ages reported above (Table S4). Sample MM4-30-04-1C (Fig. S1), collected from the northernmost margin of the Eastern Kunlun Range, cooled rapidly at ca. 50 Ma (Chen et al., 2011).

### DISCUSSION

A comparison of the Qaidam and Hoh Xil basins' stratigraphy reveals important differences in their depositional histories and topographic evolution. Qaidam basin experienced essentially continuous non-marine sedimentation in dominantly fluvial and lacustrine environments from the early Eocene through the Holocene (Yin et al., 2008b; McRivette et al., 2019). The topographic evolution of the southern edge of the Qaidam basin can be separated into three main phases (Cheng et al., 2016): (1) onset of exhumation in the Eastern Kunlun Range initiating during or possibly before the deposition of the Paleocene Lulehe Formation; (2) middle Eocene to Oligocene widening of Qaidam basin toward the south and east; and (3) a Miocene to present increase in topography of the Eastern Kunlun Range and the Altyn Tagh Ranges, progressively enclosing the Qaidam basin. This long uninterrupted history contrasts strikingly with the evolution of Hoh Xil basin, which experienced a distinct two-stage development: (1) Eocene and early Oligocene non-marine fluvial and lacustrine deposition in the Hoh Xil basin, largely similar to those existing contemporaneously in Qaidam basin; and (2) deposition of Miocene strata, characterized by lacustrine carbonate and fine-grained clastic deposits, unconformably over deformed Paleogene strata, which are only gently warped and appear to have been deposited on an extensive erosional surface (Wang et al., 2002; Wu et al., 2008).

The late Oligocene depositional hiatus in Hoh Xil basin can be attributed to deformation and uplift of the Paleogene basin sediments at this time (e.g., Liu and Wang, 2001; Wang et al., 2002). This migration has been interpreted to indicate that deformation in the Fenghuoshan region initiated as early as the early Eocene and proceeded via in-sequence development of northeast-directed thrusts (Wang et al., 2002; Zhu et

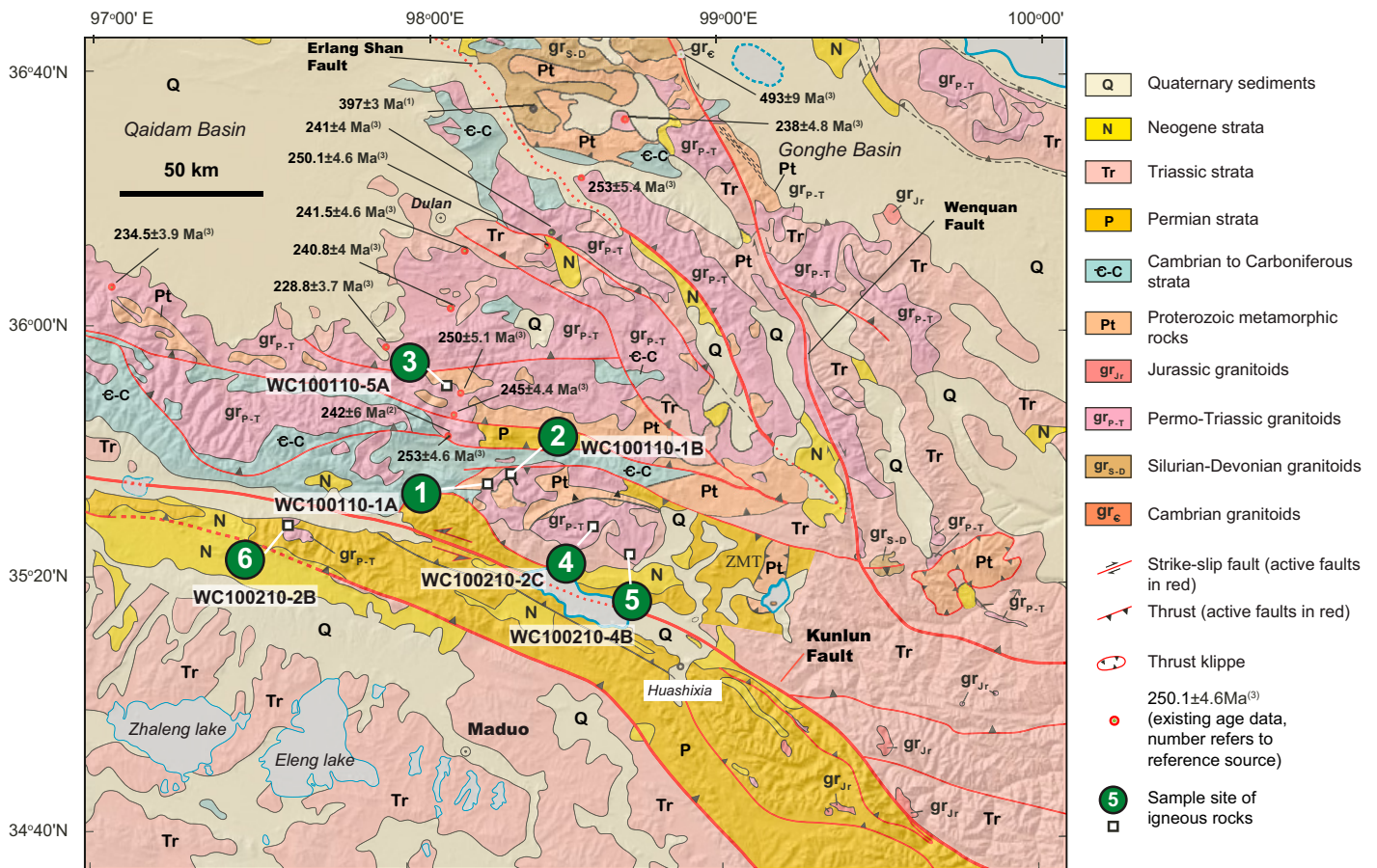


**Figure 11.** Simplified geologic map at the eastern end of the Eastern Kunlun Range, modified from C. Wu et al. (2016a). Shown in the map are locations of samples collected in this study. The map shows the sample localities with circled numbers corresponding to those listed in Table S1. ZMT—Zuimatan klippe.

al., 2006; Staisch et al., 2016). Pre-Miocene northeast-southwest crustal shortening strain across central Tibet in the Fenghuoshan area has been estimated to be ~40% (Wang et al., 2002), ~45% (>61 km shortening; Spurlin et al., 2005); and 24% (>40 km shortening; Staisch et al., 2016). Furthermore, the record of Cenozoic deformation in Qaidam basin is more complicated than in Hoh Xil basin. Paleocene to early Eocene thrusting has been documented along the northern margin of Qaidam basin, associated with the southern Qilian Shan–Nan Shan thrust belt (Yin et al., 2002, 2008a, 2008b). Interpretation of subsurface data across Qaidam basin indicates that significant deformation initiated much later along its southern margin at 29–24 Ma (Yin et al., 2008a, 2008b). Initiation of widespread uplift of the Eastern Kunlun Range in the late Oligocene, becoming increasingly more rapid, is also supported by low-temperature thermochronology (Mock et al., 1999; Jolivet et al., 2001; Wang et al., 2004; Y. Liu et al., 2005a; Yuan et al., 2006; Dai et al., 2013).

### Provenance Interpretations and Tectonic Setting of the Basins

Our inferences on the tectonic setting and depositional processes are based on the published and our new U–Pb detrital zircon dating (Figs. 6 and 14), sandstone composition analyses (Fig. 5), K–S tests (Table 1), MDS (Fig. 10), lithofacies of the sedimentary units, and field relationships. We use the relationship between detrital zircon age populations and the depositional age of the sediments to infer the tectonic setting of the basins as discussed in Cawood et al. (2012).

### Jurassic–Cretaceous Strata

For three Jurassic samples from the Southern margin of the Hoh Xil basin (Figs. 6C, 6D, and 6E), the two prominent populations with peaks at ca. 220 Ma and ca. 410 Ma correspond to the bimodal age distribution characteristic of the Kunlun batholith (e.g., C. Wu et al., 2016a). While the presence of these ages is expected in sandstones collected from Hoh Xil (e.g., Staisch et al., 2014; Li et al., 2018) and Qaidam basins (e.g., Cheng et al., 2016; Wang et al., 2017; Qian et al., 2018) flanking the Eastern Kunlun Range, their prominence in the Jurassic sandstones of the southern Hoh Xil basin–Qiangtang terrane is intriguing. Sediment supply from the north is recognized by southward paleocurrent indicators in Yanshiping Group strata (Leeder et al., 1988; Ding et al., 2013). Alternatively, the prominent Kunlun signature may also be explained by erosion of the Kunlun arc and distant transport of detrital material to the south, implying Jurassic unroofing of the Eastern Kunlun region. This hypothesis is consistent with the generally mature nature of the Yanshiping Group sediments and their “craton interior” provenance (Leeder et al., 1988; this study).

The broad detrital zircon age peaks at ca. 1870 Ma and ca. 2500 Ma in these Jurassic samples allow us to better suggest that the Jurassic sediments of the southern Hoh Xil basin–Qiangtang terrane were at least partially sourced from the Triassic flysch sequence to the north (e.g., Bruguier et al., 1997; Weislogel et al., 2006; Weislogel, 2008; Enkelmann et al., 2007; Ding et al., 2013). Furthermore, it is likely that the Jurassic sediments were derived mostly from recycling of strata in the north portion

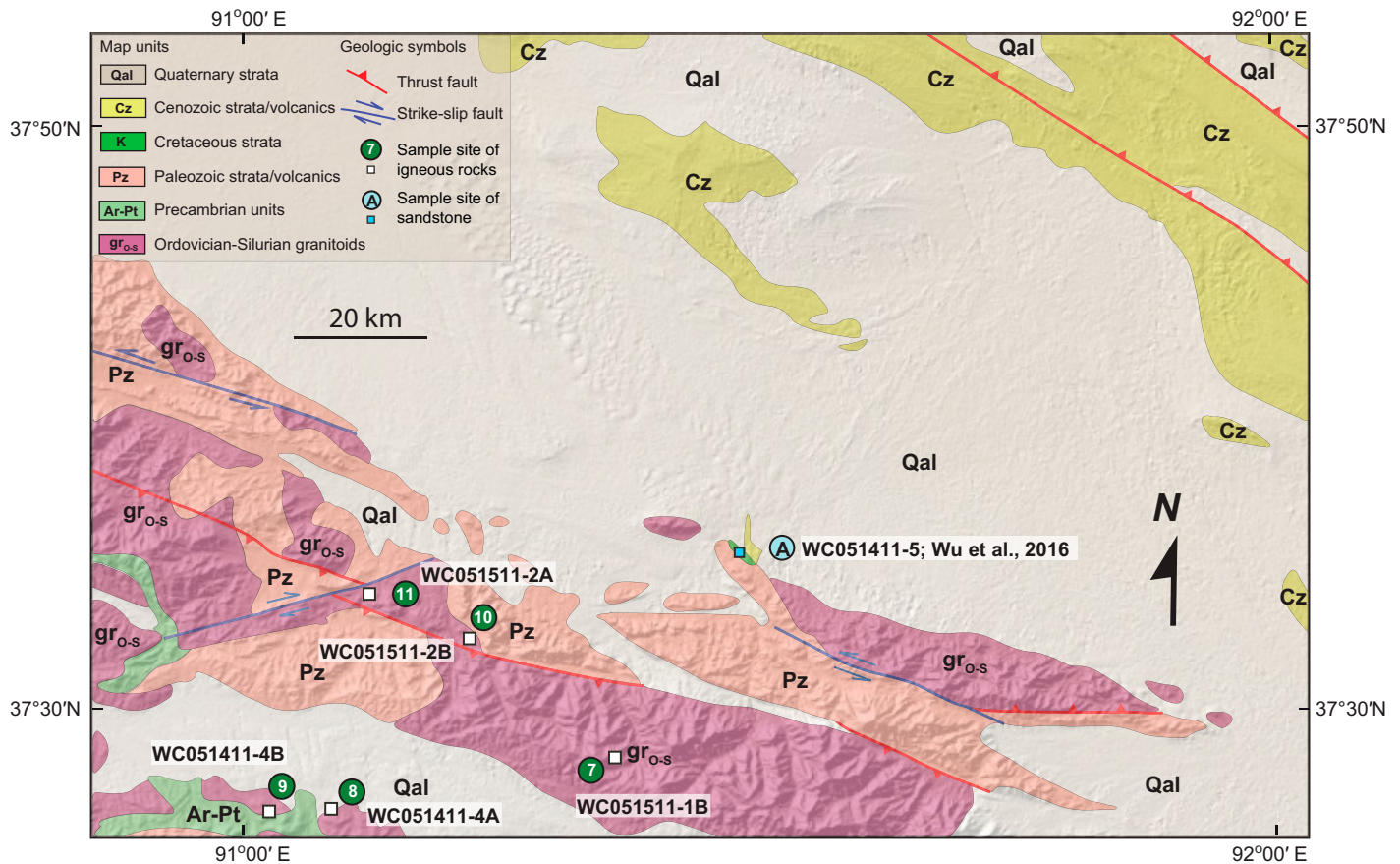


**Figure 12. Geological map of the westernmost Eastern Kunlun Range, modified from Wang et al. (2013). The map shows the sample localities with circled numbers corresponding to those listed in Table S1.**

of the Songpan-Ganzi terrane (McRivette et al., 2019). These recycled zircons may have been transported as far south as the southern margin of the Qiangtang terrane near the Bangong-Nujiang suture zone (Fig. 1), as indicated by detrital zircon results sediments located near the suture (Leier et al., 2007). However, the Mesozoic ages with ca. 170 Ma peak from the Jurassic samples do not clearly match reported geochronologic data from any potential source regions north of the central Qiangtang terrane. Granitoids exposed in association with crystalline basement along the Bangong-Nujiang suture zone have been dated to ca. 170–185 Ma (Guynn et al., 2006), suggesting that this inferred arc may have been the source for the youngest Mesozoic zircons identified as a result of north-dipping subduction of oceanic crust prior to the collision of the Lhasa and Qiangtang terranes (Guynn et al., 2006). These Jurassic samples also contain a relatively restricted cluster of Grenville ages between 750 Ma and 1220 Ma that may reflect local derivation from Paleozoic rocks exposed in the central Qiangtang terrane (Pullen et al., 2008). However, Qilian Shan also has zircons of these ages (Gehrels et al., 2003a, 2003b; Wu et al., 2017; Zuza et al., 2018), and thus, recycling of marine Paleozoic units exposed in the central Qiangtang terrane may also have been a potential source of detritus to Jurassic depositional zones to the north.

Detrital zircons from the Lower Jurassic succession are characterized solely by Neoproterozoic–Proterozoic ages (Qian et al., 2018). In marked contrast, the zircon age populations from Middle to Upper Jurassic sandstone samples contain Permian–Triassic, Late Ordovician–Devonian, Neoproterozoic, Paleoproterozoic–early Mesoproterozoic,

and Neoproterozoic–early Paleoproterozoic groups (Figs. 6F and 6G). Based on the geochronology and paleocurrent reconstructions we suggest that the Quanji massif of the southern Qilian Shan (e.g., N.S. Chen et al., 2012a; Lu, 2002; Lu et al., 2006; Gong et al., 2012; X.J. Yu et al., 2017c; Chen et al., 2013) was a discrete source area for these strata during the Early Jurassic, but the Middle–Late Jurassic sediments were sourced from an integrated drainage area including the Quanji massif (N.S. Chen et al., 2012a), Qilian Shan (e.g., Wu et al., 2017; Zuza et al., 2018), and Eastern Kunlun Range (e.g., C. Wu et al., 2016a). The marked changes in source areas between the Early and Late Jurassic provide evidence for intense deformation, uplift, and reorganization of the drainage network and source regions in the northern Qaidam region, probably related to extension during the Early Jurassic and contractional shortening starting in the Middle Jurassic.

The age spectrum of the Cretaceous sample (Fig. 6B) in the Hoh Xil basin shows two prominent populations with peaks at 236 Ma and 429 Ma, which correspond to the bimodal age distribution characteristic of the Kunlun batholith (e.g., C. Wu et al., 2016a). The broad detrital zircon age peaks at ca. 1834 Ma and ca. 822 Ma in this sample suggest that the Cretaceous sediments of the Hoh Xil basin were at least partially derived from recycling of the Triassic Songpan-Ganzi flysch sequence to the north. The age spectrum of the Cretaceous sample (Fig. 6A) suggests that its source area is local in the southern Qaidam basin, as indicated by the Kunlun arc zircon. We also note that the Cretaceous sample contains 700–800 Ma zircon grains, which are similar to the basement ages of



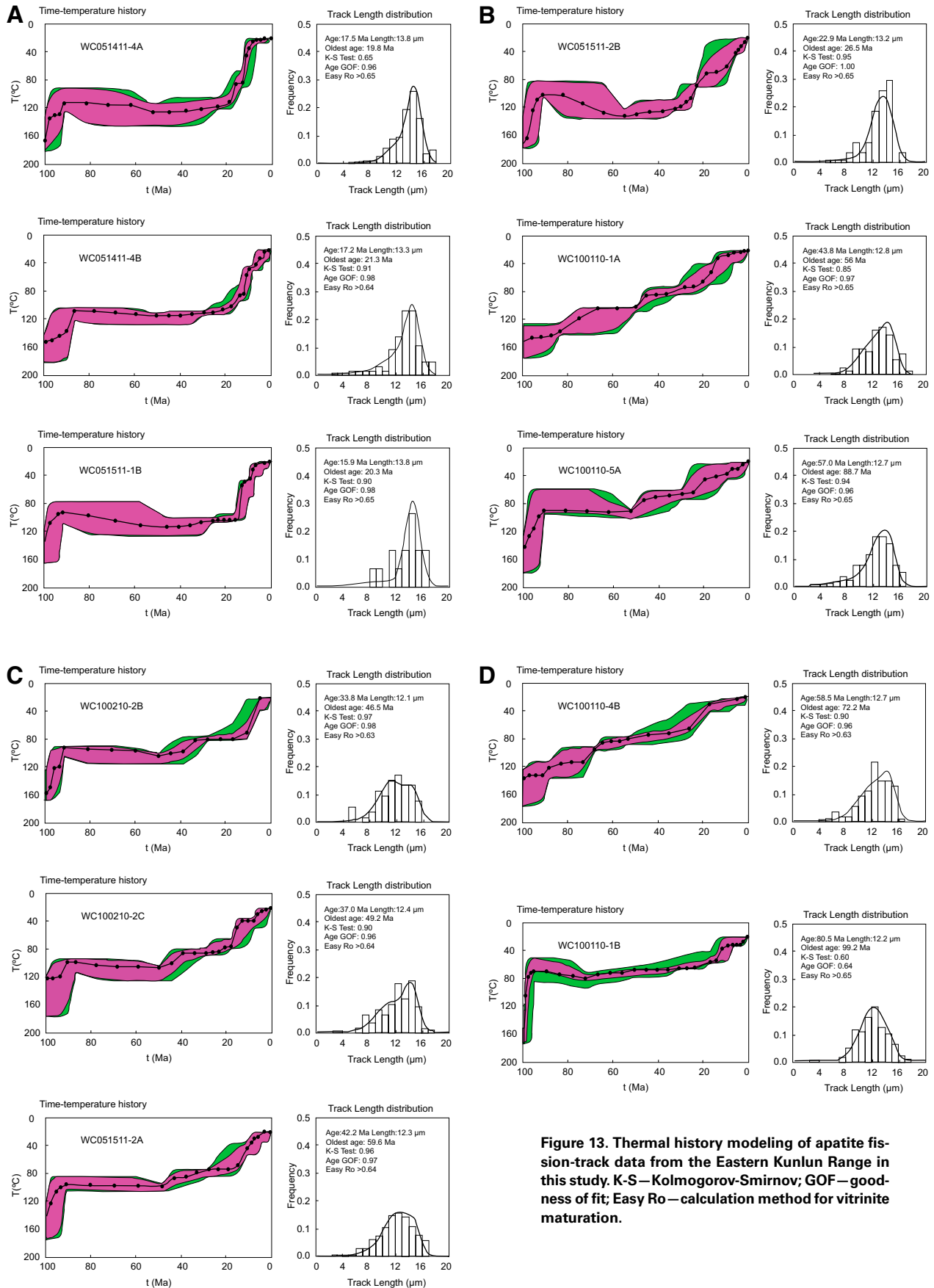


**Figure 13. Thermal history modeling of apatite fission-track data from the Eastern Kunlun Range in this study. K-S—Kolmogorov-Smirnov; GOF—goodness of fit; Easy Ro—calculation method for vitrinite maturation.**

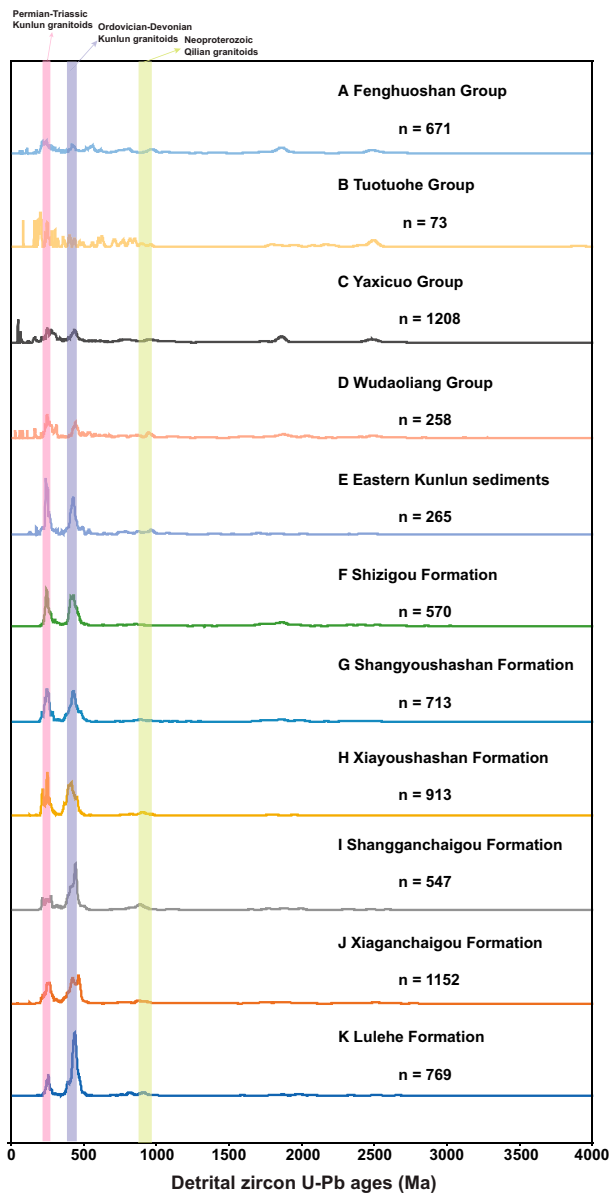


**Figure 14.** Normalized relative probability plots of detrital zircon U-Pb ages from the Cenozoic Qaidam basin, Eastern Kunlun sediments, and Hoh Xil basin from Cheng et al. (2016), Bush et al. (2016), Li et al. (2018), McRivette et al. (2019), and this study.

western South China (C. Wu et al., 2016a). Although the source areas for the Cretaceous strata are generally similar to those of the Triassic sedimentary rocks in the Eastern Kunlun area, the Cretaceous landscape must have been much more subdued than the surface topography of the same area in the Triassic. This is evident from the deposition of the mature Cretaceous arenite versus the immature Triassic arkosic sandstone in the Eastern Kunlun Range (C. Wu et al., 2016a). The abundance of quartz is likely due to chemical weathering during grain transport that removed the unstable mineral phases.

### Hoh Xil Basin

The analyzed sandstones from the Fenghuoshan, Tuotuohe, and Yaxicuo Groups exhibit two significant populations at 210–300 Ma and

390–480 Ma (Figs. 14A–14C), corresponding to the characteristic ages of the Kunlun batholith (e.g., C. Wu et al., 2016a). A third major cluster of ages spans the range 1600–2100 Ma (Figs. 7D–7G). Similar to the results for Jurassic-Cretaceous strata (Fig. 6), these age groups are consistent with significant contribution of detrital material from the Songpan-Ganzi strata upon which the Hoh Xil basin sediments are deposited on. However, this age distribution is also consistent with recycling of detritus from the thick Jurassic strata of the Qiangtang terrane to the south. This interpretation is consistent with the dominantly northward paleocurrent directions obtained for strata of the Fenghuoshan, Tuotuohe, and Yaxicuo Groups (Leeder et al., 1988; Wang et al., 2002; Cyr et al., 2005). Petrologic analyses of Paleogene sandstones point to a recycled-orogen provenance for the detrital material and a sedimentary lithology for the eroded source (Fig. 5) (Wang et al., 2002; McRivette et al., 2019; this study). While a contribution of detrital material directly from the Kunlun batholith cannot be disregarded based on the results for these sample, the batholith cannot be the sole source for the Paleocene-Oligocene strata of Hoh Xil basin (Fig. 14) (Li et al., 2018; McRivette et al., 2019).

The Miocene sandstones from the Wudaoliang Group exhibit age distributions similar to the Paleocene-Oligocene samples, with peaks at ca. 240 Ma, ca. 450 Ma, and ca. 1850 Ma (Fig. 14D). The two youngest peaks again correspond to the characteristic ages of the Kunlun batholith (e.g., C. Wu et al., 2016a). Along with smaller populations at ca. 2500 Ma, the overall distributions for the samples are consistent with derivation from recycled Triassic Songpan-Ganzi, Jurassic Qiangtang, or Hoh Xil basin Paleocene-Oligocene strata, or a combination thereof. These Miocene samples exhibit a significant number scattered Neoproterozoic detrital zircons (Fig. 14D), a pattern that is most similar to source from the Songpan-Ganzi flysch sequence. This suggests that the flysch strata were a significant contributor to the Miocene Hoh Xil strata. Thus, exclusive sourcing from the Kunlun batholith cannot account for the observed age distribution. However, unlike the Paleogene strata, limited paleocurrent data indicate southward flow for the coarse basal unit of the Wudaoliang Group (Z.F. Liu et al., 2005b). Isopach data for the Wudaoliang Group show pronounced thickening of the Miocene strata in the northern Hoh Xil basin, adjacent to the Eastern Kunlun Range (Zhu et al., 2006), suggesting that tectonic loading to the north may have contributed to basin subsidence.

The detrital zircon age results of the sandstone samples from the Fenghuoshan, Tuotuohe, and Yaxicuo Groups generally contain only minor amounts of zircons with ages close to the depositional age of the sediment. However, a significant proportion of zircon grains have ages within ca. 150 Ma of the host sediments, which may be attributed to a continental collision setting (Cawood et al., 2012). The detrital zircon ages of the early-middle Miocene Wudaoliang Group sandstones are much older than the time of sediment accumulation with <5% of grains having ages within ca. 150 Ma of the depositional age, which are interpreted as the sediments of extensional basin (Cawood et al., 2012).

### Cenozoic Eastern Kunlun Sediments

The detrital zircon age peaks at ca. 245 Ma and ca. 428 Ma in the three Neogene Eastern Kunlun Range sandstone samples (Fig. 14E) correspond to the characteristic ages of the Kunlun batholith. This is consistent with the sedimentological observations that indicate the Neogene strata are generally immature and likely derived from sources within the range proximal to the basin. A smaller peak consists of ages at 820–1100 Ma (Fig. 14E). The 820–1100 Ma age crystals may be derived from the Yidun arc (Ding et al., 2013). However, Tarim, North China, and the Qilian Shan have basement plutons with similar 820–1000 Ma ages (C. Wu et al., 2016a, 2017). One explanation for the combination of ca. 245 Ma, ca.

430 Ma, and ca. 900 Ma zircon ages is that the source region may have been the Qilian Shan (Wu et al., 2017; Zuza et al., 2018). An alternative explanation is that ca. 1.0 Ga zircons were recycled from Paleozoic and early Mesozoic sequences exposed within the Eastern Kunlun Range itself (McRivette et al., 2019). We prefer the second interpretation because it is consistent with the local derivation expected for Cenozoic Eastern Kunlun sediments. We emphasize that these units have not been adequately characterized, and future studies may test this hypothesis.

### Qaidam Basin

Normalized relative probability plots of detrital zircon ages for the late Oligocene, Miocene, and Pliocene sandstones collected from Qaidam basin (Figs. 14F–14I) all exhibit similar detrital zircon age distributions that are distinguishable from that of middle Eocene Xiaganchaigou formations sandstone samples (Fig. 14J). All samples are characterized by two prominent age populations corresponding to Kunlun batholith rocks exposed in the Eastern Kunlun Range, while Proterozoic grains, as identified in the other analyzed samples from central and northern Tibet, are not present. The absence of these ages precludes consideration of Songpan-Ganzi strata as a significant source for the late Oligocene and younger Qaidam basin sediments (Fig. 14F). Rather, the age distributions support the Kunlun batholith as the predominant source for detritus during this time. Results for the Miocene and Pliocene samples do show a slight increase in the number of grains with >700 Ma ages relative to the late Oligocene sandstone (Figs. 14F–14I). This change may reflect increased contribution of detrital material from the Qilian Shan and Altyn Tagh source regions, possibly as a result of continued left-lateral slip on the Altyn Tagh fault (Yin et al., 2002; Bush et al., 2016). The compositional trajectory displayed by Qaidam basin sandstones (Fig. 5) is consistent with our detrital zircon results that indicate younger Qaidam sediments were isolated from sedimentary sources that were important through much of the Paleogene, which is also consistent with the results of K-S testing (Table 1B) and the MDS (Fig. 10). These sources were replaced by uplifting and/or advancing thrust belts that define the modern northwestern and southern topographic boundaries of Qaidam basin (Yin et al., 2002, 2008b; Qian et al., 2018). Thus, the character of Qaidam basin sediments changed in concert with the evolution of the basin margins, with exposure of Precambrian basement rocks in Altyn Tagh Range uplifts and unroofing of voluminous igneous rocks in the Eastern Kunlun Range driving compositions toward a more mixed provenance (Zhu et al., 2018). The Eocene zircon ages were reported in early Miocene sample of Cheng et al. (2016), which is possibly derived from the Cenozoic volcanic rocks exposed on the northern margin of the Qiangtang terrane (Jolivet et al., 2003; Ding et al., 2007).

Two prominent peaks at ca. 260 Ma and ca. 430 Ma of the Xiaganchaigou Formation are characteristic of zircons ultimately derived from the Kunlun batholith (Fig. 14J). In addition, the distribution includes small populations of zircons with peaks at ca. 1.8 Ga and ca. 2.5 Ga, and several middle and late Proterozoic ages that do not constitute a clear peak. This pattern is consistent with supply of detrital material to the Eocene Qaidam basin from Songpan-Ganzi strata. Similarly, a southern derivation is suggested by the ca. 40 Ma zircon grains in the Xiaganchaigou Formation samples (Fig. 14J); potential sources for zircons of this age are all located to the south of the Eastern Kunlun Range, including scattered Cenozoic volcanic rocks and small intrusions identified in central Tibet (Roger et al., 2000; J.H. Wang et al., 2001b; Ding et al., 2003; Spurlin et al., 2005; McRivette et al., 2019) and widely exposed Paleogene igneous rocks in the Lhasa terrane (e.g., Harrison et al., 2000; Kapp et al., 2005). Furthermore, the ca. 1.8 Ga and ca. 2.5 Ga populations are also probably from the Quanji Massif in the northern Qaidam basin (e.g., Lu, 2002; Lu

et al., 2006; Gong et al., 2012; X.J. Yu et al., 2017c; Chen et al., 2013; Li et al., 2018; Zhu et al., 2018). One sample was collected from an outcrop located along the southern margin of Qaidam basin in which rare trough cross-stratification gives a mean paleocurrent direction of 358° (McRivette et al., 2019). Taken together, the detrital material deposited as part of the Xiaganchaigou Formation in Qaidam basin was transported from the south. In particular, the presence of ages corresponding to the Songpan-Ganzi flysch sequence strongly support that sedimentary transport across the Eastern Kunlun region was possible in the middle Eocene. The tectonic settings of the Xiaganchaigou Formation sandstones are possibly related to a continental collision setting (Cawood et al., 2012). The U-Pb detrital zircon ages for the Lulehe Formation support the existence of a drainage divide between the Qaidam and the Hoh Xil basins, preventing the Neoproterozoic grains of the Qiangtang terrane from reaching the Qaidam basin (Cheng et al., 2016; Bush et al., 2016) (Fig. 14K). Bush et al. (2016) suggested that the upper Lulehe Formation of the Qaidam basin was beginning to receive sediments from the Qilian Shan at this time.

### Mesozoic and Cenozoic Cooling History of the Eastern Kunlun Range

Multiple phases of Mesozoic and Cenozoic cooling and uplifting events are derived from fission-track dating and thermal history modeling of AFT ages from several plutons in the Eastern Kunlun Range. Muscovite, biotite, and K-feldspar  $^{40}\text{Ar}/^{39}\text{Ar}$  thermochronology reveal a range-wide Mesozoic cooling event that was locally overprinted by a Cenozoic cooling event at ca. 30–20 Ma (Mock et al., 1999; Y. Liu et al., 2005a; Wang et al., 2005). AFT studies suggest that the Eastern Kunlun region experienced rapid and widespread cooling at ca. 20–10 Ma, possibly related to Cenozoic range uplift in response to Indo-Asian collision (Jolivet et al., 2001; Wang et al., 2004; Y. Liu et al., 2005a; Yuan et al., 2006) (Fig. 15A). However, recent low-temperature thermochronology results have been published which suggest early Cenozoic uplift of the Eastern Kunlun Range (e.g., Clark et al., 2010; Wang et al., 2016, 2017; Liu et al., 2017b) (Fig. 15B). Our AFT results primarily reveal rapid cooling of rocks exposed in the Eastern Kunlun Range at ca. 15–20 Ma (Figs. 13 and 15A). The AFT results for sample MM4-30-04-1C indicate a rapid cooling event occurred at ca. 45 Ma, consistent with other studies of local Paleogene exhumation (e.g., Clark et al., 2010) (Fig. 15B), which may imply that contractional structures were locally developed across the forebulge, possibly having reactivated older structures (e.g., Meyers et al., 1992). This is consistent with the short-lived development of a small foreland basin which formed on the northern margin of the Eastern Kunlun Range. The forebulge may have localized the stress that led to later uplift of the Eastern Kunlun Range through development of the Kunlun transpressional system of Yin et al. (2008b). However, Cheng et al. (2016) argued for a pre-Paleocene exhumation of the Eastern Kunlun Range using detailed petrological analysis, and Dupont-Nivet et al. (2010) suggested that the Eastern Kunlun Range had already been deformed or partially uplifted before the India-Eurasia collision.

Accordingly, the Eastern Kunlun Range must have experienced a complicated Cenozoic exhumation history. Our observations of cooling and exhumation (Fig. 15A) suggest that the Eastern Kunlun Range experienced significant uplift after ca. 20 Ma. Sedimentation patterns and structural analysis of seismic sections in southern Qaidam basin suggest that initial uplift of the range began between 29 Ma and 24 Ma (Yin et al., 2008b). Although the AFT data presented here suggests slightly later exhumation (i.e., ~4 m.y. younger), we note that the Yin et al. (2008b) age is based on growth strata observed in the Qaidam basin-wide Shanganchaigou formation, which records regional deformation initiation.

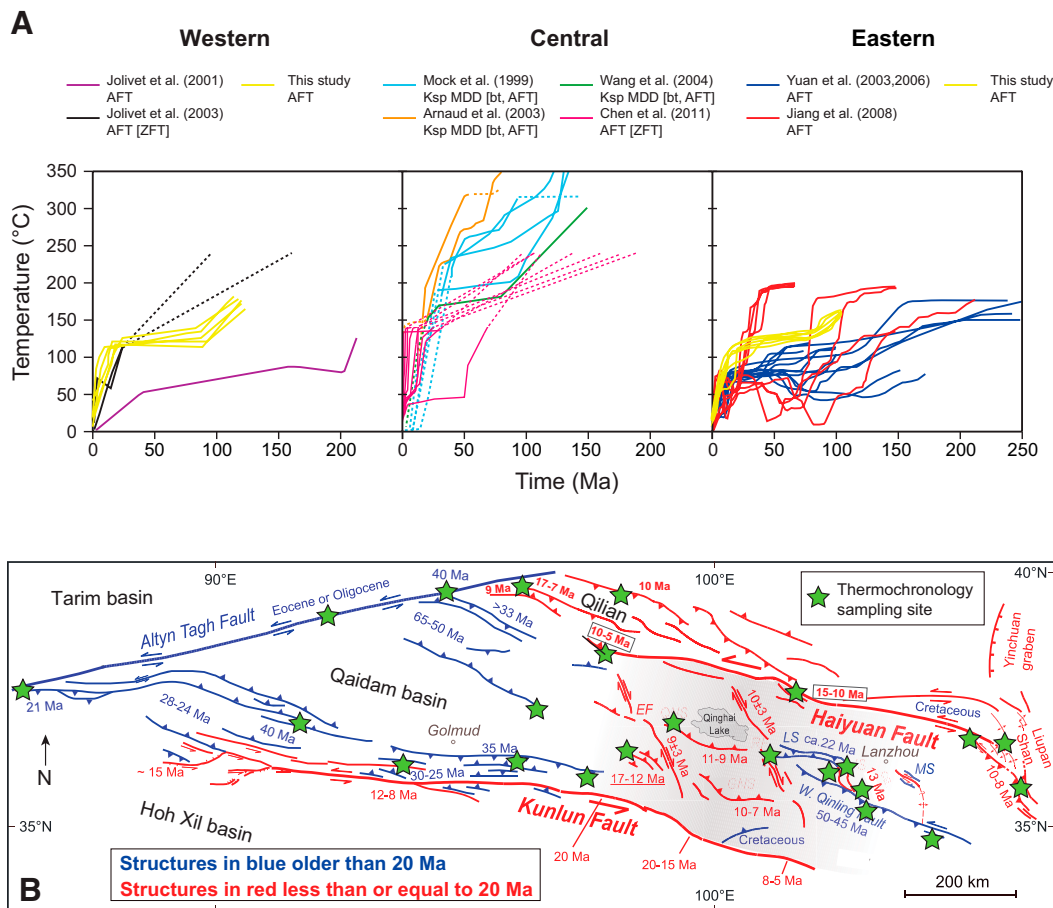


**Figure 15. (A) Compilation of modeled cooling histories from the western, central, and eastern portions of the Eastern Kunlun Range, including our new results derived from apatite fission-track (AFT) results for the western and eastern portions. Generally, results from across the range consistently show a late Cenozoic episode of rapid cooling in the Eastern Kunlun Range, which is likely in response to Indo-Asian collision-related uplift. (B) Previous thermochronology data and major Cenozoic structures from the Alтын Tagh Range, Eastern Kunlun Range, and Qilian Shan. Figure is modified from Zuzi et al. (2019), the cooling ages come from a variety of sources: e.g., Clark et al. (2010), Chen et al. (2011), Duvall et al. (2013), Wang et al. (2016), Yuan et al. (2013), Wang et al. (2017), Shi et al. (2018), Li et al. (2019), and this study. EF—Elashan Fault; LS—Laji Shan; MS—Maxian Shan; ZFT—zircon fission-track.**

The thermochronology records exhumation of relatively restricted thrust panels (Fig. 15B) that may have been uplift slightly after regional deformation initiated. Thus, we believe that these ages are compatible, showing uplift of the southern Qaidam basin and Eastern Kunlun Range in the late Oligocene–early Miocene (Fig. 15A). We note that this conclusion does not preclude the Eastern Kunlun Range to be the site of a broad structural arch prior to the Neogene. In fact, Paleogene isopach data for Qaidam basin suggest that the range was a structural high relative to its depocenters, generally located along the present-day axis of the basin (Yin et al., 2008b). The apparent lack of Eocene strata within the Eastern Kunlun Range (Pan et al., 2004) also implies that the region was a structural high. This Paleogene structural high, superposed on the Permian-Triassic Kunlun suture, may have been a forebulge induced by loading of the lithosphere by the Qilian Shan–Nan Shan thrust belt in the north and the Fenghuoshan–Nangqian thrust belt in the south. Jurassic (194–144 Ma) and Early Cretaceous (115–100 Ma) cooling and exhumation revealed by zircon fission-track ages (Chen et al., 2011) are consistent with the absence of Jurassic and Cretaceous strata across most of the study area (Fig. 15B).

### Cenozoic Basin Evolution of Central Tibet

Based on the data outlined above, we propose that the Cenozoic basins of the central and northern Tibetan plateau developed contiguously, and that the Hoh Xil and Qaidam basins originally comprised a single, large Paleo-Qaidam basin (Yin et al., 2008b). The proposed basin evolution and tectonic reconstruction are outlined below and shown in Figure 16.

In the Jurassic-Cretaceous, the Eastern Kunlun experienced a phase of unroofing, as part of widespread extension documented across north Tibet in the Mesozoic (Jolivet, 2017), which resulted in exposure and erosion of the Permian-Triassic Kunlun batholith (Fig. 16A). This hypothesis is also consistent with the results of our K-S testing (Table 1A) and MDS (Fig. 10). The unroofing of the Kunlun region in the Mesozoic supplies Kunlun Permian-Triassic batholith-age zircons rather than being derived exclusively from the Songpan-Ganzi terrane. The additional material deposited in the Yanshiping Group of the Hoh Xil basin sediments (Figs. 6C–6E) may have come from southern Qiangtang terrane and/or Qilian Shan sources, accounting for the Jurassic (ca. 150–170 Ma) and Grenville ages, respectively. The Jurassic Dameigou and Xiaomeigou formations of the Qaidam basin sediments (Figs. 6F and 6G) may have come from the Kunlun batholith. Based on our detrital zircon ages of the Cretaceous red sandstone (Fig. 6A) and its normal-fault relationship with Triassic rocks (Fig. 6E), extension-driven erosion and deposition may have continued in the Qiangtang terrane until the onset of continental collision between India and Asia. Additional material deposited in the Cretaceous strata in the southern margin of the Qaidam basin may have come from Qiangtang terrane and/or Kunlun sources, accounting for the middle Cretaceous ages (ca. 120 Ma) (Fig. 6B).

The uplift and deformation of the Jurassic-Cretaceous strata in the central-north Tibet was associated with the initiation of thrusting within the Fenghuoshan–Nangqian in the south and Qilian Shan–Nan Shan thrust belts in the north no later than the early Eocene (e.g., Leeder et al., 1988; Jolivet et al., 1999, 2001; Zhuang et al., 2011, 2018; Yuan et

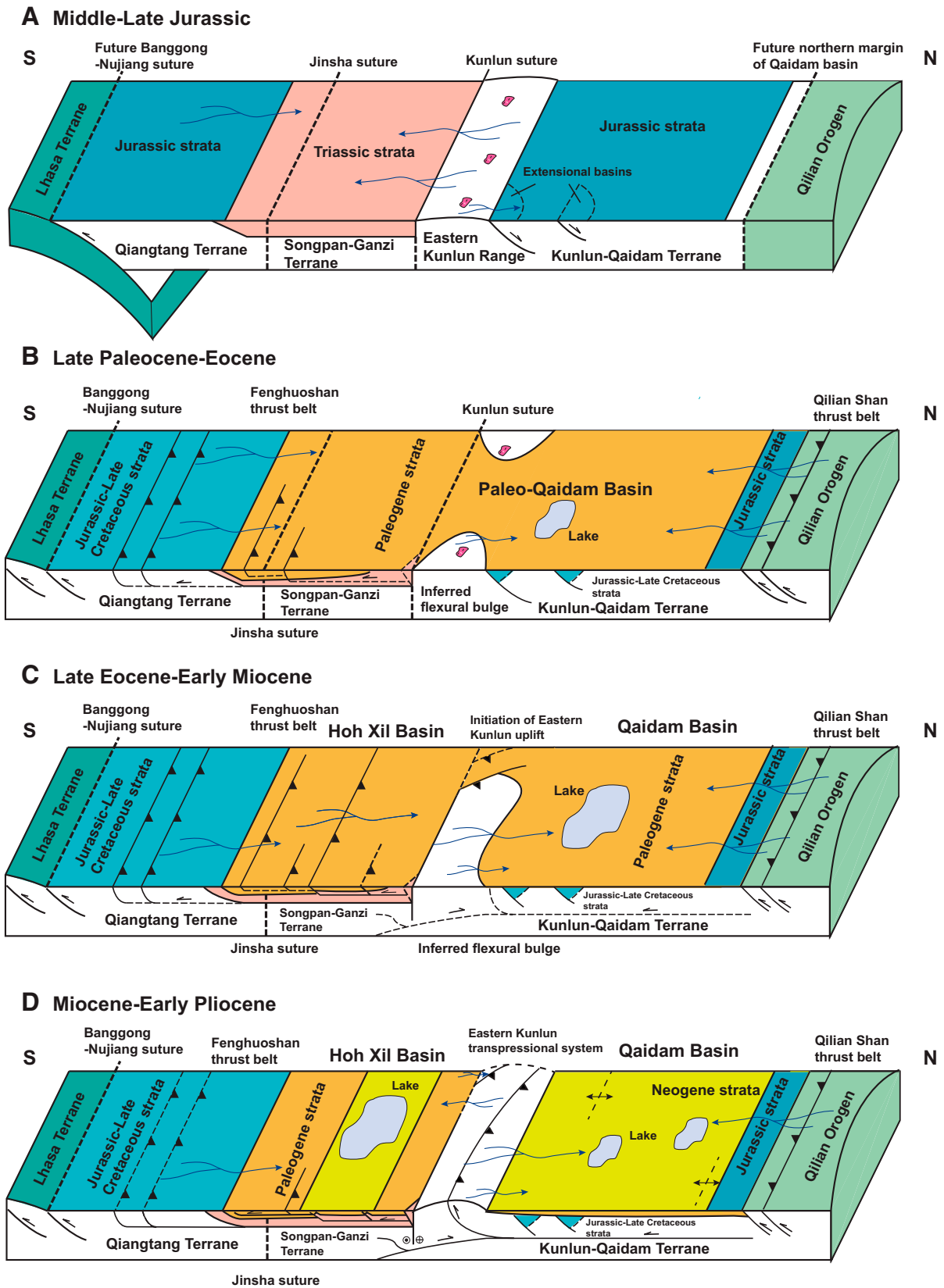


Figure 16. Block diagrams showing proposed tectonic reconstruction of the central Tibetan plateau and evolution of Cenozoic basins.

al., 2013; X.J. Yu et al., 2015, 2017d; L. Yu et al., 2017a; Horton et al., 2004; Spurlin et al., 2005; Yin et al., 2008a; Wu et al., 2011). The two thrust belts were separated by more than 500 km and the intervening topographic relative low (i.e., the Paleo-Qaidam basin) was the locus of sedimentary deposition from both sides for much of the Paleogene (Fig. 16B). Sediments were shed from Jurassic and Cretaceous strata in the south and Jurassic strata in the north into Paleo-Qaidam basin, which is consistent with paleocurrent indicators (Leeder et al., 1988; Wang et al., 2002; Cyr et al., 2005; Cheng et al., 2016). The fluvial transport systems were extensive enough to transport the material at least as far north as the present-day southern margin of Qaidam basin to be deposited as part of the early Miocene Xiaganchaigou Formation. The similar signal seen in the Adatan and Dongchaishan-Gansen sections of Cheng et al. (2016) seems to suggest that the source area for the whole southern Qaidam basin was largely homogeneous by the early Miocene. These inferences are consistent with our results of K-S testing (Table 1B) and the MDS (Fig. 10). Sedimentary material derived from the uplifting Qilian Shan–Nan Shan belt appears to have been restricted to the northern margin of Paleo-Qaidam basin. The absence of Eocene sedimentary units in the Eastern Kunlun Range, situated near the center of the Paleo-Qaidam basin, is interpreted as that thrust loading associated with the two-bounding fold-and-thrust belts (i.e., Fenghuoshan-Nangqian and Qilian Shan–Nan Shan thrust belts) may have resulted in a flexural bulge across the middle axis of this basin (Fig. 16B).

Compressive stresses resulting from the ongoing India-Eurasia collision affected the region by ca. 50 Ma and continued to be transferred farther north across Paleo-Qaidam basin to the Qilian Shan (Zuza et al., 2018) (Fig. 16C). The Triassic Anyimaqen-Kunlun-Muztagh suture may have reactivated along a zone of strain localization superposed on the inferred flexural bulge during the Miocene, which is resulted from the onset of Cenozoic uplift of the Eastern Kunlun Range (Fig. 16C) as indicated by the low-temperature thermochronologic studies discussed above (Figs. 13 and 15). This uplift may have operated as a flake tectonic system (Oxburgh, 1972), with south-directed thrusting in the Eastern Kunlun Range being fed by north-directed slip at depth (Figs. 16C and 16D). Furthermore, the northward paleoflow directions of the Miocene deposits in the eastern margin of the Qaidam basin indicate that the Eastern Kunlun Range formed a relative positive topography at this time (Cheng et al., 2016) (Fig. 16C). Rapid uplift of the Eastern Kunlun Range initiated to partition the Paleo-Qaidam basin, separate the present Qaidam basin to the north and the present Hoh Xil basin to the south (Fig. 16C). The Cenozoic uplift of the Eastern Kunlun Range is also recorded by changes in the paleocurrent directions both in the Qaidam basin (Cheng et al., 2016) and the Hoh Xil basin (Leeder et al., 1988; Wang et al., 2002; Cyr et al., 2005). In Hoh Xil basin, the northward flowing drainage systems were severely modified, and this basin transitioned from a depositional to a dominantly erosional phase, producing a widespread peneplanation surface (Wang et al., 2002). Qaidam basin received sediments from the newly uplifted Eastern Kunlun Range, as well as from the Qilian Shan to the north and/or the Altyn Tagh Range to the west (Yin et al., 2002, 2008b), which were topographic highs since the Paleocene and Oligocene as indicated by the detrital zircon data (Cheng et al., 2016; this study) (Fig. 16C).

Uplift of the Eastern Kunlun Range imparted a new tectonic load onto southern end of this range and northern margin of the Hoh Xil basin (Fig. 16D). The lacustrine carbonates of renewed sedimentation recorded in the Wudaoliang Group in Hoh Xil basin thickens toward the Eastern Kunlun Range (Liu and Wang, 2001; Zhu et al., 2006). In Qaidam basin, the Eocene zircon ages observed in an early Miocene Xiayoushshan sample of Cheng et al. (2016) is interpreted as be sourced from the Cenozoic volcanic rocks exposed on the northern margin of the Qiangtang terrane

(Jolivet et al., 2003; Ding et al., 2007). The middle and late Miocene (Shangyoushshan Formation) strata in Qaidam basin became dominated by material sourced from the Eastern Kunlun Range to the south, as suggested by the prevalence of Kunlun batholith-age zircons (Cheng et al., 2016; this study). The detrital zircon age distributions of the late Miocene–early Pliocene Shizigou Formation suggest a mixed source between the Eastern Kunlun Range to the south and the Altyn Tagh Range to the west (Cheng et al., 2016). It is important to note that the wide drainage system prevailing during the Eocene-Oligocene was not yet completely blocked, though the Eastern Kunlun Range was being increasingly rapidly uplifted, and some river systems still connected the Qaidam basin to the south (i.e., Qiangtang terrane) and west (i.e., Altyn Tagh Range) across the range (Fig. 16D).

### Implications for Tibetan Plateau Development

The potential existence of an integrated early Cenozoic Paleo-Qaidam basin has implications for the mechanisms of Tibetan plateau construction. Specifically, this wide basin (Fig. 2A) suggests that Cenozoic deformation did not progressively migrate northward following the India-Asia collision to the south as postulated in the group of continuum deformation models (e.g., England and Houseman, 1986). Instead, almost immediately after India-Asia collision, Paleocene-Eocene deformation jumped to the mechanically weak Qilian suture zone in the Qilian Shan, thus creating the northern boundary of the Paleo-Qaidam basin and the Tibetan plateau. The relatively distributed nature of active deformation in the present-day Qilian Shan argues for a weak basal detachment beneath northern Tibet that may have been assisted this early episode of deformation (Burg et al., 1994). The disintegration of this basin in the Miocene occurred as out-of-sequence thrusting as the Triassic Anyimaqen-Kunlun-Muztagh suture was reactivated during the uplift of the Eastern Kunlun Range (C. Wu et al., 2016a). Although deformation zones jump discretely across the plateau during basin formation and subsequent destruction, these patterns do not involve simple northward migration (e.g., Meyer et al., 1998; Tapponnier et al., 2001). Instead deformation exploits preexisting weaknesses, thus demonstrating the importance of mechanical anisotropy in the development of the Tibetan plateau (Kong et al., 1997; L. Chen et al., 2017b). In fact, out-of-sequence deformation is required if northern Tibet, including the Qilian Shan–Nan Shan thrust belt and Hexi Corridor foreland, has remained the northern boundary of the Himalayan-Tibetan orogen since the early Cenozoic (e.g., Clark, 2012).

Hoh Xil basin, at an elevation of ~5 km is >2 km higher than Qaidam basin (~2.8 km). If these two basins were connected in the Paleogene, there must be a viable explanation for this present-day elevation difference. Proposed models include in situ crustal thickening via crustal shortening of the Hoh Xil basin after the early Miocene (e.g., Liu and Wang, 2001; Z.F. Liu et al., 2005b; Wang et al., 2002; Wu et al., 2008; Staisch et al., 2016), flake or wedge tectonics (Oxburgh, 1972), magmatic inflation and/or thermal uplift (e.g., Molnar et al., 1993; Chen et al., 2018), and/or channel flow and lower crustal inflation (Royden, 1996; Clark and Royden, 2000).

We suggest that our observations support a combination of wedge tectonics and magmatic inflation (Chen et al., 2018) to uplift Hoh Xil basin. We do not observe any patterns of growth-strata migration that may be associated with a northward migrating topographic front due to lower-crustal flow from areas of higher topography to lower regions. Furthermore, given that the Hoh Xil basin is >2 km higher than the adjacent Qaidam basin, the channel flow process, if operating, would be expected to uplift Qaidam basin, although the strong Qaidam lithosphere may resist this process (Braitenberg et al., 2003). The cessation of Fenghuoshan

deformation in the Oligocene (Staisch et al., 2014, 2016) suggests that in situ crustal thickening was not the main driver of Hoh Xil surface uplift. The Qimen Tagh, Qaidam basin, and North Qaidam thrust systems have accommodated more Cenozoic strain than the Fenghoushan (e.g., Yin et al., 2008b; Staisch et al., 2016; Zuza et al., 2016), but are at lower elevations, which suggests crustal thickening cannot primarily lift Hoh Xil.

Neogene volcanism around Hoh Xil basin has higher La/Yb ratios than the Eocene volcanic rocks (i.e., thicker crust; Profeta et al., 2015; Farnier and Lee, 2017), and lack of Neogene volcanic rocks around Qaidam basin suggests that Neogene magmatic inflation may be at least partially responsible for uplifting Hoh Xil (Chen et al., 2018). The south-directed thrusting observed in the Eastern Kunlun Range suggests that wedge or flake tectonics is translating the Qaidam upper crust over the Eastern Kunlun Range (e.g., Yin et al., 2007a). This system may have linked with earlier Qilian Shan strain via a weak basal detachment potentially related to preexisting weaknesses associated with early Paleozoic tectonics (Burg et al., 1994; Zuza et al., 2018).

## CONCLUSIONS

A comparison of the Qaidam and Hoh Xil basins reveals important differences in their depositional histories and topographic evolution during Mesozoic-Cenozoic. The integrated results of our study of the sedimentary basins of central and northern Tibet has led to the following interpretations.

(1) Sandstone petrologic results indicate a shift from continental block to recycled-orogen provenance for Hoh Xil strata through the Cenozoic, whereas Qaidam basin continuously received sediments from recycled-orogen sources. These results are consistent with existing sedimentologic studies suggesting that Hoh Xil basin experienced two distinct stages during its evolution: a Paleogene fluvial/alluvial stage and a Neogene lacustrine stage. The Qaidam basin experienced a continuous development history during which sedimentary composition evolved in response to basin margin deformation.

(2) In Hoh Xil basin, Jurassic-Cretaceous sediments exhibit two prominent age populations at 210–290 Ma and 420–480 Ma. The Cenozoic sediments were recycled from the Jurassic rocks below that were themselves originally sourced from the Kunlun batholith. In Qaidam basin, detrital zircon results clearly distinguish the middle Eocene sandstone of the Lower and Upper Xiaganchaigou formations from the late Oligocene, Miocene, and Pliocene sandstone samples. Age characteristic of the Songpan-Ganzi terrane (ca. 1800 Ma) are recognized in Hoh Xil and Paleogene Qaidam strata, but are absent in younger Qaidam strata, which suggests emergence of a topographic barrier between the basins near the beginning of the Neogene.

(3) Our AFT data from the Eastern Kunlun Range shows that rapid cooling did not start until after ca. 20 Ma, consistent with the Paleo-Qaidam hypothesis in which the Hoh Xil and Qaidam basins were not partitioned until the beginning of the Neogene. We interpret this structural arch to be a flexural bulge induced by thrust loading of the Qilian Shan and Fenghuoshan thrust belts along the northern and southern margins of the Paleogene Paleo-Qaidam basin.

(4) An early Cenozoic Paleo-Qaidam basin implies that deformation across the Tibetan plateau did not propagate northward through time from the India-Asia collisional zone, but rather first exploited preexisting weaknesses such as in the Qilian Shan. This early thrusting established the northern margin of the plateau, and the Miocene jump in deformation to the Eastern Kunlun Range during the partitioning of the Paleo-Qaidam basin into the Qaidam and Hoh Xil sub-basins occurred out-of-sequence. This history demonstrates the importance of mechanically weak zones for the evolution and development of the Tibetan plateau.

## ACKNOWLEDGMENTS

This work was supported by the National Science Foundation of China (Project no. 41702232), the Fundamental Research Funds for the Central Universities for Chen Wu, the China University of Geosciences (Beijing) and a grant from the SINO-Probe Program administered by the Chinese Academy of Geological Sciences (SinoProbe-08-01). Fieldwork was also supported by the Qilian Mapping Program administered by the Institute of Geological Survey (Project no. 1212011121188), China University of Geosciences (Beijing). Ruixing Li is thanked for assistance in the field; Suoya Fan and Kaixuan An helped with analytical procedures. We appreciate Editor Damian Nance, Dr. Jiyuan Yin, and an anonymous reviewer for their critical, careful, and very constructive reviews that have helped improve the clarity and interpretations of the original draft. Discussions with Dr. Alex Pullen improved the ideas presented herein.

## REFERENCES CITED

- Allégre, C.J., Courtillot, V., Tapponnier, P., Hirn, A., Mattauer, M., Coulon, C., and Xu, R., 1984, Structure and evolution of the Himalaya-Tibet orogenic belt: *Nature*, v. 307, p. 17–22, <https://doi.org/10.1038/307017a0>.
- Andersen, T., 2002, Correction of common lead in U-Pb analyses that do not report <sup>204</sup>Pb: *Chemical Geology*, v. 192, p. 59–79, [https://doi.org/10.1016/S0009-2541\(02\)00195-X](https://doi.org/10.1016/S0009-2541(02)00195-X).
- Arnaud, N.O., Tapponnier, P., Roger, F., Brunel, M., Scharer, U., Chen, W., and Xu, Z., 2003, Evidence for Mesozoic shear along the western Kunlun and Altyn-Tagh fault, northern Tibet (China): *Journal of Geophysical Research*, v. 108, 2053, <https://doi.org/10.1029/2001JB000904>.
- Braitenberg, C., Wang, Y., Fang, J., and Hsu, H.T., 2003, Spatial variations of flexure parameters over the Tibet–Qinghai plateau: *Earth and Planetary Science Letters*, v. 205, no. 3–4, p. 211–224, [https://doi.org/10.1016/S0012-821X\(02\)01042-7](https://doi.org/10.1016/S0012-821X(02)01042-7).
- Bruguier, O., Lancelot, J.R., and Malavieille, J., 1997, U–Pb dating on single detrital zircon grains from the Triassic Songpan–Ganze flysch (Central China): provenance and tectonic correlations: *Earth and Planetary Science Letters*, v. 152, p. 217–231, [https://doi.org/10.1016/S0012-821X\(97\)00138-6](https://doi.org/10.1016/S0012-821X(97)00138-6).
- Burg, J.P., Davy, P., and Martinod, J., 1994, Shortening of analogue models of the continental lithosphere: new hypothesis for the formation of the Tibetan plateau: *Tectonics*, v. 13, no. 2, p. 475–483, <https://doi.org/10.1029/93TC02738>.
- Bush, M.A., Saylor, J.E., Horton, B.K., and Nie, J., 2016, Growth of the Qaidam Basin during Cenozoic exhumation in the northern Tibetan Plateau: Inferences from depositional patterns and multiproxy detrital provenance signatures: *Lithosphere*, v. 8, no. 1, p. 58–82, <https://doi.org/10.1130/L449.1>.
- Cawood, P.A., Hawkesworth, C.J., and Dhuime, B., 2012, Detrital zircon record and tectonic setting: *Geology*, v. 40, no. 10, p. 875–878, <https://doi.org/10.1130/G32945.1>.
- Chang, H., Li, L.Y., Qiang, X.K., Garzzone, C.N., Pullen, A., and An, Z.S., 2015, Magnetostratigraphy of Cenozoic deposits in the western Qaidam Basin and its implication for the surface uplift of the northeastern margin of the Tibetan Plateau: *Earth and Planetary Science Letters*, v. 430, p. 271–283, <https://doi.org/10.1016/j.epsl.2015.08.029>.
- Chen, A., Zheng, M., Shi, L., Wang, H., and Xu, J., 2017a, Magnetostratigraphy of deep drilling core 15YZK01 in the northwestern Qaidam Basin (NE Tibetan Plateau): Tectonic movement, salt deposits and their link to Quaternary glaciation: *Quaternary International*, v. 436, p. 201–211, <https://doi.org/10.1016/j.quaint.2017.01.026>.
- Chen, J.L., Yin, A., Xu, J.F., Dong, Y.H., and Kang, Z.Q., 2018, Late Cenozoic magmatic inflation, crustal thickening, and >2 km of surface uplift in central Tibet: *Geology*, v. 46, no. 1, p. 19–22, <https://doi.org/10.1130/G39699.1>.
- Chen, L., Capitanio, F.A., Liu, L., and Gerya, T.V., 2017b, Crustal rheology controls on the Tibetan plateau formation during India-Asia convergence: *Nature Communications*, v. 8, p. 15992, <https://doi.org/10.1038/ncomms15992>.
- Chen, N.S., Zhang, L., Sun, M., Wang, Q., and Kusky, T.M., 2012a, U-Pb and Hf isotopic compositions of detrital zircons from the paragneisses of the Quanji Massif, NW China: Implications for its early tectonic evolutionary history: *Journal of Asian Earth Sciences*, v. 54, p. 110–130, <https://doi.org/10.1016/j.jseaes.2012.04.006>.
- Chen, N.S., Liao, F.X., Wang, L., Santosh, M., Sun, M., Wang, Q.Y., Mustafa, H.A., 2013, Late Paleoproterozoic multiple metamorphic events in the Quanji Massif: links with Tarim and North China Cratons and implications for assembly of the Columbia supercontinent: *Precambrian Research*, v. 228, no. 102–116.
- Chen, S., Wang, H., Wei, J., Lv, Z., Gan, H., and Jin, S., 2014, Sedimentation of the Lower Cretaceous Xiangou Formation and its response to regional tectonics in the Qingxi Sag, Jiuquan Basin, NW China: *Cretaceous Research*, v. 47, p. 72–86, <https://doi.org/10.1016/j.cretres.2013.11.006>.
- Chen, X.H., Yin, A., Gehrels, G.E., Cowgill, E.S., Grove, M., Harrison, T.M., and Wang, X.F., 2003, Two phases of Mesozoic north-south extension in the eastern Altyn Tagh range, northern Tibetan Plateau: *Tectonics*, v. 22, 1053, <https://doi.org/10.1029/2001TC001336>.
- Chen, X.H., Dang, Y.Q., Yin, A., Wang, L.Q., Jiang, W.M., and Li, L., 2010, Basin mountain coupling and tectonic evolution of Qaidam Basin and its adjacent orogenic belts. Beijing: Geological Publishing House, p. 1–365 [in Chinese].
- Chen, X.H., McRivette, M.W., Li, L., Yin, A., Jiang, R.B., Wan, J.L., and Li, H.J., 2011, Thermochronological evidence for multi-phase uplift of the East Kunlun Mountains, northern Tibetan Plateau: *Geological Bulletin of China*, v. 30, no. 11, p. 1647–1660 [in Chinese with English abstract].
- Chen, X.H., Gehrels, G.E., Yin, A., Li, L., and Jiang, R.B., 2012b, Paleozoic and Mesozoic basement magmatism of Eastern Qaidam Basin, Northern Qinghai–Tibet Plateau: LA-ICP-MS zircon U-Pb geochronology and its geological significance: *Acta Geologica Sinica*, v. 86, p. 350–369, <https://doi.org/10.1111/j.1755-6724.2012.00665.x>.
- Cheng, F., Fu, S.T., Jolivet, M., Zhang, C.H., and Guo, Z.J., 2016, Source to sink relation between the Eastern Kunlun Range and the Qaidam Basin, northern Tibetan Plateau, during the Cenozoic: *Geological Society of America Bulletin*, v. 128, no. 1/2, p. 258–283, <https://doi.org/10.1130/B31260.1>.

- Chung, S.L., Chu, M.F., Zhang, Y.Q., Xie, Y.W., Lo, C.H., Lee, T.Y., Lan, C.Y., Li, X.H., Zhang, Q., and Wang, Y.Z., 2005, Tibetan tectonic evolution inferred from spatial and temporal variations in post-collisional magmatism: *Earth-Science Reviews*, v. 68, p. 173–196, <https://doi.org/10.1016/j.earscirev.2004.05.001>.
- Clark, M.K., 2012, Continental collision slowing due to viscous mantle lithosphere rather than topography: *Nature*, v. 483, no. 7387, p. 74, <https://doi.org/10.1038/nature10848>.
- Clark, M.K., and Royden, L.H., 2000, Topographic ooze: Building the eastern margin of Tibet by lower crustal flow: *Geology*, v. 28, p. 703–706, [https://doi.org/10.1130/0091-7613\(2000\)28<703:TOBTEM>2.0.CO;2](https://doi.org/10.1130/0091-7613(2000)28<703:TOBTEM>2.0.CO;2).
- Clark, M.K., Farley, K.A., Zheng, D., Wang, Z., and Duvall, A.R., 2010, Early Cenozoic faulting of the northern Tibetan Plateau margin from apatite (U-Th)/He ages: *Earth and Planetary Science Letters*, v. 296, no. 1–2, p. 78–88, <https://doi.org/10.1016/j.epsl.2010.04.051>.
- Cowgill, E., Yin, A., Harrison, T.M., and Wang, X.F., 2003, Reconstruction of the Altyn Tagh fault based on U-Pb geochronology: Role of back thrusts, mantle sutures, and heterogeneous crustal strength in forming the Tibetan Plateau: *Journal of Geophysical Research*, v. 108, 2346, <https://doi.org/10.1029/2002JB002080>.
- Cyr, A.J., Currie, B.S., and Rowley, D.B., 2005, Geochemical evaluation of Fenghuoshan Group lacustrine carbonates, North-Central Tibet: implications for the paleoaltimetry of the Eocene Tibetan Plateau: *Journal of Geology*, v. 113, p.517–533.
- Dai, J.G., Zhao, X.X., Wang, C.S., Zhu, L.D., Li, Y.L., and Finn, D., 2012, The vast proto-Tibetan Plateau: New constraints from Paleogene Hoh Xil Basin: *Gondwana Research*, v. 22, p. 434–446, <https://doi.org/10.1016/j.gr.2011.08.019>.
- Dai, J.G., Wang, C.S., Hourigan, J., and Santosh, M., 2013, Multi-stage tectono-magmatic events of the Eastern Kunlun Range, northern Tibet: Insights from U-Pb geochronology and (U-Th)/He thermochronology: *Tectonophysics*, v. 599, p. 97–106, <https://doi.org/10.1016/j.tecto.2013.04.005>.
- DeCelles, P.G., Robinson, D.M., and Zandt, G., 2002, Implications of shortening in the Himalayan fold-thrust belt for uplift of the Tibetan Plateau: *Tectonics*, v. 21, 1062, <https://doi.org/10.1029/2001TC001322>.
- Dewey, J.F., Shackleton, R.M., Chang, C., and Sun, Y., 1988, The tectonic evolution of the Tibetan Plateau: *Philosophical Transactions of the Royal Society of London. Series A, Mathematical and Physical Sciences*, v. 327, p. 379–413, <https://doi.org/10.1098/rsta.1988.0135>.
- Dickinson, W.R., 1970, Interpreting detrital modes of greywacke and arkose: *Journal of Sedimentary Research*, v. 40, p. 695–707.
- Dickinson, W.R., 1985, Interpreting provenance relations from detrital modes of sandstones, *in* Zuffa, G.G., ed., *Provenance of Arenites: NATO ASI Series C Volume 148: Dordrecht, Netherlands, D. Reidel Publishing Company*, p. 333–361, [https://doi.org/10.1007/978-94-017-2809-6\\_15](https://doi.org/10.1007/978-94-017-2809-6_15).
- Ding, L., Kapp, P., Zhong, D., and Deng, W., 2003, Cenozoic volcanism in Tibet: Evidence for a transition from oceanic to continental subduction: *Journal of Petrology*, v. 44, p. 1833–1865, <https://doi.org/10.1093/petrology/egg061>.
- Ding, L., Kapp, P., Yue, Y.H., and Lai, Q., 2007, Post collisional calc-alkaline lavas and xenoliths from the southern Qiangtang Terrane, central Tibet: *Earth and Planetary Science Letters*, v. 254, p. 28–38, <https://doi.org/10.1016/j.epsl.2006.11.019>.
- Ding, L., Yang, D., Cai, F.L., Pullen, A., Kapp, P., and Shi, R.D., 2013, Provenance analysis of the Mesozoic Hoh-Xil-Songpan-Ganzi turbidites in northern Tibet: Implications for the tectonic evolution of the eastern Paleo-Tethys Ocean: *Tectonics*, v. 32, p. 34–48, <https://doi.org/10.1002/tect.20013>.
- Ding, L., Spicer, R.A., Yang, J., Xu, Q., Cai, F., and Mehrotra, R., 2017, Quantifying the rise of the Himalaya orogen and implications for the South Asian monsoon: *Geology*, v. 45, no. 3, p. 215–218, <https://doi.org/10.1130/G38583.1>.
- Donelick, R.A., and Miller, D.S., 1991, Enhanced TINT fission track density apatites using <sup>252</sup>Cf-derived fission fragment tracks: a model and experimental observations: *Nuclear Tracks and Radiation Measurements*, v. 18, p. 301–307, [https://doi.org/10.1016/1359-0189\(91\)90022-A](https://doi.org/10.1016/1359-0189(91)90022-A).
- Dong, Y.P., He, D.F., Sun, S.S., Liu, X.M., Zhou, X.H., Zhang, F.F., Yang, Z., Cheng, B., Zhao, G.C., and Li, J.H., 2018, Subduction and accretionary tectonics of the East Kunlun orogen, western segment of the Central China Orogenic System: *Earth-Science Reviews*, v. 186, p. 231–261, <https://doi.org/10.1016/j.earscirev.2017.12.006>.
- Dupont-Nivet, G., Lippert, P.C., van Hinsbergen, D.J., Meijers, M.J., and Kapp, P., 2010, Palaeo-latitude and age of the Indo-Asia collision: Palaeomagnetic constraints: *Geophysical Journal International*, v. 182, no. 3, p. 1189–1198, <https://doi.org/10.1111/j.1365-246X.2010.04697.x>.
- Duvall, A.R., Clark, M.K., Kirby, E., Farley, K.A., Craddock, W.H., Li, C.Y., and Yuan, D.Y., 2013, Low-temperature thermochronometry along the Kunlun and Haiyuan Faults, NE Tibetan Plateau: Evidence for kinematic change during late-stage orogenesis: *Tectonics*, v. 32, p. 1190–1211, <https://doi.org/10.1002/tect.20072>.
- England, P., and Houseman, G., 1986, Finite strain calculations of continental deformation 2. Comparison with the India-Asia collision zone: *Journal of Geophysical Research*, v. 91, p. 3664–3676, <https://doi.org/10.1029/JB091iB03p03664>.
- England, P., and Houseman, G., 1989, Extension during continental convergence, with application to the Tibetan Plateau: *Journal of Geophysical Research*, v. 94, p. 17561–17569, <https://doi.org/10.1029/JB094iB12p17561>.
- Enkelmann, E., Weislogel, A., Ratschbacher, L., Eide, E., Renno, A., and Wooden, J., 2007, How was the Triassic Songpan-Ganzi basin filled? A provenance study: *Tectonics*, v. 26, TC4007, <https://doi.org/10.1029/2006TC002078>.
- Fang, X., Zhang, W., Meng, Q., Gao, J., Wang, X., King, J., Song, C., Dai, S., and Miao, Y., 2007, High-resolution magnetostratigraphy of the Neogene Huitoutala section in the eastern Qaidam basin on the NE Tibetan plateau, Qinghai province, China and its implication on tectonic uplift of the NE Tibetan plateau: *Earth and Planetary Science Letters*, v. 258, p. 293–306, <https://doi.org/10.1016/j.epsl.2007.03.042>.
- Fang, X., Song, C., Yan, M., Zan, J., Liu, C., Sha, J., Zhang, W., Zeng, Y., Wu, S., and Zhang, D., 2016, Mesozoic litho- and magneto-stratigraphic evidence from the central Tibetan Plateau for megamonsoon evolution and potential evaporites: *Gondwana Research*, v. 37, p. 110–129, <https://doi.org/10.1016/j.gr.2016.05.012>.
- Farner, M.J., and Lee, C.T.A., 2017, Effects of crustal thickness on magmatic differentiation in subduction zone volcanism. A global study: *Earth and Planetary Science Letters*, v. 470, p. 96–107, <https://doi.org/10.1016/j.epsl.2017.04.025>.
- Favre, A., Päckert, M., Pauls, S.U., Jähnig, S.C., Uhl, D., and Muellner-Riehl, A.N., 2015, The role of the uplift of the Qinghai-Tibetan Plateau for the evolution of Tibetan biotas: *Biological Reviews of the Cambridge Philosophical Society*, v. 90, no. 1, p. 236–253, <https://doi.org/10.1111/brv.12107>.
- Fu, B.H., and Awata, Y., 2007, Displacement and timing of left-lateral faulting in the Kunlun Fault Zone, northern Tibet, inferred from geologic and geomorphic features: *Journal of Asian Earth Sciences*, v. 29, no. 2–3, p. 253–265, <https://doi.org/10.1016/j.jseaes.2006.03.004>.
- Gehrels, G.E., Yin, A., and Wang, X.F., 2003a, Magmatic history of the northeastern Tibetan plateau: *Journal of Geophysical Research*, v. 108, 2423, <https://doi.org/10.1029/2002JB001876>.
- Gehrels, G.E., Yin, A., and Wang, X.F., 2003b, Detrital-zircon geochronology of the northeastern Tibetan plateau: *Geological Society of America Bulletin*, v. 115, p. 881–896, [https://doi.org/10.1130/0016-7606\(2003\)115<0881:DGOTNT>2.0.CO;2](https://doi.org/10.1130/0016-7606(2003)115<0881:DGOTNT>2.0.CO;2).
- Gehrels, G.E., Kapp, P., DeCelles, P., Pullen, A., Blakey, R., Weislogel, A., Ding, L., Guynn, J., Martin, A., McQuarrie, N., and Yin, A., 2011, Detrital zircon geochronology of pre-Tertiary strata in the Tibetan-Himalayan orogen: *Tectonics*, v. 30, TC5016, <https://doi.org/10.1029/2011TC002868>.
- Gleadow, A.J.W., 1981, Fission-track dating methods: what are the real alternatives?: *Nuclear Tracks*, v. 5, no. 1–2, p. 3–14, [https://doi.org/10.1016/0191-278X\(81\)90021-7](https://doi.org/10.1016/0191-278X(81)90021-7).
- Gleadow, A.J.W., Duddy, I.R., Green, P.F., and Lovering, J.F., 1986, Confined fission track lengths in apatite: a diagnostic tool for thermal history analysis: *Contributions to Mineralogy and Petrology*, v. 94, p. 405–415, <https://doi.org/10.1007/BF00376334>.
- Gong, S.L., Chen, N.S., Wang, Q.Y., Kusky, T.M., Wang, L., Zhang, L., Ba, J., and Liao, F.X., 2012, Early Paleoproterozoic magmatism in the Quanji Massif, north-eastern margin of the Qinghai-Tibet Plateau and its tectonic significance: *LA-ICP-MS U-Pb zircon geochronology and geochemistry: Gondwana Research*, v. 21, p. 152–166, <https://doi.org/10.1016/j.gr.2011.07.011>.
- Green, P.F., Duddy, I.R., Gleadow, A.J.W., Laslett, G.M., and Tingate, P.R., 1986, Thermal annealing of fission track in apatite 1: a qualitative description: *Chemical Geology*, v. 59, p. 237–253, [https://doi.org/10.1016/0168-9622\(86\)90074-6](https://doi.org/10.1016/0168-9622(86)90074-6).
- Guynn, J.H., Kapp, P., Pullen, A., Heizler, M., Gehrels, G., and Ding, L., 2006, Tibetan basement rocks near Amdo reveal “missing” Mesozoic tectonism along the Bangong suture, central Tibet: *Geology*, v. 34, p. 505–508, <https://doi.org/10.1130/G22453.1>.
- Hacker, B.R., Gnos, E., Ratschbacher, L., Grove, M., McWilliams, M., Sobolev, S.V., Jiang, W., and Wu, Z., 2000, Hot and dry deep crustal xenoliths from Tibet: *Science*, v. 287, p. 2463–2466, <https://doi.org/10.1126/science.2875462.2463>.
- Hao, L.L., Wang, Q., Wyman, D.A., Ou, Q., Dan, W., Jiang, Z.Q., Wu, F.Y., Yang, J.H., Long, X.P., and Li, J., 2016, Underplating of basaltic magmas and crustal growth in a continental arc: Evidence from Late Mesozoic intermediate-felsic intrusive rocks in southern Qiangtang, central Tibet: *Lithos*, v. 245, p. 223–242, <https://doi.org/10.1016/j.lithos.2015.09.015>.
- Haproff, P.J., Zuzá, A.V., and Yin, A., 2018, West-directed thrusting south of the eastern Himalayan syntaxis indicates clockwise crustal flow at the indenter corner during the India-Asia collision: *Tectonophysics*, v. 722, p. 277–285, <https://doi.org/10.1016/j.tecto.2017.11.001>.
- Harrison, T.M., Copeland, P., Kidd, W.S.F., and Yin, A., 1992, Raising Tibet: *Science*, v. 255, p. 1663–1670, <https://doi.org/10.1126/science.255.5052.1663>.
- Harrison, T.M., Yin, A., Grove, M., Lovera, O.M., Ryerson, F.J., and Zhou, X., 2000, The Zedong Window: A record of superposed Tertiary convergence in southeastern Tibet: *Journal of Geophysical Research*, v. 105, p. 19,211–19,230, <https://doi.org/10.1029/2000JB900078>.
- He, D., Dong, Y., Liu, X., Yang, Z., Sun, S., Cheng, B., and Li, W., 2016a, Tectono-thermal events in east Kunlun, northern Tibetan Plateau: evidence from zircon U-Pb geochronology: *Gondwana Research*, v. 30, p. 179–190, <https://doi.org/10.1016/j.gr.2015.08.002>.
- He, D., Dong, Y., Zhang, F., Yang, Z., Sun, S., Cheng, B., Zhou, B., and Liu, X., 2016b, The 1.0 Ga S-type granite in the East Kunlun Orogen, Northern Tibetan Plateau: implications for the Meso- to Neoproterozoic tectonic evolution: *Journal of Asian Earth Sciences*, v. 130, p. 46–59, <https://doi.org/10.1016/j.jseaes.2016.07.019>.
- He, D., Dong, Y., Liu, X., Zhou, X., Zhang, F., and Sun, S., 2018, Zircon U-Pb geochronology and Hf isotope of granitoids in East Kunlun: Implications for the Neoproterozoic magmatism of Qaidam Block, Northern Tibetan Plateau: *Precambrian Research*, v. 314, p. 377–393, <https://doi.org/10.1016/j.precamres.2018.06.017>.
- Horton, B.K., Dupont-Nivet, G., Zhou, J., Waanders, G.L., Butler, R.F., and Wang, J., 2004, Mesozoic-Cenozoic evolution of the Xining-Minhe and Dangchang basins, northeastern Tibetan Plateau: Magnetostratigraphic and biostratigraphic results: *Journal of Geophysical Research*, v. 109, B04402, <https://doi.org/10.1029/2003JB002913>.
- Hurfurd, A.J., 1990, Standardization of fission track dating calibration: recommendation by the Fission Track Working Group of the IUGS Subcommittee on Geochronology: *Chemical Geology. Isotope Geoscience Section*, v. 80, p. 171–178, [https://doi.org/10.1016/0168-9622\(90\)90025-8](https://doi.org/10.1016/0168-9622(90)90025-8).
- Hurfurd, A.J., and Green, P.F., 1983, The Zeta age calibration of fission track dating: *Chemical Geology. Isotope Geoscience Section*, v. 1, p. 285–317.
- Ingersoll, R.V., Bullard, T.F., Ford, R.L., Grimm, J.P., Pickle, J.D., and Sares, S.W., 1984, The effect of grain size on detrital modes: a test of the Gazi-Dickinson point-counting method: *Journal of Sedimentary Petrology*, v. 54, p. 103–116.
- Jackson, S.E., Pearson, N.J., Griffin, W.L., and Belousova, E.A., 2004, The application of laser ablation-inductively coupled plasma-mass spectrometry to in situ U-Pb zircon geochronology: *Chemical Geology*, v. 211, p. 47–69, <https://doi.org/10.1016/j.chemgeo.2004.06.017>.
- Jackson, W.T., Jr., Robinson, D.M., Weislogel, A.L., Shang, F., and Jian, X., 2018, Mesozoic development of nonmarine basins in the northern Yidun terrane: deposition and deformation in the eastern Tibetan Plateau prior to the India-Asia collision: *Tectonics*, v. 37, no. 8, p. 2466–2485, <https://doi.org/10.1029/2018TC004995>.



- Ji, J., Zhang, K., Clift, P.D., Zhuang, G., Song, B., and Ke, X., 2017, High-resolution magnetostratigraphic study of the Paleogene-Neogene strata in the northern Qaidam basin: implications for the growth of the northeastern Tibetan Plateau: *Gondwana Research*, v. 46, p. 141–155, <https://doi.org/10.1016/j.gr.2017.02.015>.
- Jiang, R.B., Chen, X.H., Dang, Y.Q., Yin, A., Wang, L.Q., Jiang, W.M., Wan, J.L., Li, L., and Wang, X.F., 2008, Apatite fission track evidence for two phases Mesozoic-Cenozoic thrust faulting in eastern Qaidam basin: *Chinese Journal of Geophysics*, v. 51, p. 117–125.
- Jin, C., Liu, Q., Liang, W., Roberts, A.P., Sun, J., Hu, P., and Duan, Z., 2018, Magnetostratigraphy of the Fenghuoshan Group in the Hoh Xil Basin and its tectonic implications for India-Eurasia collision and Tibetan Plateau deformation: *Earth and Planetary Science Letters*, v. 486, p. 41–53, <https://doi.org/10.1016/j.epsl.2018.01.010>.
- Jolivet, M., 2017, Mesozoic tectonic and topographic evolution of Central Asia and Tibet: a preliminary synthesis, in Brunet, M.-F., et al., eds., *Geological Evolution of Central Asian Basins and the Western Tien Shan Range*: Geological Society, London, Special Publications, v. 427, p. 19–55, <https://doi.org/10.1144/SP427.2>.
- Jolivet, M., Brunel, M., Roger, F., Tapponnier, P., Arnaud, N., and Seward, D., 1999, Exhumation history of the Altyn Shan with evidence for the timing of the subduction of the Tarim block beneath the Altyn Tagh system, North Tibet: *Comptes Rendus de l'Académie des Sciences, Série 2, Sciences de la Terre et des Planètes*, v. 31, p. 749–755.
- Jolivet, M., Brunel, M., Seward, D., Xu, Z., Yang, J., Roger, F., Tapponnier, P., Malavieille, J., Arnaud, N., and Wu, C., 2001, Mesozoic and Cenozoic tectonics of the northern edge of the Tibetan plateau: fission-track constraints: *Tectonophysics*, v. 343, p. 111–134, [https://doi.org/10.1016/S0040-1951\(01\)00196-2](https://doi.org/10.1016/S0040-1951(01)00196-2).
- Jolivet, M., Brunel, M., Seward, D., Xu, Z., Yang, J., Malavieille, J., Roger, F., Leyreloup, A., Arnaud, N., and Wu, C., 2003, Neogene extension and volcanism in the Kunlun Fault Zone, northern Tibet: New constraints on the age of the Kunlun Fault: *Tectonics*, v. 22, 1052, <https://doi.org/10.1029/2002TC001428>.
- Kang, L., Liu, L., Cao, Y.T., Wang, C., Yang, W.Q., and Zhu, X.H., 2011, Geochemistry, zircon LA-ICP-MS U-Pb ages and Hf isotopes of Hongliuguo moyite from north Altyn Tagh tectonic belt: *Geological Bulletin of China*, v. 30, p. 1066–1076 [in Chinese with English abstract].
- Kapp, P., Yin, A., Harrison, T.M., and Ding, L., 2005, Cretaceous-Tertiary shortening, basin development, and volcanism in central Tibet: *Geological Society of America Bulletin*, v. 117, p. 865–878, <https://doi.org/10.1130/B25595.1>.
- Kapp, P., DeCelles, P.G., Gehrels, G.E., Heizler, M., and Ding, L., 2007a, Geological records of the Lhasa-Qiangtang and Indo-Asian collisions in the Nima area of central Tibet: *Geological Society of America Bulletin*, v. 119, p. 917–933, <https://doi.org/10.1130/B26033.1>.
- Kapp, P., DeCelles, P.G., Leier, A.L., Fabijanic, J.M., He, S., Pullen, A., Gehrels, G.E., and Ding, L., 2007b, The Gangdese retroarc thrust belt revealed: *GSA Today*, v. 17, p. 4–9, <https://doi.org/10.1130/GSAT01707A.1>.
- Ke, X., Ji, J.J., Zhang, K.X., Kou, X.H., Song, B.W., and Wang, C.W., 2013, Magnetostratigraphy and anisotropy of magnetic susceptibility of the lulehe formation in the Northeastern Qaidam basin: *Acta Geologica Sinica*, v. 87, p. 576–587, <https://doi.org/10.1111/1755-6724.12069>.
- Ketcham, R.A., Donelick, R.A., Carlson, W.D., 1999, Variability of apatite fission-track annealing kinetics: III. Extrapolation to geological time scales: *The American Mineralogist*, v. 84, no. 9, p. 1235–1255.
- Ketcham, R.A., Donelick, R.A., and Donelick, M.B., 2000, AFTSolve: A program for multi-kinetic modeling of apatite fission-track data: *Geological Materials Research*, v. 2, no. 1, p. 1–32.
- Ketcham, R.A., Carter, A., Donelick, R.A., Barbarand, J., and Hurford, A.J., 2007, Improved modeling of fission-track annealing in apatite: *The American Mineralogist*, v. 92, no. 5-6, p. 799–810, <https://doi.org/10.2138/am.2007.22281>.
- Kong, X., Yin, A., and Harrison, T.M., 1997, Evaluating the role of preexisting weakness and topographic distributions in the Indo-Asian collision by use of a thin shell numerical model: *Geology*, v. 25, p. 527–530, [https://doi.org/10.1130/0091-7613\(1997\)025<0527:ETROPW>2.3.CO;2](https://doi.org/10.1130/0091-7613(1997)025<0527:ETROPW>2.3.CO;2).
- Laslett, G.M., Green, P.F., Duddy, I.R., and Gleadow, A.J.W., 1987, Thermal annealing of fission tracks in apatite; 2: a quantitative analysis: *Chemical Geology. Isotope Geoscience Section*, v. 65, p. 1–13, [https://doi.org/10.1016/0168-9622\(87\)90057-1](https://doi.org/10.1016/0168-9622(87)90057-1).
- Leeder, M.R., Smith, A.B., and Yin, J., 1988, Sedimentology, palaeoecology and palaeoenvironmental evolution of the 1985 Lhasa to Golmud Geotraverse: *Philosophical Transactions of the Royal Society of London. Series A, Mathematical and Physical Sciences*, v. 327, p. 107–143, <https://doi.org/10.1098/rsta.1988.0123>.
- Leier, A.L., Kapp, P., Gehrels, G.E., and DeCelles, P.G., 2007, Detrital zircon geochronology of Carboniferous-Cretaceous strata in the Lhasa terrane, southern Tibet: *Basin Research*, v. 19, p. 361–378, <https://doi.org/10.1111/j.1365-2117.2007.00330.x>.
- Li, B., Chen, X., Zuza, A.V., Hu, D., Ding, W., Huang, P., and Xu, S., 2019, Cenozoic cooling history of the North Qilian Shan, northern Tibetan Plateau, and the initiation of the Haiyuan fault: Constraints from apatite- and zircon-fission track thermochronology: *Tectonophysics*, v. 751, p. 101–124, <https://doi.org/10.1016/j.tecto.2018.12.005>.
- Li, J.G., Peng, J.G., and Batten, D.J., 2015, Palynomorph assemblages from the Fenghuoshan Group, southern Qinghai, China: Their age and palaeoenvironmental significance: *Science Bulletin*, v. 60, no. 4, p. 470–476, <https://doi.org/10.1007/s11434-014-0677-8>.
- Li, J.X., Qin, K.Z., Li, G.M., Richards, J.P., Zhao, J.X., and Cao, M.J., 2014, Geochronology, geochemistry, and zircon Hf isotopic compositions of Mesozoic intermediate-felsic intrusions in central Tibet: Petrogenetic and tectonic implications: *Lithos*, v. 198, p. 77–91, <https://doi.org/10.1016/j.lithos.2014.03.025>.
- Li, L., Garzzone, C.N., Pullen, A., and Chang, H., 2016, Early-middle Miocene topographic growth of the northern Tibetan Plateau: Stable isotope and sedimentation evidence from the southwestern Qaidam basin: *Palaeogeography, Palaeoclimatology, Palaeoecology*, v. 461, p. 201–213, <https://doi.org/10.1016/j.palaeo.2016.08.025>.
- Li, L., Garzzone, C.N., Pullen, A., Zhang, P., and Li, Y., 2018, Late Cretaceous-Cenozoic basin evolution and topographic growth of the Hoh Xil Basin, central Tibetan Plateau: *Geological Society of America Bulletin*, v. 130, p. 499–521, <https://doi.org/10.1130/B31769.1>.
- Liao, F.X., Zhang, L., Chen, N.S., Sun, M., Santosh, M., Wang, Q.Y., and Hassan, A.M., 2014, Geochronology and geochemistry of meta-mafic dykes in the Quanjia Massif, NW China: Paleoproterozoic Evolution of the Tarim Craton and implications on the Assembly of the Columbia Supercontinent: *Precambrian Research*, v. 249, p. 33–56, <https://doi.org/10.1016/j.precamres.2014.04.015>.
- Liu, D., Shi, R., Ding, L., Huang, Q., Zhang, X., Yue, Y., and Zhang, L., 2017a, Zircon U-Pb age and Hf isotopic compositions of Mesozoic granitoids in southern Qiangtang, Tibet: Implications for the subduction of the Bangong-Nujiang Tethyan Ocean: *Gondwana Research*, v. 41, p. 157–172, <https://doi.org/10.1016/j.gr.2015.04.007>.
- Liu, D., Li, H., Sun, Z., Pan, J., Wang, M., and Wang, H., 2017b, AFT dating constrains the Cenozoic uplift of the Qimen Tagh Mountains, Northeast Tibetan Plateau, comparison with LA-ICPMS zircon U-Pb ages: *Gondwana Research*, v. 41, p. 438–450, <https://doi.org/10.1016/j.gr.2015.10.008>.
- Liu, D.L., Shi, R.D., Ding, L., and Zou, H.B., 2018, Late Cretaceous transition from subduction to collision along the Bangong-Nujiang Tethys: New volcanic constraints from central Tibet: *Lithos*, v. 296–299, p. 452–470, <https://doi.org/10.1016/j.lithos.2017.11.012>.
- Liu, L., Wang, C., Chen, D., Zhang, A., and Liou, J.G., 2009, Petrology and geochronology of HP-UHP rocks from the South Altyn Tagh, northwestern China: *Journal of Asian Earth Sciences*, v. 35, no. 3-4, p. 232–244, <https://doi.org/10.1016/j.jseas.2008.10.007>.
- Liu, Y., Genser, J., Neubauer, F., Jin, W., Ge, X., Handler, R., and Takasu, A., 2005a, <sup>40</sup>Ar/<sup>39</sup>Ar mineral ages from basement rocks in the Eastern Kunlun Mountains, NW China, and their tectonic implications: *Tectonophysics*, v. 398, p. 199–224, <https://doi.org/10.1016/j.tecto.2005.02.007>.
- Liu, Z.F. and Wang, C.S., 2001, Facies analysis and depositional systems of Cenozoic sediments in the Hoh Xil basin, northern Tibet: *Sedimentary Geology*, v. 140, p. 251–270, [https://doi.org/10.1016/S0037-0738\(00\)00188-3](https://doi.org/10.1016/S0037-0738(00)00188-3).
- Liu, Z.F., Zhao, X., Wang, C.S., Liu, S., and Yi, H., 2003, Magnetostratigraphy of Tertiary sediments from the Hoh Xil basin: implications for the Cenozoic tectonic history of the Tibetan plateau: *Geophysical Journal International*, v. 154, p. 233–252, <https://doi.org/10.1046/j.1365-246X.2003.01986.x>.
- Liu, Z.F., Wang, C.S., Jin, W., Yi, H.S., Zheng, H.B., Zhao, X.X., and Li, Y.L., 2005b, Oligo-Miocene depositional environment of the Tuotuohe basin, central Tibetan plateau: *Acta Sedimentologica Sinica*, v. 23, p. 210–217.
- Liu-Zeng, J., Tapponnier, P., Gaudemer, Y., and Ding, L., 2008, Quantifying landscape differences across the Tibetan plateau: Implications for topographic relief evolution: *Journal of Geophysical Research. Earth Surface*, v. 113, F4, <https://doi.org/10.1029/2007JF000897>.
- Lu, H.J., and Xiong, S.F., 2009, Magnetostratigraphy of the Dahonggou section, northern Qaidam Basin and its bearing on Cenozoic tectonic evolution of the Qilian Shan and Altyn Tagh Fault: *Earth and Planetary Science Letters*, v. 288, p. 539–550, <https://doi.org/10.1016/j.epsl.2009.10.016>.
- Lu, S.N., 2002, Preliminary Study of Precambrian Geology in the North Tibet-Qinghai Plateau: Geological Publishing House, Beijing, p. 1–125 [in Chinese with English abstract].
- Lu, S.N., Yu, H.F., and Li, H.K., 2006, Research on Precambrian Major Problems in China: Geological Publishing Press, Beijing, p. 1–206 [in Chinese with English abstract].
- McRivette, M.W., Yin, A., Chen, X.H., and Gehrels, G.E., 2019, Cenozoic basin evolution of the central Tibetan plateau as constrained by U-Pb detrital zircon geochronology, sandstone petrology, and fission-track thermochronology: *Tectonophysics*, v. 751, p. 150–179, <https://doi.org/10.1016/j.tecto.2018.12.015>.
- Meyer, B., Tapponnier, P., Bourjot, L., Metivier, F., Gaudemer, Y., and Zhaitai, C., 1998, Crustal thickening in Gansu-Qinghai, lithospheric mantle subduction, and oblique, strike-slip controlled growth of the Tibet plateau: *Geophysical Journal International*, v. 135, p. 1–47, <https://doi.org/10.1046/j.1365-246X.1998.00567.x>.
- Meyers, J.H., Suttner, L.J., Furer, L.C., May, M.T., and Soreghan, M.J., 1992, Intrabasinal tectonic control on fluvial sandstone bodies in the Cloverly Formation (Early Cretaceous), west-Central Wyoming, USA: *Basin Research*, v. 4, p. 315–335.
- Miller, C., Schuster, R., Klötzli, U., Frank, W., and Purtscheller, F., 1999, Postcollisional potassic and ultrapotassic magmatism in SW Tibet: Geochemical and Sr-Nd-Pb-O isotopic constraints for mantle source characteristics and petrogenesis: *Journal of Petrology*, v. 40, p. 1399–1424, <https://doi.org/10.1093/ptro/j/40.9.1399>.
- Mo, X.X., Dong, G.C., Zhao, Z.D., Guo, T., Wang, L., and Chen, T., 2005, Timing of magma mixing in the Gangdese magmatic belt during the India-Asia collision: Zircon SHRIMP U-Pb dating: *Acta Geologica Sinica*, v. 79, p. 66–76, <https://doi.org/10.1111/j.1755-6724.2005.tb00868.x>.
- Mo, X.X., Zhao, Z.D., Deng, J., Flower, M., Yu, X., and Wang, L., 2006, Petrology and geochemistry of postcollisional volcanic rocks from the Tibetan plateau: Implications for lithosphere heterogeneity and collision-induced asthenosphere flow, in Dilek, Y., and Pavlides, S., eds., *Postcollisional Tectonics and Magmatism in the Mediterranean Region and Asia*: Geological Society of America Special Paper, v. 409, p. 507–530, [https://doi.org/10.1130/2006.2409\(24\)](https://doi.org/10.1130/2006.2409(24)).
- Mo, X.X., Hou, Z.Q., Niu, Y.L., Dong, G.C., Qu, X.M., Zhao, Z.D., and Yang, Z.M., 2007, Mantle contributions to crustal thickening during continental collision: Evidence from Cenozoic igneous rocks in southern Tibet: *Lithos*, v. 96, p. 225–242, <https://doi.org/10.1016/j.lithos.2006.10.005>.
- Mock, C., Arnaud, N.O., and Cantagrel, J.M., 1999, An early unroofing in northeastern Tibet? Constraints from <sup>40</sup>Ar/<sup>39</sup>Ar thermochronology on granitoids from the eastern Kunlun range (Qianghai, NW China): *Earth and Planetary Science Letters*, v. 171, p. 107–122, [https://doi.org/10.1016/S0012-821X\(99\)00133-8](https://doi.org/10.1016/S0012-821X(99)00133-8).
- Molnar, P., England, P., and Martinod, J., 1993, Mantle dynamics, the uplift of the Tibetan Plateau, and the Indian monsoon: *Reviews of Geophysics*, v. 31, p. 357–396, <https://doi.org/10.1029/93RG02030>.
- Molnar, P., Boos, W.R., and Battisti, D.S., 2010, Orographic controls on climate and paleoclimate of Asia: thermal and mechanical roles for the Tibetan Plateau: *Annual Review of Earth and Planetary Sciences*, v. 38, p. 77–102.

- Murphy, M.A., Yin, A., Harrison, T.M., Dürr, S.B., Chen, Z., Ryerson, F.J., Kidd, W.S.F., Wang, X., and Zhou, X., 1997, Did the Indo-Asian collision alone create the Tibetan plateau?: *Geology*, v. 25, p. 719–722, [https://doi.org/10.1130/0091-7613\(1997\)025<0719:DTIACA>2.3.CO;2](https://doi.org/10.1130/0091-7613(1997)025<0719:DTIACA>2.3.CO;2).
- Nie, S.Y., Yin, A., Rowley, D.B., and Jin, Y.G., 1994, Exhumation of the Dabie Shan ultra-high pressure rocks and accumulation of the Songpan-Ganzi flysch sequence, central China: *Geology*, v. 22, p. 999–1002, [https://doi.org/10.1130/0091-7613\(1994\)022<0999:EOTDSU>2.3.CO;2](https://doi.org/10.1130/0091-7613(1994)022<0999:EOTDSU>2.3.CO;2).
- Oxburgh, E.R., 1972, Flake tectonics and continental collision: *Nature*, v. 239, no. 5369, p. 202, <https://doi.org/10.1038/239202a0>.
- Pan, G.T., Ding, J., Yao, D., and Wang, L., 2004, Geological map of Qinghai-Xiang (Tibet) plateau and adjacent areas: Chengdu Institute of Geology and Mineral Resources: China Geological Survey, Chengdu, Chengdu Cartographic Publishing House, scale 1:1,500,000.
- Profeta, L., Ducea, M.N., Chapman, J.B., Paterson, S.R., Gonzales, S.M.H., Kirsch, M., and DeCelles, P.G., 2015, Quantifying crustal thickness over time in magmatic arcs: *Scientific Reports*, v. 5, 17786, <https://doi.org/10.1038/srep17786>.
- Pullen, A., Kapp, P., Gehrels, G.E., Vervoort, J.D., and Ding, L., 2008, Triassic continental subduction in central Tibet and Mediterranean-style closure of the Paleo-Tethys Ocean: *Geology*, v. 36, p. 351–354, <https://doi.org/10.1130/G24435A.1>.
- Qian, T., Wang, Z.X., Liu, Y.Q., Liu, S.F., Gao, W.L., Li, W.P., Hu, J.J., and Li, L.L., 2018, Provenance analysis of the Jurassic northern Qaidam Basin: Stratigraphic succession and LA-ICP-MS geochronology: *Scientia Sinica Terrae*, v. 48, p. 224–242 [in Chinese].
- Qinghai BGMR (Bureau of Geology and Mineral Resources), 1991, Regional geology of Qinghai Province: Beijing, Geological Publishing House, 662 p. [in Chinese with English summary].
- Reid, A., Wilson, C.J.L., Lui, S., Pearson, N., and Belousova, E., 2007, Mesozoic plutons of the Yidun arc, SW China: U/Pb geochronology and Hf isotopic signature: *Ore Geology Reviews*, v. 31, p. 88–106, <https://doi.org/10.1016/j.oregeorev.2004.11.003>.
- Rieser, A.B., Neubauer, F., Liu, Y., and Ge, X., 2005, Sandstone provenance of northwestern sectors of the intracontinental Cenozoic Qaidam basin, western China: tectonic vs. climatic control: *Sedimentary Geology*, v. 177, p. 1–18, <https://doi.org/10.1016/j.sedgeo.2005.01.012>.
- Rieser, A.B., Liu, Y., Genser, J., Neubauer, F., Handler, R., Friedl, G., and Ge, X.H., 2006a, <sup>40</sup>Ar/<sup>39</sup>Ar ages of detrital white mica constrain the Cenozoic development of the intracontinental Qaidam Basin, China: *Geological Society of America Bulletin*, v. 118, p. 1522–1534, <https://doi.org/10.1130/B25962.1>.
- Rieser, A.B., Liu, Y., Genser, J., Neubauer, F., Handler, R., and Ge, X.H., 2006b, Uniform Permian <sup>40</sup>Ar/<sup>39</sup>Ar detrital mica ages in the eastern Qaidam Basin (NW China): where is the source?: *Terra Nova*, v. 18, p. 79–87, <https://doi.org/10.1111/j.1365-3121.2005.00666.x>.
- Robinson, D.M., Dupont-Nivet, G., Gehrels, G.E., and Zhang, Y., 2003, The Tula uplift, northwestern China: Evidence for regional tectonism of the northern Tibetan Plateau during late Mesozoic–early Cenozoic time: *Geological Society of America Bulletin*, v. 115, p. 35–47, [https://doi.org/10.1130/0016-7606\(2003\)115<0035:TTUNCE>2.0.CO;2](https://doi.org/10.1130/0016-7606(2003)115<0035:TTUNCE>2.0.CO;2).
- Roger, R., Tapponnier, P., Arnaud, N., Schärer, U., Brunel, M., Xu, Z., and Yang, J., 2000, An Eocene magmatic belt across central Tibet: mantle subduction triggered by the Indian collision?: *Terra Nova*, v. 12, p. 102–108, <https://doi.org/10.1046/j.1365-3121.2000.123282.x>.
- Roger, F., Arnaud, N., Gilder, S., Tapponnier, P., Jolivet, M., Brunel, M., Malavieille, J., Xu, Z., and Yang, J., 2003, Geochronological and geochemical constraints on Mesozoic suturing in east central Tibet: *Tectonics*, v. 22, 1037, <https://doi.org/10.1029/2002TC001466>.
- Roger, F., Malavieille, J., Leloup, P.H., Calassou, S., and Xu, Z., 2004, Timing of granite emplacement and cooling in the Songpan-Garzê Fold Belt (eastern Tibetan Plateau) with tectonic implications: *Journal of Asian Earth Sciences*, v. 22, p. 465–481, [https://doi.org/10.1016/S1367-9120\(03\)00089-0](https://doi.org/10.1016/S1367-9120(03)00089-0).
- Royden, L.H., 1996, Coupling and decoupling of crust and mantle in convergent orogens: Implications for strain partitioning in the crust: *Journal of Geophysical Research*, v. 101, p. 17,679–17,705, <https://doi.org/10.1029/96JB00951>.
- Ryan, W.B.F., Carbotte, S.M., Coplan, J.O., O'Hara, S., Melkonian, A., Arko, R., Weissel, R.A., Ferrini, V., Goodwillie, A., Nitsche, F., Bonczkowski, J., and Zensky, R., 2009, Global multi-resolution topography synthesis: *Geochemistry Geophysics Geosystems*, v. 10, Q03014, <https://doi.org/10.1029/2008GC002332>.
- Saylor, J.E., and Sundell, K.E., 2016, Quantifying comparison of large detrital geochronology data sets: *Geosphere*, v. 12, no. 1, p. 203–220, <https://doi.org/10.1130/GES01237.1>.
- Shi, W., Wang, F., Yang, L., Wu, L., and Zhang, W., 2018, Diachronous growth of the Altyn Tagh Mountains: Constraints on propagation of the northern Tibetan margin from (U-Th)/He dating: *Journal of Geophysical Research*, *Solid Earth*, v. 123, p. 6000–6018, <https://doi.org/10.1029/2017JB014844>.
- Smith, A.B., and Xu, J., 1988, Palaeontology of the 1985 Tibet Geotraverse, Lhasa to Golmud: *Philosophical Transactions of the Royal Society of London. Series A, Mathematical and Physical Sciences*, v. 327, p. 53–105, <https://doi.org/10.1098/rsta.1988.0122>.
- Sobel, E.R., and Arnaud, N., 1999, A possible middle Paleozoic suture in the Altyn Tagh, NW China: *Tectonics*, v. 18, no. 1, p. 64–74, <https://doi.org/10.1029/1998TC000023>.
- Spurlin, M.S., Yin, A., Horton, B.K., Zhou, J.Y., and Wang, J.H., 2005, Structural evolution of the Yushu-Nangqian region and its relationship to synconvergent igneous activity, east-central Tibet: *Geological Society of America Bulletin*, v. 117, p. 1293–1317, <https://doi.org/10.1130/B25572.1>.
- Staisch, L.M., Niemi, N.A., Chang, H., Clark, M.K., Rowley, D.B., and Currie, B.S., 2014, A Cretaceous-Eocene depositional age for the Fenghuoshan Group, Hoh Xil Basin: Implications for the tectonic evolution of the northern Tibetan Plateau: *Tectonics*, v. 33, p. 281–301, <https://doi.org/10.1002/2013TC003367>.
- Staisch, L.M., Niemi, N.A., Clark, M.K., and Chang, H., 2016, Eocene to late Oligocene history of crustal shortening within the Hoh Xil Basin and implications for the uplift history of the northern Tibetan Plateau: *Tectonics*, v. 35, no. 4, p. 862–895, <https://doi.org/10.1002/2015TC003972>.
- Sun, Z., Feng, X., Li, D., Yang, F., Qu, Y., and Wang, H., 1999, Cenozoic Ostracoda and palaeoenvironments of the northeastern Tarim basin, western China: *Palaeogeography, Palaeoclimatology, Palaeoecology*, v. 148, p. 37–50, [https://doi.org/10.1016/S0031-0182\(98\)00174-6](https://doi.org/10.1016/S0031-0182(98)00174-6).
- Sun, Z., Yang, Z., Pei, J., Ge, X., Wang, X., Yang, T., Li, W., and Yuan, S., 2005, Magnetostratigraphy of Paleogene sediments from northern Qaidam Basin, China: Implications for tectonic uplift and block rotation in northern Tibetan plateau: *Earth and Planetary Science Letters*, v. 237, p. 635–646, <https://doi.org/10.1016/j.epsl.2005.07.007>.
- Tapponnier, P., Xu, Z.Q., Roger, F., Meyer, B., Arnaud, N., Wittlinger, G., and Yang, J.S., 2001, Oblique stepwise rise and growth of the Tibet plateau: *Science*, v. 294, p. 1671–1677, <https://doi.org/10.1126/science.105978>.
- Volkmer, J.E., Kapp, P., Guynn, J.H., and Lai, Q., 2007, Cretaceous-Tertiary structural evolution of the north central Lhasa terrane, Tibet: *Tectonics*, v. 26, TC6007, <https://doi.org/10.1029/2005TC001832>.
- Wang, C.S., Yi, H. S., Li, Y., Deng, B., Liu, D. Z., Wang, G. Z., and Lin, J.H., 2001a, The Geological Evolution and Prospective Oil and Gas Assessment of the Qiangtang Basin in Northern Tibetan Plateau: Beijing, Geological Publishing House [in Chinese with English abstract].
- Wang, C.S., Liu, Z.F., Yi, H., Liu, S., and Zhao, X., 2002, Tertiary crustal shortening and pe-nephanation in the Hoh Xil region: implications for the tectonic history of the northern Tibetan plateau: *Journal of Asian Earth Sciences*, v. 20, p. 211–223, [https://doi.org/10.1016/S1367-9120\(01\)00051-7](https://doi.org/10.1016/S1367-9120(01)00051-7).
- Wang, C.S., Zhao, X.X., Liu, Z., Lippert, P.C., Graham, S.A., Coe, R.S., Yi, H., Zhu, L., Liu, S., and Li, Y., 2008, Constraints on the early uplift history of the Tibetan plateau: *Proceedings of the National Academy of Sciences of the United States of America*, v. 105, p. 4987–4992, <https://doi.org/10.1073/pnas.0703595105>.
- Wang, C.S., Gao, R., Yin, A., Wang, H.Y., Zhang, Y.X., Guo, T.L., Li, Q.S., and Li, Y.L., 2011, A mid-crustal strain-transfer model for continental deformation: A new perspective from high-resolution deep seismic-reflection profiling across NE Tibet: *Earth and Planetary Science Letters*, v. 306, p. 279–288, <https://doi.org/10.1016/j.epsl.2011.04.010>.
- Wang, F., Lo, C.H., Li, Q., Yeh, M.W., Wan, J., Zheng, D., and Wang, E., 2004, Onset timing of significant unroofing around Qaidam basin, northern Tibet, China: constraints from <sup>40</sup>Ar/<sup>39</sup>Ar and FT thermochronology on granitoids: *Journal of Asian Earth Sciences*, v. 24, p. 59–69, <https://doi.org/10.1016/j.jseaes.2003.07.004>.
- Wang, F., Feng, H., Shi, W., Zhang, W., Wu, L., Yang, L., Wang, Y., Zhang, Z., and Zhu, R., 2016, Relief history and denudation evolution of the northern Tibetan margin: Constraints from <sup>40</sup>Ar/<sup>39</sup>Ar and (U-Th)/He dating and implications for far-field effect of rising plateau: *Tectonophysics*, v. 675, p. 196–208, <https://doi.org/10.1016/j.tecto.2016.03.001>.
- Wang, J.H., Yin, A., Harrison, T.M., Grove, M., Zhang, Y.Q., and Xie, G.H., 2001b, A tectonic model for Cenozoic igneous activities in the eastern Indo-Asian collision zone: *Earth and Planetary Science Letters*, v. 188, p. 123–133, [https://doi.org/10.1016/S0012-821X\(01\)00315-6](https://doi.org/10.1016/S0012-821X(01)00315-6).
- Wang, L.Q., Pan, G.T., Ding, J., and Yao, D.S., compiler., 2013, Geological Map of the Tibetan Plateau at a scale of 1:1.5 M with explanations: Beijing, Geological Publishing House, 288 p.
- Wang, W.T., Zheng, W.J., Zhang, P.Z., Li, Q., Kirby, E., Yuan, D.Y., Zheng, D.W., Liu, C.C., Wang, Z.C., Zhang, H.P., and Pang, J.Z., 2017, Expansion of the Tibetan Plateau during Neogene: *Nature Communications*, v. 8, p. 15887, <https://doi.org/10.1038/ncomms15887>.
- Wang, X., Qiu, Z., Li, Q., Wang, B., Qiu, Z., and Meng, Q., 2007, Vertebrate paleontology, biostratigraphy, geochronology, and paleoenvironment of Qaidam basin in northern Tibetan plateau: *Palaeogeography, Palaeoclimatology, Palaeoecology*, v. 254, p. 363–385, <https://doi.org/10.1016/j.palaeo.2007.06.007>.
- Wang, Y., Zhang, X., Wang, E., Zhang, J., Li, Q., and Sun, G., 2005, <sup>40</sup>Ar/<sup>39</sup>Ar thermochronological evidence for formation and Mesozoic evolution of the northern-central segment of the Altyn Tagh fault system in the northern Tibetan Plateau: *Geological Society of America Bulletin*, v. 117, p. 1336–1346, <https://doi.org/10.1130/B25685.1>.
- Weislogel, A.L., 2008, Tectonostratigraphic and geochronological constraints on evolution of the northeast Paleotethys from the Songpan-Ganzi complex, central China: *Tectonophysics*, v. 451, p. 331–345, <https://doi.org/10.1016/j.tecto.2007.11.053>.
- Weislogel, A.L., Graham, S.A., Chang, E.Z., Wooden, J.L., Gehrels, G.E., and Yang, H., 2006, Detrital zircon provenance of the Late Triassic Songpan-Ganzi complex: Sedimentary record of collision of the North and South China blocks: *Geology*, v. 34, p. 97–100, <https://doi.org/10.1130/G21929.1>.
- Weislogel, A.L., Graham, S.A., Chang, E.Z., Wooden, J.L., and Gehrels, G.E., 2010, Detrital zircon provenance from three turbidite depocenters of the Middle–Upper Triassic Songpan-Ganzi complex, central China: Record of collisional tectonics, erosional exhumation, and sediment production: *Geological Society of America Bulletin*, v. 122, no. 11–12, p. 2041–2062, <https://doi.org/10.1130/B26606.1>.
- Williams, H., Turner, S., Kelley, S., and Harris, N., 2001, Age and composition of dikes in Southern Tibet: New constraints on the timing of east-west extension and its relationship to postcollisional volcanism: *Geology*, v. 29, p. 339–342, [https://doi.org/10.1130/0091-7613\(2001\)029<0339:AACODI>2.0.CO;2](https://doi.org/10.1130/0091-7613(2001)029<0339:AACODI>2.0.CO;2).
- Wu, C., Yin, A., Zusa, A.V., Zhang, J.Y., Liu, W.C., and Ding, L., 2016a, Pre-Cenozoic geologic history of the central and northern Tibetan Plateau and the role of Wilson cycles in constructing the Tethyan orogenic system: *Lithosphere*, v. 8, no. 3, p. 254–292, <https://doi.org/10.1130/L494.1>.
- Wu, C., Zusa, A.V., Yin, A., Liu, C.F., Reith, R.C., Zhang, J.Y., Liu, W.C., and Zhou, Z.G., 2017, Geochronology and geochemistry of Neoproterozoic granitoids in the central Qilian Shan of northern Tibet: Reconstructing the amalgamation processes and tectonic history of Asia: *Lithosphere*, v. 9, no. 4, p. 609–636.
- Wu, C., Zusa A.V., Chen X.H., Ding L., Levy, D.A., Liu C.F., Liu, W.C., Jiang, T., and Stockli, D.F., 2019, Tectonics of the Eastern Kunlun Range: Cenozoic reactivation of a Paleozoic-early Mesozoic orogeny: *Tectonics*, <https://doi.org/10.1029/2018TC005370> (in press).
- Wu, C.L., Yang, J.S., Yao, S.Z., Zeng, L.S., Chen, S.Y., Li, H.B., Qi, X.X., Wooden, J.L., and Mazdab, F.L., 2005, Characteristics of the granitoid complex and its zircon SHRIMP dating at the south margin of the Bashikaocong Basin, North Altun, NW China: *Yanshi Xuebao*, v. 21, p. 846–858 [in Chinese with English abstract].

- Wu, C.L., Lei, M., Wu, D., Zhang, X., Cheng, H.J., and Li, T.X., 2016b, Zircon U-Pb dating of Paleozoic granite from South Altun and response of the magmatic activity to the tectonic evolution of the Altun Orogenic Belt: *Acta Geologica Sinica*, v. 90, p. 2276–2315 [in Chinese with English abstract].
- Wu, L., Xiao, A., Wang, L., Shen, Z., Zhou, S., Chen, Y., and Guan, J., 2011, Late Jurassic–early Cretaceous northern Qaidam basin, NW China: implications for the earliest Cretaceous intracontinental tectonism: *Cretaceous Research*, v. 32, no. 4, p. 552–564, <https://doi.org/10.1016/j.cretres.2011.04.002>.
- Wu, Z.H., Barosh, P.J., Wu, Z., Hu, D., Zhao, X., and Ye, P., 2008, Vast early Miocene lakes of the central Tibetan plateau: *Geological Society of America Bulletin*, v. 120, p. 1326–1337, <https://doi.org/10.1130/B26043.1>.
- Xia, W., Zhang, N., Yuan, X., Fan, L., and Zhang, B., 2001, Cenozoic Qaidam basin, China: A stronger tectonic inverted, extensional rifted basin: *The American Association of Petroleum Geologists Bulletin*, v. 85, p. 715–736.
- Yang, F., Ma, Z., Xu, T., and Ye, S., 1992, A Tertiary paleomagnetic stratigraphic profile in Qaidam basin: *Yanshi Xuebao*, v. 13, p. 97–101.
- Yin, A., 2010, Cenozoic tectonic evolution of Asia: A preliminary synthesis: *Tectonophysics*, v. 488, p. 293–325, <https://doi.org/10.1016/j.tecto.2009.06.002>.
- Yin, A., and Harrison, T.M., 2000, Geologic evolution of the Himalayan-Tibetan orogen: *Annual Review of Earth and Planetary Sciences*, v. 28, p. 211–280, <https://doi.org/10.1146/annurev.earth.28.1.211>.
- Yin, A., and Nie, S., 1996, A Phanerozoic palinspastic reconstruction of China and its neighboring regions, in Yin, A., and Harrison, T.M., *The tectonic evolution of Asia*: New York, Cambridge University Press, p. 442–485.
- Yin, J., Xu, J., Liu, C., and Li, H., 1988, The Tibetan plateau: regional stratigraphic context and previous work: *Philosophical Transactions of the Royal Society of London. Series A, Mathematical and Physical Sciences*, v. 327, p. 5–52, <https://doi.org/10.1098/rsta.1988.0121>.
- Yin, A., Harrison, T.M., Ryerson, F.J., Chen, W.J., Kidd, W.S.F., and Copeland, P., 1994, Tertiary structural evolution of the Gangdese thrust system, southeastern Tibet: *Journal of Geophysical Research*, v. 99, p. 18,175–18,201, <https://doi.org/10.1029/94JB00504>.
- Yin, A., Rumelhart, P.E., Butler, R., Cowgill, E., Harrison, T.M., Foster, D.A., Ingersoll, R.V., Zhang, Q., Zhou, X.Q., Wang, X.F., Hanson, A., and Raza, A., 2002, Tectonic history of the Altyn Tagh fault system in northern Tibet inferred from Cenozoic sedimentation: *Geological Society of America Bulletin*, v. 114, p. 1257–1295, [https://doi.org/10.1130/0016-7606\(2002\)114<1257:THOTAT>2.0.CO;2](https://doi.org/10.1130/0016-7606(2002)114<1257:THOTAT>2.0.CO;2).
- Yin, A., Dang, Y., Zhang, M., McRivette, M.W., Burgess, W.P., and Chen, X.H., 2007a, Cenozoic tectonic evolution of Qaidam basin and its surrounding regions (Part 2): Wedge tectonics in southern Qaidam basin and the Eastern Kunlun Range, in Sears, J.W., et al., eds., *Whence the Mountains? Inquiries into the Evolution of Orogenic Systems: A Volume in Honor of Raymond A. Price*: Geological Society of America Special Paper, v. 433, p. 369–390, [https://doi.org/10.1130/2007.2433\(18\)](https://doi.org/10.1130/2007.2433(18)).
- Yin, A., Manning, C.E., Lovera, O., Menold, C.A., Chen, X.H., and Gehrels, G.E., 2007b, Early Paleozoic tectonic and thermomechanical evolution of ultrahigh-pressure (UHP) metamorphic rocks in the northern Tibetan plateau, northwest China: *International Geology Review*, v. 49, p. 681–716, <https://doi.org/10.2747/0020-6814.49.8.681>.
- Yin, A., Dang, Y.Q., Wang, L.C., Jiang, W.M., Zhou, S.P., Chen, X.H., Gehrels, G.E., and McRivette, M.W., 2008a, Cenozoic tectonic evolution of Qaidam basin and its surrounding regions (Part 1): The southern Qilian Shan-Nan Shan thrust belt and northern Qaidam basin: *Geological Society of America Bulletin*, v. 120, p. 813–846, <https://doi.org/10.1130/B26180.1>.
- Yin, A., Dang, Y., Zhang, M., Chen, X.H., and McRivette, M.W., 2008b, Cenozoic tectonic evolution of Qaidam basin and its surrounding regions (Part 3): Structural geology, sedimentation, and regional tectonic reconstruction: *Geological Society of America Bulletin*, v. 120, p. 847–876, <https://doi.org/10.1130/B26232.1>.
- Yu, L., Xiao, A., Wu, L., Tian, Y., Rittner, M., Lou, Q., and Pan, X., 2017a, Provenance evolution of the Jurassic northern Qaidam Basin (West China) and its geological implications: evidence from detrital zircon geochronology: *International Journal of Earth Sciences*, v. 106, no. 8, p. 2713–2726, <https://doi.org/10.1007/s00531-017-1455-z>.
- Yu, S., Zhang, J.X., Li, S.Z., Sun, D.Y., Li, Y.S., Liu, X., Guo, L.L., Suo, Y.H., Peng, Y.B., and Zhao, X.L., 2017b, Paleoproterozoic granulite-facies metamorphism and anatexis in the Oulongbuluke Block, NW China: Respond to assembly of the Columbia supercontinent: *Precambrian Research*, v. 291, p. 42–62, <https://doi.org/10.1016/j.precamres.2017.01.016>.
- Yu, X.J., Huang, B.C., Guan, S.W., Fu, S.T., Cheng, F., Cheng, X., Zhang, T., and Guo, Z.J., 2014, Anisotropy of magnetic susceptibility of Eocene and Miocene sediments in the Qaidam Basin, Northwest China: implication for Cenozoic tectonic transition and depocenter migration: *Geochimica Geophysica Geosystems*, v. 15, p. 2095–2108, <https://doi.org/10.1002/2014GC005231>.
- Yu, X.J., Guo, Z., and Fu, S., 2015, Enderheic or exorheic: differential isostatic effects of Cenozoic sediments on the elevations of the cratonic basins around the Tibetan Plateau: *Terra Nova*, v. 27, no. 1, p. 21–27, <https://doi.org/10.1111/ter.12126>.
- Yu, X.J., Fu, S., Wang, Z., Li, Q., and Guo, Z.J., 2017c, The discovery of early Paleoproterozoic high-Na trondhjemite in the northeastern Qaidam basin: Evidence from the drilling core samples: *Precambrian Research*, v. 298, p. 615–628, <https://doi.org/10.1016/j.precamres.2017.04.002>.
- Yuan, W.M., Zhang, X.T., Dong, J.Q., Tang, Y.H., Yu, F.S., and Wang, S.C., 2003, A new vision of the intracontinental evolution of the eastern Kunlun Mountains, Northern Qinghai-Tibet plateau, China: *Radiation Measurements*, v. 36, p. 357–362, [https://doi.org/10.1016/S1350-4487\(03\)00151-3](https://doi.org/10.1016/S1350-4487(03)00151-3).
- Yuan, W.M., Dong, J., Wang, S., and Carter, A., 2006, Apatite fission track evidence for Neogene uplift in the eastern Kunlun Mountains, northern Qinghai-Tibet plateau, China: *Journal of Asian Earth Sciences*, v. 27, p. 847–856, <https://doi.org/10.1016/j.jseas.2005.09.002>.
- Yuan, D.Y., Ge, W.P., Chen, Z.W., Li, C.Y., Wang, Z.C., and Roe, G.H., 2013, The growth of north-eastern Tibet and its relevance to large-scale continental geodynamics: A review of recent studies: *Tectonics*, v. 32, p. 1358–1370, <https://doi.org/10.1002/tect.20081>.
- Zhang, K.J., Zhang, Y.X., Xia, B.D., and He, Y.B., 2006, Temporal variations of Mesozoic sandstone compositions in the Qiangtang block, northern Tibet (China): Implications for provenance and tectonic setting: *Journal of Sedimentary Research*, v. 76, p. 1035–1048, <https://doi.org/10.2110/jsr.2006.089>.
- Zhang, L.Y., Ding, L., Pullen, A., Xu, Q., Liu, D.L., Cai, F.L., Yue, Y.H., Lai, Q.Z., Shi, R.D., Ducea, M.H., Kapp, P., and Chapman, A., 2014, Age and geochemistry of western Hoh-Xil-Songpan-Ganzi granitoids, northern Tibet: Implications for the Mesozoic closure of the Paleo-Tethys ocean: *Lithos*, v. 190, p. 328–348, <https://doi.org/10.1016/j.lithos.2013.12.019>.
- Zhu, L., Wang, C., Zheng, H., Xiang, F., Yi, H., and Liu, D., 2006, Tectonic and sedimentary evolution of basins in the northeast of Qinghai-Tibet Plateau and their implication for the northward growth of the Plateau: *Palaeogeography, Palaeoclimatology, Palaeoecology*, v. 241, p. 49–60, <https://doi.org/10.1016/j.palaeo.2006.06.019>.
- Zhu, W., Wu, C., Wang, J., and Zhou, T., 2018, Provenance analysis of detrital monazite, zircon and Cr-spinel in the northern Tibetan Plateau: Implications for the Paleozoic tectonothermal history of the Altyn Tagh and Qimen Tagh Ranges: *Basin Research*, <https://doi.org/10.1111/bre.12333> (in press).
- Zhuang, G., Hourigan, J.K., Ritts, B.D., and Kent-Corson, M.L., 2011, Cenozoic multiple-phase tectonic evolution of the northern Tibetan Plateau: Constraints from sedimentary records from Qaidam basin, Hexi Corridor, and Subei basin, northwest China: *American Journal of Science*, v. 311, no. 2, p. 116–152, <https://doi.org/10.2475/02.2011.02>.
- Zhuang, G., Johnstone, S.A., Hourigan, J., Ritts, B., Robinson, A., and Sobel, E.R., 2018, Understanding the geologic evolution of Northern Tibetan Plateau with multiple thermochronometers: *Gondwana Research*, v. 58, p. 195–210, <https://doi.org/10.1016/j.gr.2018.02.014>.
- Zuza, A.V., Cheng, X., and Yin, A., 2016, Testing models of Tibetan Plateau formation with Cenozoic shortening estimates across the Qilian Shan–Nan Shan thrust belt: *Geosphere*, v. 12, p. 501–532, <https://doi.org/10.1130/GES01254.1>.
- Zuza, A.V., Yin, A., Lin, J., and Sun, M., 2017, Spacing and strength of active continental strike-slip faults: *Earth and Planetary Science Letters*, v. 457, p. 49–62, <https://doi.org/10.1016/j.epsl.2016.09.041>.
- Zuza, A.V., Wu, C., Reith, R.C., Yin, A., Li, J.H., Zhang, J.Y., Zhang, Y.X., Wu, L., and Liu, W.C., 2018, Tectonic evolution of the Qilian Shan: An early Paleozoic orogen reactivated in the Cenozoic: *Geological Society of America Bulletin*, v. 130, no. 5–6, p. 881–925, <https://doi.org/10.1130/B31721.1>.
- Zuza, A.V., Wu, C., Wang, Z., Levy, D.A., Li, B., Xiong, X., and Chen, X., 2019, Underthrusting and duplexing beneath the northern Tibetan Plateau and the evolution of the Himalayan-Tibetan orogen: *Lithosphere*, v. 2, p. 209–231, <https://doi.org/10.1130/L1042.1>.

MANUSCRIPT RECEIVED 9 JANUARY 2019

REVISED MANUSCRIPT RECEIVED 26 FEBRUARY 2019

MANUSCRIPT ACCEPTED 2 APRIL 2019